CLOSING THE LOOP: A COMBINED COMPUTATIONAL MODELING AND EXPERIMENTAL APPROACH PROVIDES NOVEL INSIGHTS INTO IMMUNE CELL SIGNALING SYSTEMS AND THEIR GLOBAL EFFECTS.

by

Robert Patrick Sheehan Jr

Bachelors of Science in Quantitative Biology, University of Delaware, 2007

Submitted to the Graduate Faculty of

School of Medicine in partial fulfillment

of the requirements for the degree of

Doctor of Philosophy

University of Pittsburgh

2016

UNIVERSITY OF PITTSBURGH

SCHOOL OF MEDICINE

This dissertation was presented

by

Robert Patrick Sheehan Jr

It was defended on

July 22, 2016

and approved by

Robin E. Lee, PhD, Department of Computational and Systems Biology

Penelope A. Morel, MD, Department of Immunology

Gilles Clermont, MD, Department of Critical Care Medicine

Russell S. Schwartz, PhD, Computational Biology Department, Carnegie Mellon University

Dissertation Advisor: James R. Faeder, PhD, Department of Computational and Systems Biology

CLOSING THE LOOP: A COMBINED COMPUTATIONAL MODELING AND EXPERIMENTAL APPROACH PROVIDES NOVEL INSIGHTS INTO IMMUNE CELL SIGNALING SYSTEMS AND THEIR GLOBAL EFFECTS.

Robert Patrick Sheehan Jr, PhD

University of Pittsburgh, 2016

Systems biology is an approach that marries complimentary disciplines, encouraging the use of quantitative methods to help define, explain, and predict biological processes. By building computational models of biological systems, we can pose new biologically motivated questions and make falsifiable, quantitative predictions. In this thesis I will discuss the cycle of model building and experimental validation, and how it has provided insight into poorly and understood systems and allowed us to predict the effects of perturbations on these systems, which could have real and significant effects in human health and medicine. First, we model the activation of neutrophils in sepsis. By fitting a single model to two sets of data, coming from animals that survive and succumb to the same bacterial challenge, we create a realistic representation of biological variation, showing how a single network architecture can lead to different outcomes. Additionally, this method allows us to identify markers for sepsis susceptibility and identify and optimize a potential treatment option to lead to improved outcomes. Next, we model signaling downstream of the T cell receptor, and how this leads to differentiation decision making in CD4 T cells. By modeling the dynamics of this signaling network under varying antigen doses, we are able to identify network elements critical to dose discrimination, leading to the production of

Treg cells following low dose stimulation and Th cells following high dose stimulation. We can then perturb these elements of the network, to potentially fine tune mature T cell populations to alter the trajectories of autoimmune disorders or cancer. Finally, we model the dynamics of IL-17 signaling. This allows us to understand how ubiquitin scaffolds form following cytokine stimulation, leading to the activation of NF-κB, and how the ubiquitin editing enzyme A20 acts as a negative feedback regulator by breaking these chains. This allows us to better understand ubiquitin oligomerization as a fulcrum in the system, and how changes in A20 and ubiquitin binding proteins lead to different profiles of NF-κB activation and could play a role in inflammatory disorders.

TABLE OF CONTENTS

LIST OF TABLES

LIST OF FIGURES

LIST OF EQUATIONS

ACKNOWLEDGEMENTS

I would like to thank my advisor, Dr. James Faeder. You have been the best mentor I could have hoped for to guide my growth as a scientist, an academic, and a person. You were one of the main reasons I came to Pittsburgh, and it couldn't have turned out better. I will sincerely miss our long chats about not only science, but sports, politics, and life, and I just hope I can continue to carry on the Faeder lab zeal for rule-based modeling, high quality science, and pushing the bounds of biology.

I would like to thank Dr. Robin Lee. Although you were only here for the last couple of years of my degree, you did so much to help me better understand the greater biological context of my work, and opened up a new world of experiments for me to consider. Your advice and support in my search for a postdoc and my move to Boston have been invaluable.

I would like to thank my collaborators, Dr. Sarah Gaffen and Dr. Penny Morel for teaching me what it means to be a biologist, and how to expand my thinking beyond the realm of modeling and how to ask the right questions to do meaningful biological research. I would also like to thank the members of the Gaffen Lab, in particular Juan Agustin Cruz, Dr. Abhishek Garg, and Dr. Michelle Simpson-Abelson for patiently teaching a humble computationalist how to do experiments with at least a modicum of competence.

I would like to thank all of the past and present members of the Faeder lab, in particular Dr. Leonard Harris, Dr. Justin Hogg, Dr. John Sekar, and Dr. Jose Juan Tapia. You guys taught

me how to be a productive grad student, and how to make the most of my time in the Faeder lab. Your mentorship helped to get me on my feet and on the right path, and your friendship made the long days and long lab meetings so much more enjoyable.

To my family, Mom, Dad, and Christina, I never would have even made it to graduate school, and certainly never finished without all of your love and support. Thank you for helping to make all of my education possible, for coming to visit every year in Pittsburgh, and for being my support system and sounding board for all of these years, when I just need to tell someone about the vultures I see outside of my apartment.

And finally, to my amazing wife Jen, I would be lost without your love and support. You've been by my side through all the late nights of coding, the early mornings of writing, and all the coffee in between. You're the only one who could keep me sane and keep me moving forward through this whirlwind of a dissertation on top of a move to a new city. I can't wait for all of our new adventures in Boston, and only hope I can return all of the love, and the unending help you've given me during this long process.

1.0 INTRODUCTION

1.1 A SYTEMS BIOLOGY APPROACH

1.1.1 Systems biology as an evolving field and a useful tool

Systems biology as a field is still relatively new and in the process of being defined. It encompasses work from many fields, including molecular biology, immunology, biochemistry, mathematics, computer sciences, and physics, drawing pieces from each and integrating them to push in new directions. All new scientific fields, like species, arise by descent with modification [1]. Systems biology has arisen by making modifications on these stalwart fields, and is prominently populated by researchers who pride themselves on attempting to cross disciplines and learn the basics of other fields. However, as the field grows in prominence, new scientists can be trained with a more coherent and focused path, codifying the ideas and needs of the field of systems biology, and allowing the field to grow, flourish, and better contribute to the greater scientific community.

The evolution of biology has created a clear need for the growth of systems biology. Changes in data collection as well as understanding have led to the need for new methods of analysis and explanation. Big data has become a reality and a shift in focus from individual components and steady state behavior to network connectivity and dynamical changes [2,3]

requires a different tool set to study. We now strive to understand not only how individual elements function, but how these pieces can fit together to form functional and robust systems. The need to expand from individual components to consider systems and networks has been summarized in the following quotations from H. Kitano and J. Gunawardena: “We now think we know most of the genes and the interesting question is no longer characterizing this or that gene but, rather, understanding how the various molecular components collectively give rise to phenotype and physiology” [4]; “While and understanding of genes and proteins continues to be important, the focus is on understanding a system’s structure and dynamics” [5].

The study of these larger scale systems introduces many new challenges. One complication is that these systems often rely on multiple different time and length scales. It can be quite difficult to study events that happen on the order of seconds, such as protein-protein interactions, minutes, such as transcription and translation, hours or days, such as the time course of a disease in an individual, and even longer times such as the spread of disease in a population. Labs set up to study the short time scales are often ill equipped to also track longer time scales. Often the shortest and longest scales are difficult-to-impossible to measure and can require very expensive studies. This is where mathematics and computer science can open new avenues. We can easily simulate events that take place on scales ranging less than a second to over many years, with varying degrees of coarse graining [6].

This approach of studying large and complex systems as a whole is where the interests of traditional biologists and new systems biologists overlap, and how they can work together for mutual benefit. Both groups can find common ground on the systems they are interested in, and systems biologists can take the questions and hypotheses of biologists, formalize their assumptions, identify new questions, and model their systems. This is helpful in many ways. The

wealth of new techniques available, in addition to the thought process and formalisms of systems biologists, can contribute to clarification of the core concepts of biology by directly addressing and writing down assumptions.

Modeling can contribute to biology on multiple fronts. It both helps us formalize the assumptions we bring to a question, and also allows us to reach new conclusions that we can take away. In short, as Gunawardena explains, “a mathematical model is a logical machine for converting assumptions into conclusions. If the model is correct and we believe its assumptions then we must, as a matter of logic, believe its conclusions” [7]. Well-constructed models will give useful predictions (conclusions) we can take back to the lab to test. We can confirm these predictions, solidifying new biological knowledge, or refute the prediction, forcing us to reexamine and reconsider our assumptions, often leading to new biological knowledge as well. The types of insights we gain from these predictions are particularly useful because they are mechanistic in nature. Rather than searching for correlations, we specifically search for causality, because, as Wenying Shou states: “statistical correlations on their own do not constitute understanding. Rather, it is when a mechanistic explanation of the regularities or patterns is developed from underlying principles, while relying on as few assumptions as possible, that a theory is born” [8]. Modeling allows us to convert assumptions and preliminary data into new mechanistic conclusions that take the form of falsifiable predictions.

Getting the most out of this potential collaboration between biologists and modelers requires the two groups to work closely together. This requires both groups to be clear in their goals and abilities, and to be generous in understanding the needs and limitations of the other. Modelers clearly expressing the data they require and the specific questions they can answer, and biologists being open to unusual experiments, sharing their data, and gaining enough

understanding of the model to request their own computational experiments will go a long way to improve collaborations and greatly improve scientific output.

1.1.2 Iterative collaborations allow experimental results and model predictions to add to each other

Gold standard science comes not just from collaborations born of convenience, but long standing partnerships which take the form of a cycle, as experiments inform model development, the model informs new experiments, and new data informs further model refinement. This format functions the best when the two sides are in close contact, and can create a uniform plan for attack. The interests of a modeler and experimentalist may not always align, but planning out combined efforts in an efficient way can lead to very quick progress [9].

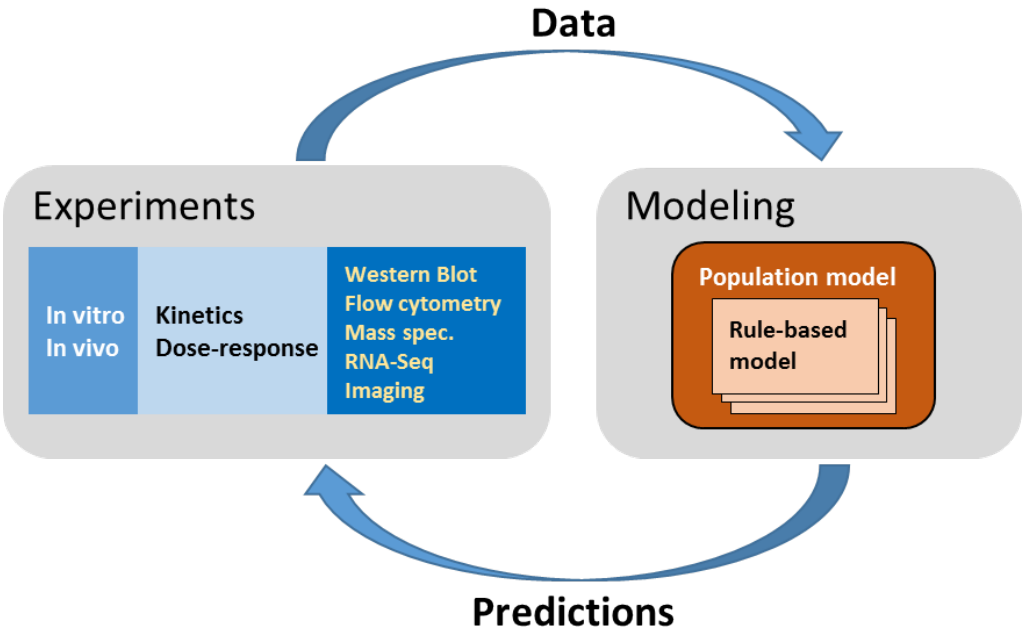

Figure 1 An iterative cycle composed of experimentalists and computationalists exchanging data leads to optimal advancement in both fields.

One reason this close collaboration is so important is the difficulty in building and calibrating new models, and the large barrier of entry this can present. A substantial amount of data are typically needed to accurately calibrate a model, and the larger and more detailed the model is, the more data are required. Often these data are difficult to collect, typically including time course experiments and sometimes requiring very specific time points. Often this will involve experiments that otherwise would not be done. This means modelers either needs the training, time, and motivation to perform these experiments themselves, or needs a collaborator willing to go out of their way to do experiments on their behalf.

The bright side is that a properly calibrated model can provide a lot of benefit in return for the experimentalist. A single model can generate a wealth of predictions and hypotheses and can be used repeatedly. While generating predictions may seem to be solely the domain of the modeler, this is again an area that benefits from collaboration. An experienced experimentalist in the field can sort through potential predictions and their corresponding experiments and decide which will be the most fruitful to pursue, based on interest in the field and feasibility of experiments. A clever experimentalist can even propose their own simulation scenarios that they would like to test, making their own experimental plans more efficient by using a computational test run. Additionally, experiments testing model predictions have an inherently low downside. Novel predictions that are confirmed are obviously interesting findings. But even when a prediction fails, new understanding can be gained. A failed prediction can often tell us even more, because it tells us something is wrong or missing from the model. It tells us our assumptions were flawed, and this can lead to its own kind of new biological finding. It may call into question long standing canon, or point researchers in the direction of a missing piece of the puzzle. Even “obvious” predictions made by a model provide us useful information on whether

the model is working correctly, and lend additional validity to future predictions. Nearly all model predictions and their corresponding experiments provide tangible benefit to both the modelers and experimentalists. All new experimental data, whether these confirm or refutes the model, can then be used to improve the model, or lead to expansion of the model in interesting directions. This cycle of model developments, predictions, and experiments make up the backbone of systems biology and lead to the quickest and most robust advancement of the field.

1.2 BIOLOGICAL BACKGROUND

1.2.1 Cell signaling methods are well suited to modeling studies

Within a good systems biology collaboration, a key point is picking the right systems to model that will benefit the most from the methods being used. Cell signaling networks are such a system that often benefit from computational modeling. These systems consist of complex networks, which computationalists are used to dealing with. These networks have many common motifs, such as feedback and feedforward loops [10], that can lead to predictable mathematical behaviors such as oscillations, bistable switches, and pulses, which computationalists are used to analyzing [11]. Additionally, these systems contain a great degree of overlap in terms of biological mechanisms. Repeated themes including protein-protein binding, phosphorylation events leading to changes in binding and catalytic activity, and trafficking of key components between different compartments allow a modeler to work on multiple systems with a baseline level of understanding. In this work, I focus on three systems, neutrophil signaling and activation leading to sepsis, T cell receptor signaling leading to CD4+ T cell differentiation, and IL-17

receptor signaling leading to NF-κB activation, which use many of these well-studied network motifs and signaling mechanisms to exert dramatic effects on the global immune response.

1.2.2 Immunological cell signaling systems

Sepsis is a case ripe for systems-level study. It involves many different scales, including the molecular level of receptor activation and cell signaling, whole cell phenotypic changes, cell population migration and behavior, the spread of inflammation, and whole organ failure. Many specific mechanisms underlying sepsis have been well studied, but a systems level understanding is still lacking. Because of this, clinical treatments are still poor [12,13], and it still has a near 20% mortality rate [14–17]. Through mathematical modeling, we can begin to tie signaling dynamics to changes in cell behavior. By calibrating our model to experimental data from septic and non-septic animals exposed to the same bacterial challenge, we can make real predictions of markers of sepsis susceptibility and progression. It also allows us to quantitatively test treatments that act on a molecular level, and predict the effects on a wider scale in terms of survival.

CD4+ T cell differentiation is controlled by signaling downstream of the T cell receptor, but has wide ranging effects. Naïve CD4+ cells can develop into immune-activating Th cells and immune-suppressive Treg cells. The balance of these populations plays a key role in many different scenarios. Too few Tregs can lead to overactive immune responses to self-antigens and the development of autoimmune disorders [18]. Too many Tregs can lead to a decrease in the ability of the immune system to target tumors in cancer patients [19,20]. By understanding how the balance of these cell populations change with changes in signaling we can learn how to better target immunotherapies and improve outcomes in these scenarios. Our previous modeling efforts indicated that differences in the signaling response to different doses of antigens played a critical

role in the differentiation decision making process [21]. By using this insight and continuing to iterate through the experimental-modeling loop we can identify key mechanisms in the signaling pathway, such as positive feedback loops resulting in a switch in activation state, that determine the differentiation outcome, and how by targeting elements in this loop we can change outcomes.

IL-17 signaling is another case study in signaling dynamics exerting a far reaching effect. Activation of the transcription factor NF-κB downstream of the IL-17 receptor leads to the transcription of pro-inflammatory genes. Defects in this pathway have been linked to inflammatory disorders such as psoriasis [22–24] and Rheumatoid Arthritis [25], so better understanding the control of NF-κB could have a substantial clinical impact. A key inhibitor of NF-κB that could play a role in these disorders is the ubiquitin editing enzyme A20 [26,27]. A20 acts as a negative feedback element, as it is an NF-κB-induced gene that reduces the activation of NF-κB by breaking ubiquitin scaffolds that are required for the activation of kinases necessary for IκB degradation and subsequent NF-κB activation. The growth and maintenance of these ubiquitin scaffolds is an important step in the signaling pathway, but it is difficult to measure and track experimentally using traditional biochemical methods. By building a unique mathematical model with a specific focus on ubiquitin oligomerization and A20's ubiquitin editing mechanisms, and calibrating it to experimental data, we can predict the growth dynamics and typical sizes of ubiquitin, as well as the activation dynamics their binding partners. This allows us to gain new understanding into how a known key player, A20, functions, and make quantitative predictions about how changes to its function affect signaling dynamics and resultant inflammation.

1.3 COMPUTATIONAL BACKGROUND

1.3.1 Modeling methods

To model all of these different systems we have to choose methods to match both system and question being answered. There exist many methods for model specification and model simulation, and each have their own strengths and weaknesses that make them suitable for modeling different kinds of systems and answering different kinds of questions [28].

1.3.1.1 Ordinary differential equations Ordinary differential equation (ODE) networks are one of the most common forms of mathematical model [29]. They are simulated deterministically and deal well with low complexity systems but can scale poorly in terms of model specification. Model simulation is generally fast and lends itself to well established methods of analysis [11]. Well suited to handling large populations and provides extensive flexibility.

They have been extensively used in modeling various aspects of the immune system in, a wide variety of contexts and with different approaches [30,31]. Simple, phenomenological models that focus on a small number of generalized components have been used to model a wide range of immune behaviors. These models may involve a small amount of mechanistic detail, such as a receptor binding a ligand, or a pathogen with realistic population growth and decay. However, they will also contain more abstract elements, such as generic changes in activation state, or transition between phenotypes that involve a series of more complex mechanisms, but are simplified to a single step to allow for easier simulation, easier analysis, and to facilitate the building of larger scope models. This type of model has been used to great effect in studying inflammatory pathways, where a less detailed approach is beneficial due to the sheer complexity

involved in considering numerous overlapping signaling pathways. These pathways can experience crosstalk complicated by autocrine and paracrine signaling [32–36], and the many inflammatory cytokines and other mediators that are produced, which can also have many overlapping effects on the system [37,38]. Many models have tried to tackle these problems, at a variety of different scales. Models have attempted to understand the dynamics of the inflammatory response to specific challenges in a quasi-mechanistic fashion by explicitly modeling certain elements of interest, and grouping other mediators into a smaller number of abstract variables [39,40]. Alternatively, more abstract, statistical approaches have been used to identify inflammatory markers indicative of patient outcomes, in the absence of mechanistic detail [41]. A more coarse-grained approach, focusing on the dynamics of gross populations of cells, rather than the molecular detail inside of a single cell, has also led to increased understanding of the pathology of inflammation in sepsis [42]. By zooming out to an even more coarse-grained level of detail, epidemiological models can assess the spread of a disease throughout a population, while ignoring the details of a single individual [43–45]. These use cases illustrate the great extent to which phenomenological ODE models allow for case-specific coarse graining to tackle immunological problems at many levels of detail, including the level of molecular interactions, cell population dynamics, the growth of disease in an individual, and the spread of disease in populations. However, ODE models can also utilize a greater level of detail, maintaining greater fidelity to biological mechanisms.

More detailed models are often used with the goal of achieving greater mechanistic detail, and gaining insight into specific players in a system of interest. JAK-STAT signaling pathways received significant modeling attention as a seemingly simple but important system in the immune response triggered by many factors. The kinetics were predicted in early models [46]

and additional studies followed suit, focusing on the details of specific JAK-STAT combinations [47–49] and specific cell types [50,51]. These models can also be reduced back to simpler, more phenomenological models for additional analysis [52].

It is common for modeling literature to build over time in this manner, with studies building on each other to add additional information or analysis to an old model, or creating new models to attack the system from a different angle, and fill more gaps in knowledge. A classic example of this phenomenon is modeling of signaling through the epidermal growth factor (EGFR) receptor [53]. There is a large swath of literature examining the dynamics of this signaling cascade [54–56]. Many additional studies have been performed over the years to study various aspects of the system such as how information is passed from the ligand-induced signal to response [57–59], the complexity of interactions [60–62], the effects of receptor endocytosis and trafficking [63–65], the role of the pathway in cancer [66–68]. A similar effect can be seen in the NF-κB modeling field [69], where a large number of different groups have modeled various aspects of the associated pathways, as discussed in section 4.1.1.

1.3.1.2 Boolean modeling In Boolean modeling [70] elements are represented as binary variables that take the values 0, representing the inactive state, or 1, representing the active state. Variable states are determined using a set of logical rules which are constructed using standard logical operators such as AND, OR, and NOT. These models are typically simulated stochastically with a series of update rounds which can represent the passage of time where each variable is updated synchronously or asynchronously [70,71].

This method is beneficial for modeling very large networks in a coarse grained and qualitative manner. There are no explicit parameters in a Boolean model, reducing the need to calibrate models to experimental data. This allows models to scale up to much larger sizes

without the need for increasing numbers of experiments. This makes the models suitable for exploring different network architectures, and understanding all possible behaviors arising from a given architecture. The difficulty of integrating quantitative experimental data and lack of explicit time make it difficult to make quantitative predictions, but do allow for qualitative predictions and can be used to understand the flow of information within a network.

Boolean modeling has been used to great effect in modeling many different types of biological systems, allowing for the inclusion of large complex sets of interactions [72]. Boolean modeling is a popular technique for modeling gene regulatory networks [73,74], and has been expanded to add mechanistic detail, such as considering ligands and subsequent transcription factor activation [75]. Using these techniques to model signaling pathways has become common since they scale well, allowing for the modeling of crosstalk and signaling downstream of multiple of multiple receptors [76]. Signaling pathways influencing the differentiation of CD4 T cells have been modeled a number of times, including various levels of mechanistic detail, ranging from small models focused on identifying minimal mechanisms needed to recover the observed phenomenon [77] to larger models encompassing multiple receptors, signaling intermediates, and resulting gene products [78,79]. Additional work has focused on other effects downstream of the TCR, including activation in response to infection and cell survival decision making [80,81].

1.3.1.3 Rule-based modeling Rule-based modeling is a modeling approach where the model is specified in human-readable modeling languages such as the BioNetGen Language (BNGL) [82,83]. Model elements are specified as structured objects, allowing for the specification of site-specific dynamics. In a cell signaling context these sites can represent binding sites, catalytic domains and sites for post-translational modifications. The dynamics of model behavior are

controlled by user-defined rules that most commonly represent biochemical events controlled by mass action kinetics.

This method is well suited to modeling cell signaling systems due to its transparent fidelity to the biological system, as rules can be written to correspond directly to actual mechanisms. Additionally, it elegantly handles the problem of combinatorial complexity in model specification that arises in modeling signaling networks. The “don’t care, don’t write” convention [84] that allows for model components that do not impact a reaction to be omitted from a rule has the effect of greatly reducing the number of rules that need to be written in comparison to the number of equations required in an equivalent ODE model, particularly when accounting for the building of large complexes and oligomerization, which are common to signaling systems.

BioNetGen models are also flexible in that they can be simulated using a variety of methods. They can be simulated deterministically as a set of ODEs using the CVODE solver [85], or stochastically using an iteration of Gillespie’s method for stochastic simulations of chemical kinetics [86]. These methods have been used to model immune signaling networks in a great deal of detail [30]. Important systems modeled in the past have been reexamined in more detail as rule-based models, such as negative feedback in TLR4 signaling [87], kinetic proofreading and bistability in TCR activation [88], and JAK-STAT signaling [89]. Additional modeling studies have added significant understanding into how positive negative feedback affect the activation of both T cells [90,91] and B cells [92].

Rule-based models can also be simulated in a stochastic network-free framework using the NFsim software [93], which does not require the generation of the network of all possible reactions, making the simulation of models with a very large or even an infinite number of

species possible. This method has proved useful in simulating large signaling networks, such as that downstream of the T cell receptor [94], and in systems involving oligomerization reactions, such as in TNFR aggregation [95] and CaMKII activation [96].

1.3.1.4 Parameter estimation The final necessary computational piece is parameter estimation. Using experimental data to estimate these values and calibrate the data to quantitative dynamics of the system allows us to make quantitative predictions with our model. This requires carefully selected experimental data that captures the key dynamical features, such as complex but important dynamics like oscillations, and needs to be sufficient to constrain the model to realistic behavior. We use two methods for efficient parameter estimation. First, Bayesian parallel tempering, which utilizes traditional Markov Chain Monte Carlo (MCMC) methods to sample the Bayesian posterior distribution P(**p**|**y**), of each parameter efficiently. It is implemented in the software suite known as PTempEst (https://github.com/RuleWorld/ptempest). This method works efficiently with ODE models. Second, we utilize a genetic algorithm based approach implemented in the BioNetFit software [97], which works efficiently with models encoded in NFsim.

1.4 THESIS OUTLINE

This thesis presents a systems biology approach to modeling three separate immunological signaling systems, with a goal of gaining new understanding and making novel predictions. In Chapter 2 I will present an ODE model of neutrophil activation through two cell surface receptors, CXCR1 and CXCR2, and its implications in sepsis. Using this model, I will make predictions on the efficacy of a proposed sepsis treatment. In Chapter 3 I will present two models

of T cell receptor signaling and its impact on CD4 T cell differentiation, one a Boolean model, and one a rule-based model. I will identify signaling mechanisms leading to a threshold separating Th and Treg differentiation and predict interventions to shift this threshold. In Chapter 4 I will present a rule-based model of IL-17 receptor signaling leading to the activation of NF-κB and predict how the mechanisms of A20 affect ubiquitin scaffold formation and the dynamics of NF-κB

2.0 NEUTROPHIL ACTIVATION LEADING TO SEPSIS CAN POTENTIALLY BE TREATED USING AN EXTRACORPOREAL DEVICE TARGETING NEUTROPHIL SURFACE RECEPTORS

Adapted from Malkin AD, Sheehan RP, Mathew S, Federspiel WF, Redl H, Clermont G. (2015) A neutrophil phenotype model for extracorporeal treatment of sepsis. *PLOS Comput BIol* 11(10): e1004314. doi:10.1371/journal.pcbi.1004314. A full description of my contributions to this work is given in Section 2.5.

2.1 INTRODUCTION

Sepsis, a systemic inflammatory response due to an infection, affects 900,000 Americans per year and its incidence is expected to increase over the next 10-20 years as the population ages [17]. While it is acknowledged that sepsis is a growing problem, its associated mortality rate has remained persistently high for the last 20 years and is currently near 20% [14–17]. Sepsis is now the leading cause of in-hospital death in the United States, yet there are no FDA approved specific treatments [98]. While understanding of the underlying mechanisms in sepsis has been rapidly improving, translation to clinically effective treatments has proven very challenging [12,13]. Much of this difficulty translating treatments may be the diversity and complexity of individual immune response and patient population [99,100]. These complexities lend

themselves well to computational modeling, which can help integrate these complexities into a unified pathophysiological framework and optimize potential treatments [101].

Neutrophils are one of the first responders to sites of inflammation and play a critical role in the innate immune response. When effective, neutrophils migrate from the bloodstream through endothelial walls to the site of inflammation by sensing gradients of chemokines, which bind to neutrophil cell surface receptors. In early stages of sepsis neutrophils potentially play a duplicitous role, both actively fighting the invading pathogen but also contributing to undesirable systemic inflammation, which often leads to multiple organ dysfunction, immune paralysis, or death [102,103]. Neutrophils' roles in sepsis are well recognized but the dynamics of multiple phenotypes and their impact on treatments is not fully understood. A key chemokine impacting neutrophil behavior and phenotype is interleukin-8 (IL-8). IL-8 signals through functionally distinct surface receptors CXCR-1/2, which are primarily expressed on neutrophils. CXCR-1 is primarily responsible for activating phospholipase D [104], which mediates respiratory burst and other pathogen killing functions. CXCR-2 has been shown to stimulate migratory functions such as chemotaxis and diapedesis [105,106].

The motivation of this work is to use computational modeling of CXCR-1/2 signaling, and the associated dynamics in neutrophil phenotype composition, to explore whether modifying this dynamic could be exploited to favorably impact outcome in sepsis. A population based mechanistic computational model, which incorporates both receptor level dynamics and neutrophil response to pathogen, was developed to explore the mechanisms involved in sepsis progression and calibrated in septic baboons. Furthermore, an experimental extracorporeal treatment which modulates CXCR-1/2 receptor levels was evaluated *in silico* using the model framework. The computational model described in this manuscript provides a physiologic

rationale for neutrophil's CXCR-1/2 mediated activity in sepsis, delivers insight into the overriding mechanisms involved, and suggests that interventions aiming to modulate phenotypic composition are time sensitive.

2.2 METHODS

2.2.1 Experimental data set protocol

After general anesthesia, instrumentation and a 30 minute stabilization period, sixteen baboons (*Papio ursinus*) weighing between 19 and 32 kg were infused with 2 x 10^9 CFU *Escherichia coli* per kg over a two-hour period as described previously [107]. Thereafter, antibiotic therapy was delivered (gentamycin 4mg/kg twice a day). Eight animals were placed in an acute study lasting 6 days, while another eight were placed in the chronic study intended to last 28 days. All animals were observed for a 4-hour period after bacteria infusion then 11, 23, 35, 47, 72 hour and 6 days after infusion. Pathogen counts in blood, IL-8, creatinine, white blood cell, neutrophil elastase / α1-PI complex, and other physiologic parameters and biomarkers were gathered at multiple time point. For animals in the chronic study an additional time point was collected at 28 days. At the end of the study period, the baboons were again anesthetized for measurements and thereafter sacrificed with an overdose of pentobarbital. This study was approved by the Institutional Animal Care and Use Committee at Biocon Research Institute and animals were treated according to NIH guidelines.

2.2.2 Model framework and description

A simplified mechanistic model of IL-8 mediated activation of CXCR-1/2 receptors and neutrophil response to a pathogen was developed based on available literature information and general knowledge of acute inflammatory response. Receptor level dynamics and systemic parameters were coupled with multiple neutrophil phenotypes to generate dynamic populations of activated neutrophils which reduce pathogen load, and/or primed neutrophils which cause adverse tissue damage when misdirected. Mathematical representation of the interactions detailed in Fig 1. were generated using ordinary differential equation (ODE) framework with the rate of interactions described by mass action kinetics or Hill type kinetics [108,109]. The interactions included in the model gives rise to 16 ODE state variables and 43 rate parameters.

In brief, the model is initiated by a pathogen load, which represents a bacterial inoculation. Presence of pathogen leads to continued growth as well as IL-8 and fMLP cytokine production. IL-8 is generated indirectly from pathogen generation from responding phagocytic mononuclear cells [110]. IL-8 initiates CXCR-1/2 activation in the receptor level, which in turn generates neutrophil phenotype change. Depending on phenotype, neutrophils may cause either pathogen elimination or misdirected tissue damage. A systemic damage indicator represents overall patient health. Increased systemic damage results in further IL-8 generation [111,112], resulting in a positive feedback loop. This simplified system captures the basic functionality of acute IL-8 mediated immune response to pathogen and is capable providing valuable feedback on potential therapeutic treatments modulating these mechanisms. A more detailed description of model equations follows.

Pathogen: Equation (1) describes the population of foreign pathogen. Base pathogen growth rate increases linearly with pathogen until approaching a carrying capacity at elevated pathogen loads. In addition to basal pathogen death, the Neutrophil kill/migrate phenotype is capable of decreasing pathogen population through diapedesis, followed by targeted phagocytosis [102,113,114].

Equation 1

$$\frac{dP}{dt} = k_{PG}P - k_{P-N_{K/M}}N_{K/M}P - \frac{k_p P}{k_p^d + P} - k_{pL}P^2$$

Ligands: Interleukin-8 (IL-8) and fMLP:

In the model, neutrophils progress through multiple phenotypes which dictate neutrophil migratory, phagocytic, and antibiotic activity. The association of chemokine IL-8 with the surface CXCR-1/2 triggers the transition of basal neutrophils to functional phenotypes. Previously characterized receptor surface activation, internalization, and recycling rates of CXCR-1/2 are utilized to predict receptor levels and neutrophil phenotypes in response to systemic IL-8 stimulation [105,115]. IL-8 production rate is a function of elevated pathogen and tissue damage [116,117]. Both terms are represented as Hill Equations in Equation (2). While IL-8 is not directly linked to pathogen levels, this simplified representation captures IL-8 release from macrophages and endothelial cells in response to infection.

Equation 2

$$\frac{dC_{IL8}}{dt} = \frac{k_{IL8-P}P}{k_{IL8-P}^d + P} + \frac{k_{IL8-D}D^2}{k_{IL8-D}^d + D^2} - k_{IL8}C_{IL8}$$

Equation (3) characterizes a general pro-inflammatory pathway, which is independent of CXCR-1/2 activation has been added to represent alternate means of neutrophil induced pathogen activation. This generic pathway is not modeled using receptor level dynamics and directly transitions the N_{Basal} (N_B) population to $N_{Killing/Migratory}$ ($N_{K/M}$).The generic proinflammatory ligand growth is dictated by pathogen level.

Equation 3

$$\frac{dC_{fMLP}}{dt} = \frac{k_{fMLP}P}{k_{fMLP}^{d} + P} - k_{fMLP-D}C_{fMLP}$$

Neutrophil Surface Receptors CXCR-1 & CXCR-2:

Receptor level dynamics dictate neutrophils advancement into one of four phenotypes depending on CXCR-1/2 surface activation. Each receptor can occupy one of the three states, namely free surface receptor, surface receptor bound to IL-8 and internalized receptor bound to IL-8 [118]. Equation (4) and Equation (5) describe CXCR-1 surface and internalized populations, which have been non-dimensionalized to remove the free receptor state. Equivalent equations are present for CXCR-2. The active surface state was modeled as the dynamic condition which drives neutrophil population phenotype change [55]. This model makes the assumption that CXCR-1/2 receptors are conserved.

Equation 4

$$\frac{dC_{R1s}}{dt} = k_{f1}C_{IL8}\left(1 - C_{R1s} - C_{R1i}\right) - k_{r1}C_{R1s} - k_{i1}C_{R1s}$$

Equation 5

$$\frac{dC_{R1i}}{dt} = k_{i1}C_{R1s} - k_{i1'}C_{R1i}$$

Neutrophil Phenotype:

Equation (6) represents the resting state (N_B) represents basal neutrophils which have not been stimulated by IL-8 or other proinflammatory stimuli. These neutrophils are mobile in blood, but not capable of causing systemic damage or utilizing their anti-pathogen capacity without transitioning to another phenotype. All neutrophils begin in this basal state prior to activation and priming. Without stimulation, neutrophil growth and death rates are in equilibrium, however growth rate increases with the introduction of pathogen, which has been expressed through a filter equation to produce a physiologic time delay [102,119]. CXCR-1/2 surface complex levels dictate the transition rates of N_B to the $N_{Migratory}$ (N_M) or $N_{killing}$ (N_K) phenotypes. Additionally, there is a direct pathway to transition N_B to $N_{K/M}$. This mechanism represents a general proinflammatory process independent of CXCR-1/2 signaling. A filter equation was generated in Equation (7). This function fits the physiologic delay between pathogen generation and increased neutrophils entering circulation.

Equation 6

$$\frac{dN_B}{dt} = k_{NG}\left(1 + \frac{k_{N_B-G}F}{k^d_{N_B-G} + F}\right) - k_{N_{K-IL8}}N_B C_{R1s} - k_{N_{M-IL8}}N_B C_{R2s} - k_{N_B}N_B - k_{fMLP-N_B}N_B$$

Equation 7

$$\frac{dF}{dt} = k_{filter\_on}P - k_{filter\_off}F$$

Equation (8) contains neutrophils which have been activated via IL-8 mediated CXCR-2 stimulation.

Equation 8

$$\frac{dN_M}{dt} = k_{N_M - IL8}N_B C_{R2s} - k_{N_M - N_K - IL8}N_M C_{R1s} - k_{N_M}N_M$$

Equation (9) characterizes the killing phenotype (N_K), representing neutrophils which have been activated via IL-8 mediated CXCR-1 stimulation. N_K neutrophils are capable of untargeted cytotoxic activity, resulting in systemic organ damage. The CXCR-1/2 surface population dictates transition rates into phenotypes. Neutrophil elastase / α1-PI complex was utilized in the model to fit N_K neutrophil population. As shown in Equation (10) levels of neutrophil elastase / α1-PI complex equate to levels of circulating N_K phenotypes.

Equation 9

$$\frac{dN_K}{dt} = k_{N_K - IL8}N_B C_{R1s} - k_{N_K - N_M - IL8}N_K C_{R2s} - k_{N_K}N_K$$

Equation 10

$$\frac{dC_{elas}}{dt} = k_{NE}\frac{dN_K}{dt}$$

Both N_M and N_K phenotypes are capable of progressing to the $N_{K/M}$ phenotype through CXCR-1/2 surface receptor activation. This neutrophil state ($N_{K/M}$), shown in Equation (11), represents neutrophils which have been activated through both CXCR-1 and CXCR-2 and are capable of target pathogen removal, effectively fighting infection. The pathogen equation (Equation (1)) contains a term which dictates pathogen death in response to $N_{K/M}$ levels. Once activated through CXCR-1/2 neutrophils are not capable of returning to the basal N_B phenotype.

Equation 11

$$\frac{dN_{K/M}}{dt} = k_{N_K - N_M - IL8} N_K C_{R2s} + k_{N_M - N_K - IL8} N_M C_{R1s} - k_{N_{K/M}} N_{K/M} + k_{fMLP - N_B} N_B$$

Damage:

A systemic damage indicator (Equation (12)) was developed to represent overall animal health. Damage is increased by the population of N_K and decays gradually as tissue and organs recover. Creatinine, a biomarker for kidney function, was utilized in Equation (13) as an indicator for the damage term ensemble computation. Creatinine is maintained at a constant level in the absence of damage, but systemic levels increase with damage as body's ability to clear creatinine decreases [120].

Equation 12

$$\frac{dD}{dt} = k_{D-N_K} N_K \left(1 - D\right) - k_D D$$

Equation 13

$$\frac{dC_{creat}}{dt} = k_{creat-P} - k_{creat} \left(1 - D\right) C_{creat}$$

The model uses empirical time series of Pathogen (CFU), IL-8 (nM), creatinine (mM), White Blood Cell count (10^3 cells/μl), and neutrophil elastase / α1-PI complex (ng/ml) for computation of the ensemble. State variables and their initial conditions are listed in Table 1.

2.2.3 Parameter estimation

The model contains 38 parameters, 13 of which are fixed based on literature data (Table 1). Parameter values were inferred using a Bayesian parallel tempering approach [121,122], which utilizes traditional Markov Chain Monte Carlo (MCMC) methods to sample the Bayesian posterior distribution P(p|y), the probability of parameter set p given data y, given by the Bayes formula

$$P(\boldsymbol{p}\,|\,\boldsymbol{y}) = \frac{L(\boldsymbol{y}\,|\,\boldsymbol{p})\theta(\boldsymbol{p})}{\int L(Y\,|\,\boldsymbol{p})\theta(\boldsymbol{p})}$$

where L(**y**|**p**) is the likelihood of observing **y** for a model with parameters **p**, θ(**p**) is the prior distribution, and $\int L(Y\,|\,\boldsymbol{p})\theta(\boldsymbol{p})$ is the normalizing constant. Additional sampling efficiency is gained by running multiple parallel chains evolving at different temperatures. Higher temperature increases the likelihood of acceptance of proposed steps. This allows the high temperature chains to move more freely through the parameter space, avoiding getting stuck in local minima. This results in more efficient exploration of parameter space [123,124] a method we have applied extensively in parameter estimation of practically unidentifiable complex non-linear models [101,125,126]. This resulted in the creation of parameter ensembles, where each

parameter is represented by a posterior distribution, rather than a single value. Free parameters were fit separately to the survivor and non-survivor experimental data sets, resulting in two parameter ensembles representing surviving and non-surviving animals.

2.2.3.1 Bayesian priors Prior distributions were selected for each parameter. In each case uniform priors were used, with a suitably large range so as to encompass all reasonable parameter values. This was ideal due to the limited prior knowledge and phenomenological nature of many of the parameters. Tighter ranges were enforced on select parameters as required to avoid non-physiologic model behavior. All candidate parameter values were selected from these pre-defined priors.

2.2.3.2 Parameter set fitness Fitness (log likelihood) of candidate parameters sets was determined by the difference between model simulations and experimental data, as determined by the sum of squared residuals cost function,

$$Fitness = \sum_{i,j,k} w_{i,j,k} * \frac{\left(y_{i,j,k} - \hat{y}_{i,j,k}\right)^2}{2\sigma_{i,j,k}^{\ 2}}$$

Where $w_{i,j,k}$ is a weighting function, $y_{i,j,k}$ is the output for a simulation with a single set of parameters, $\hat{y}_{i,j,k}$ is the experimental mean, and $\sigma_{i,j,k}$ $\sigma_{i,j,k}$ is the experimental standard deviation at time point *i*, observable *j*, and data set *k*. No additional penalties or constraints were added to parameter selection. To ensure proper fitting of the pathogen observable a threshold was added to change all values below the experimental limit of detection (4.4 CFU) to 0.

2.2.3.3 Parallel tempering To efficiently sample the posterior distribution, six separate Markov chains were run, initiated with parameter values randomly selected from the supplied prior distributions which met a maximum energy criterion. Each chain was initiated with a temperature and step size parameter which controlled the chain's ability to fully explore the parameters space. Chains were allowed to swap from a higher temperature to a lower temperature every 25 steps to allow for local sampling of newly found local minima. Step size and temperature parameters dynamically changed every 6,250 and 2,500 steps respectively to attempt to reach an ideal step acceptance rate of 23% [127], and swap rates of 15%-30%. Once these targets were reached, the temperature schedule and step sizes were fixed. Parameter sets were saved every 25 steps. Full exploration of parameter space was confirmed by examining, for each parameter, the frequency histogram of its full marginal posterior distribution, confirming that it spanned the prior domain.

We measured convergence and chain stationarity using the Gelman-Rubin criteria [128,129]. All parameters had converged with a potential scale reduction factor (PSRF) < 1.1 following 200,000 (x25) MCMC steps. Another 100,000 steps were taken to build a posterior distribution for each parameter that would be used for all model analysis and simulation. This ensured that all samples from the burn-in time for each chain were discarded, and only samples from the correct stationary distribution were used. The ensemble of all parameter sets from the lowest chain comprised the computed ensemble (posterior distribution).

2.2.4 Selection of key parameters

In order to better capture the underlying biological differences between animals that survive and those that die following the same challenge we attempted to identify the most important

parameters in determining animal fate. After computing ensembles for survivors and non-survivors, we performed regularized logistic regression, forward conditional stepwise logistic regression, and backward conditional logistic regression to identify a subset of parameters that are most indicative of outcome. Predictors consisted of all estimated parameters of both ensembles, and the indicator variable was the source (survivor or non-survivor) of the ensemble. Parameters were selected that were considered significant by all three methods, leaving a set of seven key parameters.

2.2.5 Model fitting

A second round of model fitting was then performed. In this round, 18 of the 25 parameters were fit simultaneously to both data sets, resulting in identical parameter values in the two ensembles. The seven parameters identified as being significant were fit twice, once against the survivor data set and once against the non-survivor data set, resulting in different parameter values across the two ensembles. This resulted in a smaller and more focused difference between the final ensembles.

2.2.6 Global sensitivity analysis

Global Sensitivity analysis was done to determine the independent and correlated contributions of rate parameters on cumulative damage. Area under the damage curve was chosen as the system output. To reduce the computational cost of GSA, Random Sampling High Dimensional Model Representation (RS-HDMR) approach was used [130]. Here, a multivariate output function (eg. AUC_D) was approximately represented by weighted optimal expansion functions

(called as component functions). The expansion coefficients of these functions were determined by least-squares regression simultaneously from one set of Monte Carlo samples. In general, for input vector, $\bar{x} = [x_1, x_2, ..., x_n]$ of rate parameters, in an n–dimensional space, a multivariate output function, $f(\bar{x})$, is approximated by a sum of terms including the mean (f_0) and the component functions (g_l). Mathematically,

$$f(\bar{x}) = f_0 + \sum_{l=1}^{2^n-1} g_l$$

Here, the index l indicates all possible combinations of the input parameters. In practice, not all component functions are significant and an F-test can be used to determine which component function should be excluded from the expansion [131]. For our work, we evaluated the variance based Sobol' indices using these component functions. The workflow adopted here starts with generation of Monte Carlo samples of the rate parameters from the ensembles obtained by the parallel tempering approach. Since they come from the ensemble, information on the covariance between the parameter distributions for the population of survivors and non-survivors is retained. Next, a detailed procedure is followed which includes simultaneous construction of all the component functions, removal of non-significant component functions using an F-test ratio score, re-evaluation of component functions and finally evaluation of the Sobol' sensitivity indices. The first order Sobol' sensitivity indices which capture the influence of a single parameter (but averaged over the other parameters) are defined as:

$$S_l = \frac{Cov(f(\bar{x}), g_l(\bar{x}))}{\sigma^2}, \; l = 1, 2, 3, ..., n$$

Here, σ^2 is the total variance in the output and $Cov(\bullet)$ is the covariance between the output function and each of the first order component functions. For clarity, the component function, g_l, is written as a function of $\bar{x}$ but in reality it is only a function of the input parameter for which it is defined (for example, x_l) and not the entire vector. Further, this sensitivity index is a sum of two terms that capture independent (S_l^a) and correlated contributions (S_l^b) of the input, which are defined as:

$$S_l^a = \frac{\langle g_l(\bar{x}), g_l(\bar{x}) \rangle}{\sigma^2}$$

and

$$S_l^b = \frac{\sum_{\substack{k=1 \\ k \neq l}}^{n} \langle g_l(\bar{x}), g_k(\bar{x}) \rangle}{\sigma^2}.$$

The inner products, $\langle \bullet \rangle$, are defined as:

$$\langle g_k(\bar{x}), g_l(\bar{x}) \rangle = \int_{x_1} \dots \int_{x_n} w(\bar{x}) g_k(\bar{x}) g_l(\bar{x}) dx_1 \dots dx_n$$

and $w(\bar{x})$ is the probability density function of the inputs informed by the parameter ensembles. Similar equations can be written for the higher order component functions and sensitivity indices. Further details on the evaluation of the component function for various types of models are given in [130,132,133]. To determine the importance of a given parameter, it is necessary to

combine all the important sensitivity indices (all orders) into a total sensitivity index, which for a parameter i can be defined as:

$$S_{T_i} = S_i + \sum_{\substack{j=1 \\ j \neq i}}^{n} S_{ij} + \sum_{\substack{j<k=1 \\ j,k \neq i}}^{n} S_{ijk} + \ldots\ldots$$

For most systems, very high order interactions are negligible and therefore, indices until the third order are sufficient, with most systems requiring only until the second order terms [130]. In this work, we constructed a third order RS-HDMR. All GSA computations were performed using the ExploreHD software (Aerodyne Research Inc., MA, USA).

2.2.7 Treatment framework

2.2.7.1 Treatment implementation After model fitting and analysis, a potential extracorporeal treatment was introduced (See Fig 7.). The extracorporeal treatment directly modulates CXCR-1/2 levels of circulating neutrophils, limiting passage of N_B to N_K and N_M. This mechanism of limiting CXCR-1/2 surface levels is modeled solely in the receptor level equations of the model. A heaviside function is used to turn treatment on and off at various treatment times. The k_{ft1} parameter represents treatment effectiveness, which combines device size, efficacy, efficiency and flow rate. Equation (14) is the modified CXCR-1 surface receptor equation which includes the Heaviside function. Equation (15) characterizes the trapped receptor state of CXCR-1. Similarly Equation (16) and Equation (17) are constructed for CXCR-2 and its associated trapped receptor state.

Equation 14

$$\frac{dC_{R1s}}{dt} = k_{f1}C_{IL8}\left(1 - C_{R1s} - C_{R1i} - C_{R1t}\right) - k_{r1}C_{R1s} - k_{i1}C_{R1s} + k_{ft1'}C_{R1t} - Heaviside\left(t, k_{treat-on}, k_{treat-off}\right)k_{ft1}\left(1 - C_{R1s} - C_{R1i} - C_{R1t}\right)$$

Equation 15

$$\frac{\mathrm{dC_{R1t}}}{\mathrm{dt}} = \mathrm{Heaviside}\left(\mathrm{t}, \mathrm{k_{treat-on}}, \mathrm{k_{treat-off}}\right)\mathrm{k_{ft1}}\left(1 - \mathrm{C_{R1s}} - \mathrm{C_{R1i}} - \mathrm{C_{R1t}}\right) - \mathrm{k_{ft1'}C_{R1t}}$$

Equation 16

$$\frac{dC_{R2s}}{dt} = k_{f2}C_{IL8}\left(1 - C_{R2s} - C_{R2i} - C_{R2t}\right) - k_{r2}C_{R2s} - k_{i2}C_{R2s} + k_{ft2'}C_{R2t} - Heaviside\left(t, k_{treat-on}, k_{treat-off}\right)k_{ft2}\left(1 - C_{R2s} - C_{R2i} - C_{R2t}\right)$$

Equation 17

$$\frac{\mathrm{dC_{R2t}}}{\mathrm{dt}} = \mathrm{Heaviside}\left(\mathrm{t}, \mathrm{k_{treat-on}}, \mathrm{k_{treat-off}}\right)\mathrm{k_{ft2}}\left(1 - \mathrm{C_{R2s}} - \mathrm{C_{R2i}} - \mathrm{C_{R2t}}\right) - \mathrm{k_{ft2'}C_{R2t}}$$

2.2.7.2 Classification of patient outcome In order to implement and evaluate treatment frameworks, simulated patient survivorship needed to be explicitly labeled. This was accomplished using a logistic regression classifier as specified by the machine learning software Weka [134]. The estimated parameter ensemble was partitioned into a training set and test set to

build the classifier, using 20% of the ensemble as training data. Two features were used for training, total accumulated damage measured by area under the curve of the damage time course for each patient, as well as the peak damage experienced by the patient. Training with these features resulted in a classifier that could label a patient as surviving or dying after being exposed to a specific infection and possible treatment.

2.3 RESULTS

2.3.1 Computation of parameter ensembles explaining survivor and non-survivor dynamics

Of the 16 baboons subjected to bacterial infusion, 11 (69%) died and 5 (31%) survived, with death occurring within 6 days of bacterial infusion. Based on these two systemic outcomes, a thorough investigation of the model (see Methods section & Fig 2) was completed to identify parameter regimes that explain the dynamics of each group of the responders.

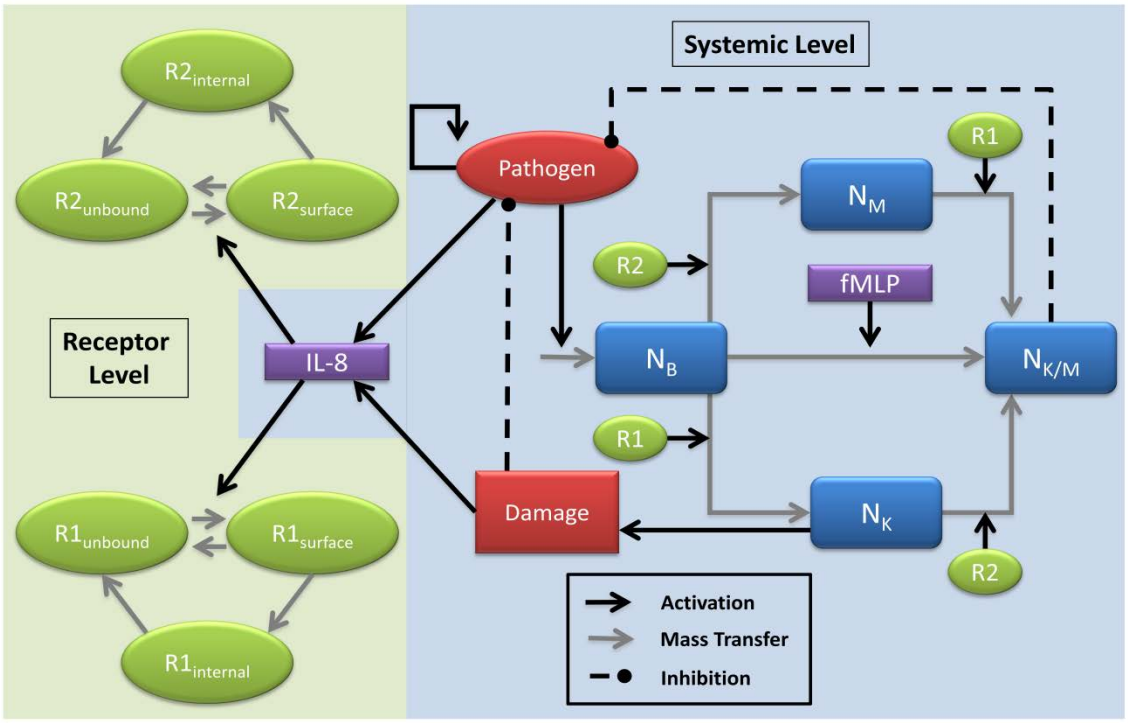

Figure 2 Model diagram detailing neutrophil phenotypes and critical feedback loops.

The system is divided into modules based on the level at which the interactions occur. The systemic level includes the interactions between the pathogen (P), four neutrophil phenotypes (basal: N_B, migratory: N_M, killing: N_K and killing and migratory: $N_{K/M}$) and chemokine IL-8. The receptor level interactions include the intracellular dynamics of CXCR-1/2, namely activation, internalization and recycling. Two types of feedback occur between the two levels, active surface receptors can trigger the phenotype conversion of the neutrophils and IL-8 produced at the systemic level triggers the trafficking of the receptors. A CXCR-1/2 independent activation via fMLP is included to model general pro-inflammatory response. The systemic damage (D) indicates the overall damage (direct and indirect) caused by the action of the killer neutrophils.

The initial conditions for the state variables of the ODE were fixed to simulate experimental stimulation (Table 1). Among the rate parameters, some were fixed to literature values. These included pathogen growth and decay rates, basal decay rates of naïve neutrophils,

CXCR-1/2 internalization and recycling rates and creatinine decay rate (See fixed parameters in Tables 2 and 3). Remaining parameters were estimated by generating parameter ensembles using a Bayesian parallel tempering approach that fit our model to the survivor and non-survivor experimental data sets (see Methods). We conducted the parameter estimation process in two rounds. In round one, the model was fitted to the two data sets separately. By fitting to the two data sets separately, we were able to effectively show that the model was capable of replicating both lethal and non-lethal outcomes through only a change in few parameters. In an attempt to classify the underlying differences, we identified the parameters that were most influential in determining the outcome (survivor or non-survivor) of an individual using stepwise logistic regression. This resulted in a list of seven key parameters. These parameters tend to control the rate at which neutrophils grow and how quickly they can change phenotypes, which play a critical role in determining how quickly and severely the animal will respond to the infection.

Table 1 Initial Conditions

No.	Symbol	Description	Initial Condition–Survivors	Initial Condition–Non-Survivors	Units
1	P	Pathogen	1000	1000	CFU
2	N_B	Basal neutrophils	4.4	5.06	10^3 cells/μl
3	N_K	Neutrophils with killer phenotype	0.0	0.0	10^3 cells/μl
4	N_M	Neutrophils with migratory phenotype	0.0	0.0	10^3 cells/μl
5	$N_{K/M}$	Neutrophils with dual phenotype	0.0	0.0	10^3 cells/μl
6	C_{IL8}	Systemic IL-8 concentration	0.0	0.0	nM
7	D	Global tissue damage	0.0	0.0	unitless
8	C_{R1s}	Surface CXCR1 population	0.0	0.0	unitless
9	C_{R1i}	Internalized CXCR1 population	0.0	0.0	unitless
10	C_{R2s}	Surface CXCR2 population	0.0	0.0	unitless
11	$C_{R\ 2i}$	Internalized CXCR2 population	0.0	0.0	unitless
12	C_{creat}	Creatinine	91.5455	102.4	nM
13	F	Filter term	0.0	0.0	unitless
14	C_{R1t}	CXCR1 trapped	0.0	0.0	unitless
15	C_{fMLP}	fMLP	0.0	0.0	nM
16	C_{elas}	Neutrophil elastase / α1-PI complex	0.0	0.0	ng/ml
17	WBC	Total white blood cells	4.4	5.06	10^3 cells/μl

doi:10.1371/journal.pcbi.1004314.t001

Table 2 Shared Parameter Values

No.	Symbol	Description	Fixed/Fitted	Mean	Std. Dev.	Units
1	k_{PG}	Pathogen growth	Fixed	1	0	$Hour^{-1}$
2	$k_{PG-N_{K/M}}$	Neutrophil induced pathogen death	Fitted	145.5391	0.040553	$(Hour *10^3 cells/\mu l)^{-1}$
3	k_{PL}	Pathogen population limit	Fitted	1.6533E-7	2.3409E-7	$(Hour*CFU)^{-2}$
4	k_P	Pathogen decay	Fitted	271.9904	352.4858	CFU/Hour
5	k_p^d	Pathogen decay	Fixed	1000	0	CFU
6	k_{N_B}	Basal neutrophil natural	Fixed	0.1	0	$Hour^{-1}$
7	k_{N_K}	Killer neutrophil decay	Fitted	0.0330	0.0275	$Hour^{-1}$
8	k_{N_M}	Migratory neutrophil decay	Fitted	0.1244	0.1936	$Hour^{-1}$
9	$k_{N_{K/M}}$	Migratory-Killer neutrophil decay	Fitted	0.1176	0.1772	$Hour^{-1}$
10	$k_{N_M-N_K-IL8}$	IL-8 induced migratory neutrophil to neutrophil migratory-killer transition	Fitted	168.7708	260.7247	$Hour^{-1}$
11	k_{IL8-P}	Pathogen induced IL-8 production	Fitted	2.7810E-6	2.0441E-6	$Hour^{-1}$
12	k_{IL8-D}	Tissue damage induced IL-8 production	Fitted	5.7938E-9	7.9615E-9	$nM*Hour^{-1}$
13	k_{IL8}	IL-8 decay	Fitted	0.3352	0.0261	$Hour^{-1}$
14	k_{D-N_K}	Tissue damage induced by killer neutrophils	Fitted	0.0319	0.0285	$(Hour *10^3 cells/\mu l)^{-1}$
15	k_D	Damage recovery rate	Fitted	7.0147	8.8870	$Hour^{-1}$
16	k_{filter_on}	Filter production rate	Fitted	6.1698E-4	8.2047E-4	$(CFU*Hour)^{-1}$
17	k_{r1}	Dissociation constant for R1 receptors	Fixed	79.2	0	$Hour^{-1}$
18	k_{r2}	Dissociation constant for R2 receptors	Fixed	79.2	0	$Hour^{-1}$
19	k_D	Affinity constant for IL-8 to the receptors	Fixed	2.5E-3	0	$Hour^{-1}$
20	k_{i1}	Internalization rate for IL-8-R1 complex	Fixed	5.196	0	$Hour^{-1}$
21	$k_{i1'}$	Recycle rate for R1	Fixed	0.612	0	$Hour^{-1}$
22	k_{i2}	Internalization rate for IL-8-R2 complex	Fixed	20.796	0	$Hour^{-1}$
23	$k_{i2'}$	Recycle rate for R2	Fixed	0.144	0	$Hour^{-1}$
24	k_{fMLP}	Pathogen induced fMLP production	Fitted	5.9866E-7	1.3864E-6	$nM*Hour^{-1}$
25	k_{fMLP}^d	Pathogen induced fMLP production	Fitted	622.9280	1.6952E3	CFU
26	k_{fMLP-D}	Pathogen induced fMLP decay	Fitted	9.8425E4	1.7303E5	$Hour^{-1}$
27	k_{fMLP-N_B}	fMLP induced basal neutrophil to migratory-killer phenotype transition	Fitted	0.0021	0.0025	$Hour^{-1}$
28	k_{ne}	Scaling of Nk cells to neutrophil elastase / α1-PI complex levels	Fitted	0.0351	0.0209	ng/cell

doi:10.1371/journal.pcbi.1004314.t002

Table 3 Unique Parameter Vales

No.	Symbol	Description	Fixed/ Fitted	Mean—Survivor	Std. Dev.–Survivor	Mean–Non-survivor	Std. Dev.–Non-survivor	Units
1	k_{NG}	Neutrophil baseline growth rate, based on 12 h life	Fixed	0.506	0	0.54417	0	10^3 cells/ (μl *Hour)
2	k_{creat}	Creatinine decay rate	Fixed	0.1591	0	0.1792	0	$Hour^{-1}$
3	k_{N_B-G}	Pathogen influenced neutrophil growth	Fitted	6.6447E5	1.5092E6	6.4953E5	1.0063E6	unitless
4	$k_{N_B-G}^d$	Pathogen influenced neutrophil growth (denominator)	Fitted	8.8322E4	1.7149E5	5.5590E4	9.0741E4	unitless
5	k_{N_K-IL8}	IL-8 induced neutrophil basal to killer phenotype transition	Fitted	8.9617E3	4.9596E3	4.5302E4	2.6386E4	$Hour^{-1}$
6	k_{N_M-IL8}	IL-8 induced neutrophil basal to migratory phenotype transition	Fitted	4.8740E3	6.5289E3	2.9804E3	6.6655E3	$Hour^{-1}$
7	$k_{N_K-N_M-IL8}$	IL-8 induced killer neutrophil to neutrophil migratory-killer transition	Fitted	3.9436	12.6137	5.9631	16.7691	$Hour^{-1}$
8	k_{IL8-P}^d	Pathogen induced IL-8 production	Fitted	1.2814E4	1.2646E4	1.2841E4	1.4198E4	CFU
9	k_{filter_off}	Filter decay rate	Fitted	0.0813	0.0145	0.1407	0.0328	$Hour^{-1}$

doi:10.1371/journal.pcbi.1004314.t003

Once these differentiating parameters were identified, we put the model through a second round of estimation. In the second round, the model was fit to both data sets simultaneously; allowing only the seven previously identified key parameters to vary between the survivor and non-survivor subpopulations (see Table 3). Additionally, two fixed parameters were allowed to take different values across the two populations to maintain the appropriate initial conditions in creatinine and white blood cell count. This step resulted in two new parameter ensembles that were identical in 28 parameters but varied in nine parameters. This second step enabled us to better crystallize the differences between animals that survived and those that died. These ensembles are biologically more relevant as we expect the animals' immune responses to be highly similar, with small but important differences indicating susceptibility to a septic insult. Resulting full marginal distributions for each of the 7 parameters were statistically different across survivor and non-survivor populations (Fig 3). The final mean values and the standard deviation of all the estimated parameters are summarized in Tables 2 and 3.

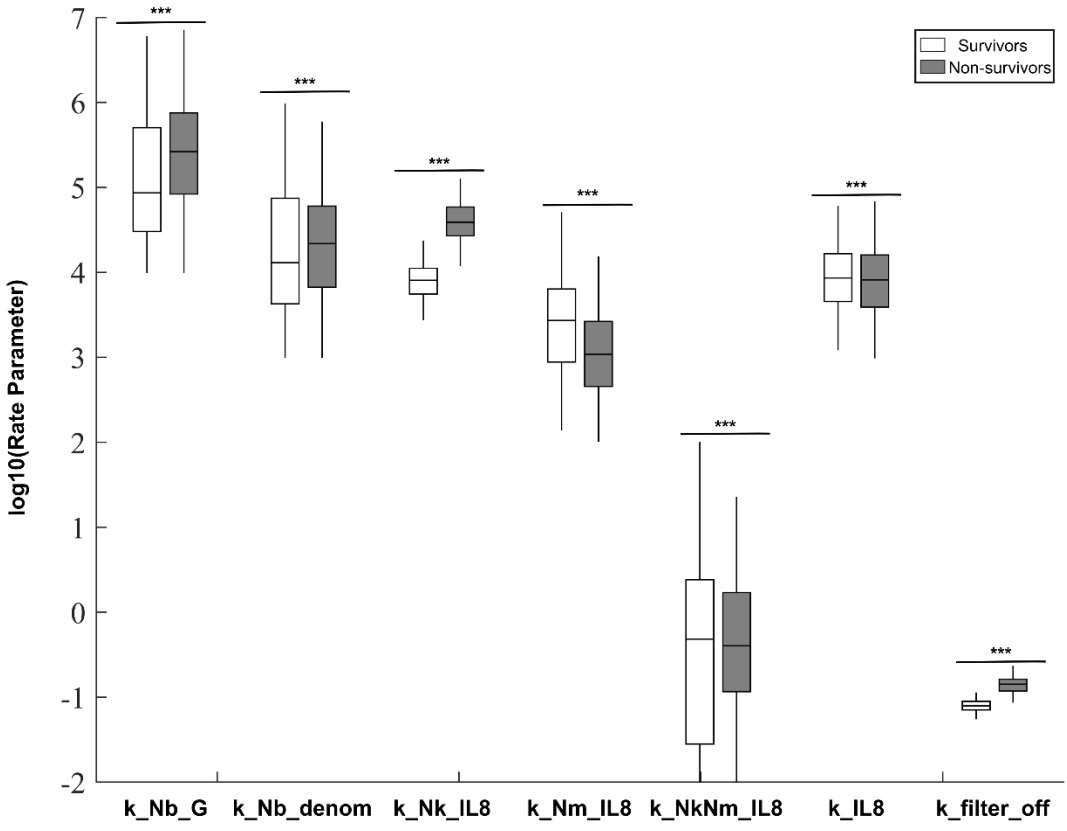

Figure 3 Posterior distributions of parameters allowed to vary across ensembles.

Each parameter was fit separately to data from surviving and non-surviving animals. Values for the mean, 25th-75th percentile, and 2.5th to 97.5th percentiles are shown. Parameters distributions were compared using a two-sample Kolmogorov-Smirnov test. *p<0.05, **p<0.01, ***p<0.001.

2.3.2 Features of survivor and non-survivor dynamics

2.3.2.1 Trained model outcomes The two ensembles resulted in model fits that faithfully recreate the key features of the surviving and non-surviving data sets (Fig 4). Pathogen dynamics showed a transient behavior, with the model predicting a slightly higher peak for non-survivors. The ensembles captured the transient peak in IL-8 that occurs early after infection,

with the non-surviving population exhibiting a higher maximum peak. The predicted neutrophil populations also tracked well with the experimental results, with circulating basal neutrophils exhibiting a strong initial decline in abundance as the cells are activated and migrate to the site of infection, followed by a growth phase as the body compensates for the infection, and finally a return to baseline levels. While both surviving and non-surviving populations exhibited this trend, the surviving populations had a noticeably higher peak in basal neutrophils during the growth phase. Levels of neutrophil elastase / α1-PI complex in the blood, indicative of the killing and damage causing function of activated neutrophils, peaks around 15 hours post-infection. The non-surviving population showed a stronger and longer lasting peak, which is captured by the model. Creatinine, a measure of kidney health, increased to higher and more sustained levels in non-surviving animals, as kidney health decreases and creatinine was not as efficiently cleared.

2.3.2.2 Model predictions The model also made predictions in the absence of observable data on the dynamics of neutrophil phenotypes (Fig 5 & Fig 6). Although both populations had similar peaks in fully activated neutrophils, allowing them both to fight off the infection on similar time scales as predicted experimentally, they showed strong differences in other populations. Non-survivors showed a significantly stronger spike in damage-causing killer neutrophils, while survivors showed a stronger spike in migratory neutrophils. This can also be seen in the parameter ensembles, as neutrophils in non-survivors had an increased proclivity to activate their killing function in response to IL-8, while neutrophils in survivors were faster to activate their

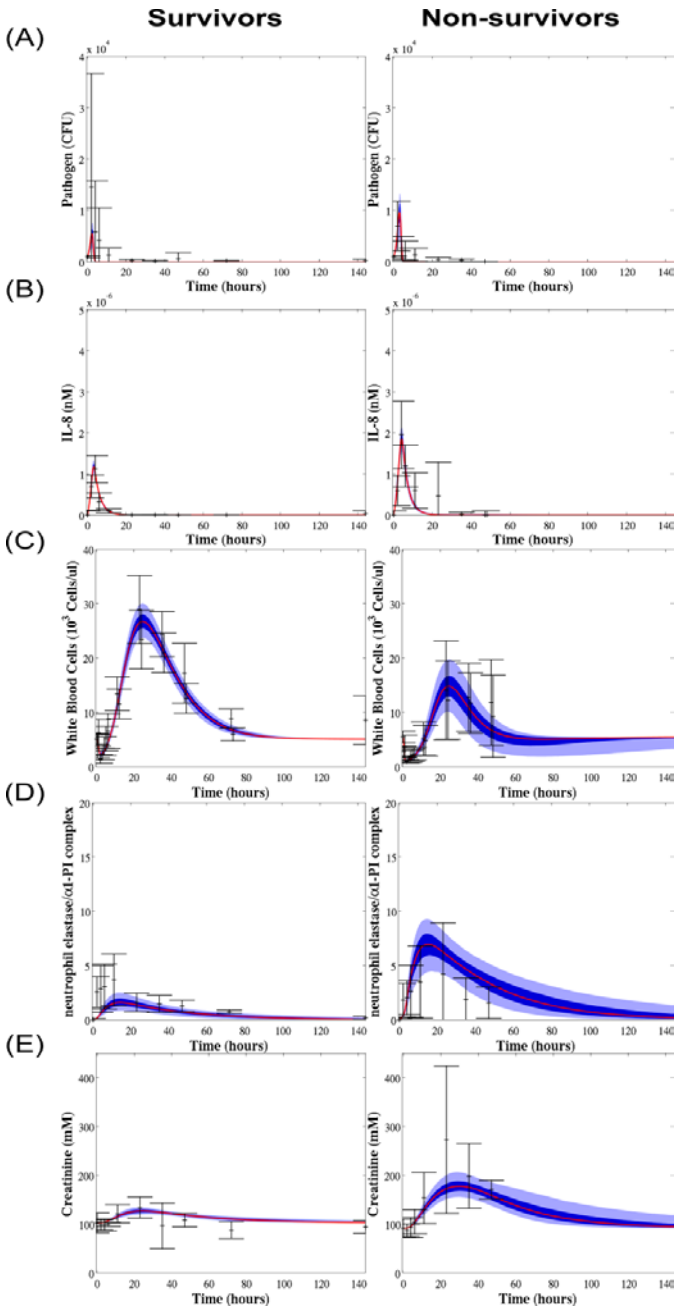

Figure 4 Simulated model fits with their experimental training data.

Mean (red), 25th-75th percentile (dark blue), and 5th-95th percentile trajectories of the simulated ensemble are shown. Experimental data points are shown in black with error bars representing one standard deviation above and below the mean. Results are shown for surviving (left) and non-surviving (right) animals for all observables with corresponding experimental data; (A) pathogen levels, (B) free IL-8 levels, (C) white blood cell counts, (D) neutrophil elastase / α1-PI complex levels, and (E) creatinine levels.

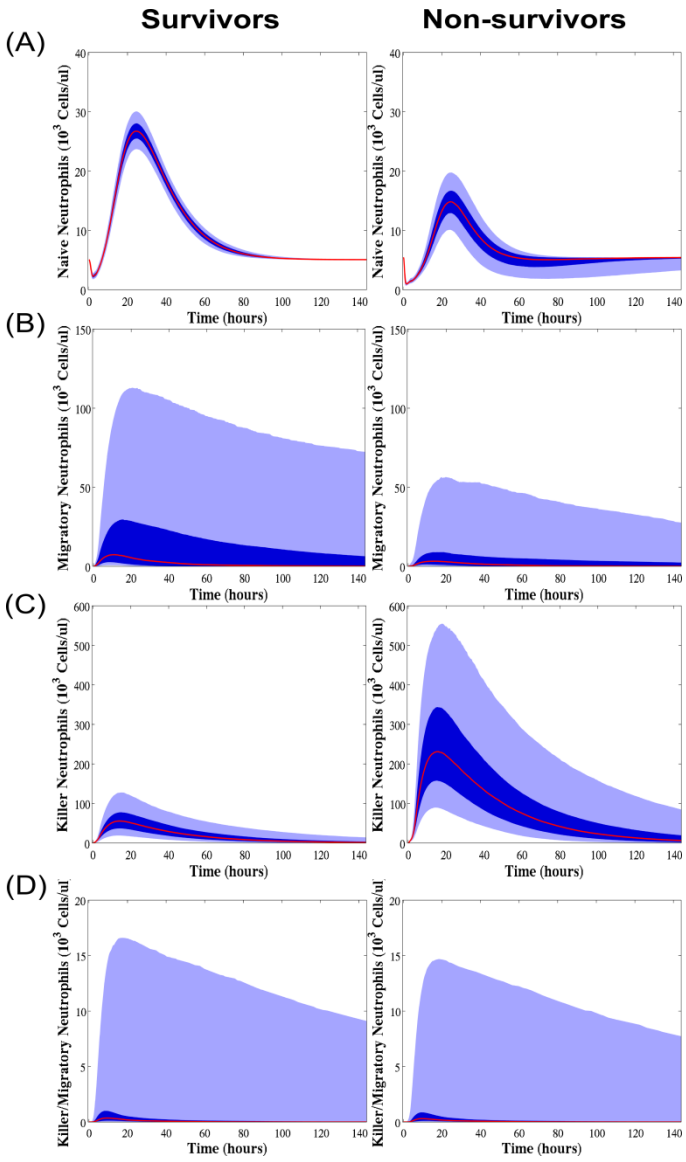

Figure 5 Model predictions for neutrophil phenotype dynamics following infection.

Mean (red), 25th-75th percentile (dark blue), and 5th-95th percentile trajectories of the simulated ensemble are shown. Predictions are shown for surviving (left) and non-surviving (right) animals for the four neutrophil phenotypes considered in the model; (A) basal neutrophils, which were calibrated with white blood cell count data, as well as (B) migratory neutrophils, (C) killer neutrophils, and (D) killer/migratory neutrophils for which there is no experimental data.

migratory functions (Fig 3). Generating similar numbers of fully activated neutrophils, but through differing intermediate activation populations, could be an explanation for how these two animal populations controlled infection with similar dynamics, while still experiencing differing fates.

At the receptor level, underlying activation of CXCR-1/2 was transient in both the survivors and non-survivors. Compared to the neutrophil dynamics which was slow and spread across few hours, receptor dynamics was very fast. Most of the receptors were in the free state, and internalized CXCR-1 is recycled faster than CXCR-2. Among the active receptors, there was one order of magnitude higher level of internalized CXCR-1 receptors than the surface bound CXCR-1 receptors, while this difference is two orders of magnitude for CXCR-2. Non-survivors had higher levels of the surface and internalized active receptors. This can be explained by the higher peak in IL-8 levels for the non-survivors than the survivors (Fig 3.). But, survivors had very close levels of CXCR-1 and -2 bound receptors and non-survivors had slightly higher levels of bound CXCR-1 than bound CXCR-2. These small differences in the peak levels of the receptors coupled with differences in the transition rates were sufficient to result in different neutrophil phenotype levels in the two populations, a key prediction from the ensemble modeling process.

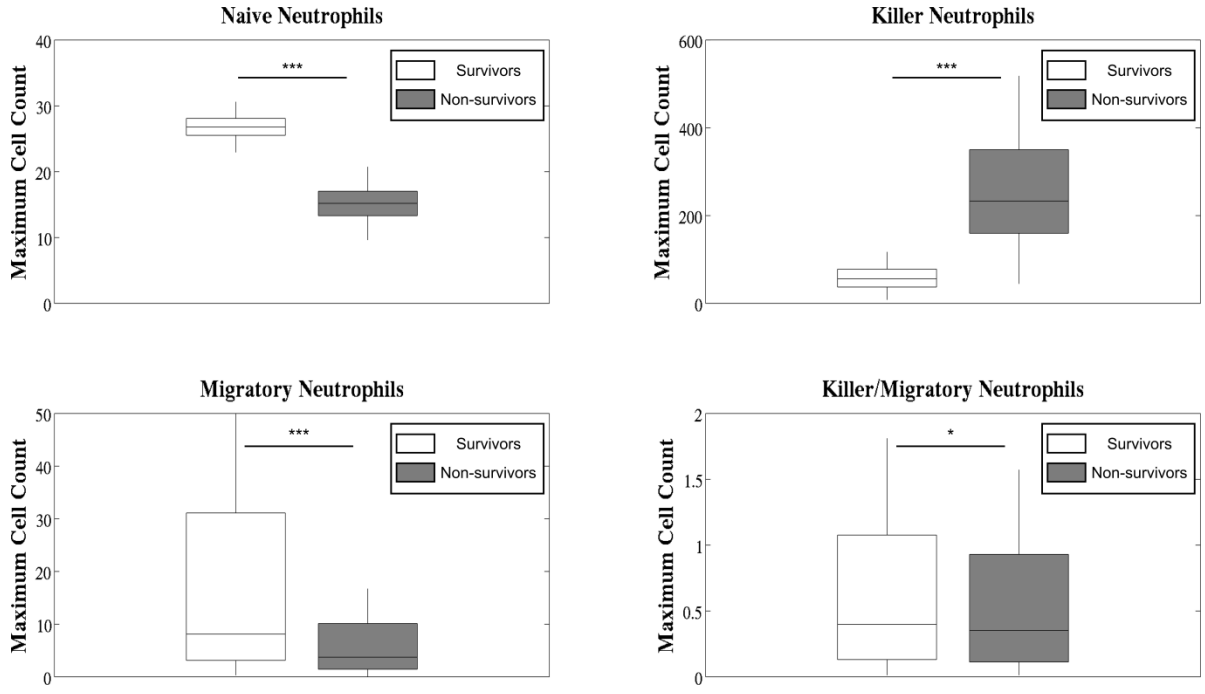

Figure 6 Model predictions for maximal levels of each neutrophil phenotype compared across ensembles.

Maximal values for each neutrophil phenotype from each trajectory in both ensembles were recorded. Values for the mean, 25th-75th percentile, and 2.5th to 97.5th percentiles are shown. Distributions were compared using a two sample T-test. *$p<0.05$, **$p<0.01$, ***$p<0.001$.

2.3.3 Factors modulating cumulative damage in the two populations

Until now, the focus was on deriving parametric ensembles explaining the mechanism of sepsis progression in each population. In this section, the sensitivity of sepsis-mediated damage to different model parameters (and hence different processes in the network) was evaluated for each population. Area under the damage curve (AUC_D) was used as an output metric of cumulative damage from sepsis. The analysis was done in two steps. First the sensitive parameters affecting damage in each population was identified to check if similar parameters were responsible for modulating damage within each population. Next, the two populations were combined to identify

the parameters primarily responsible a switch from a low to a high damage region. Since the model is highly nonlinear, a global sensitivity analysis (GSA) based on variance decomposition was chosen. This method decomposes the total variance in the output into variance and co-variance contributions from each rate parameter and its higher order combinations. To reduce computational cost, a meta-model based approximation was done (See Materials and Methods). The meta-model method called Random Sampling High Dimensional Model Representation (or RS-HDMR), decomposes the output function (AUC_D) into a set of component functions that includes the mean followed by first order effects of each parameter and other higher order effects resulting from parameter combinations. The degree of sensitivity of a parameter or its combination with other parameters (as a set) is captured by Sobol' index which by definition is the fraction of the total output variance attributed to the selected parameter set. To perform GSA, 4000 samples were generated from the parameter distributions of the two ensembles and the dynamics of the damage term was simulated for the survivors and the non-survivors. Fig. 7A shows the AUC_D distributions for each ensemble. As expected, the survivors show lower levels of cumulative damage than the non-survivors. The coefficient of variation was higher for the non-survivors (CV = 1.98) as compared to the survivors (CV = 0.32). When GSA was performed on the survivor and non-survivor samples separately and in combination, it was found that a third order RS-HDMR contributed close to 95% of the variance for both the populations. However, most of the important contributions were from the parameters constituting highly ranked first order indices.

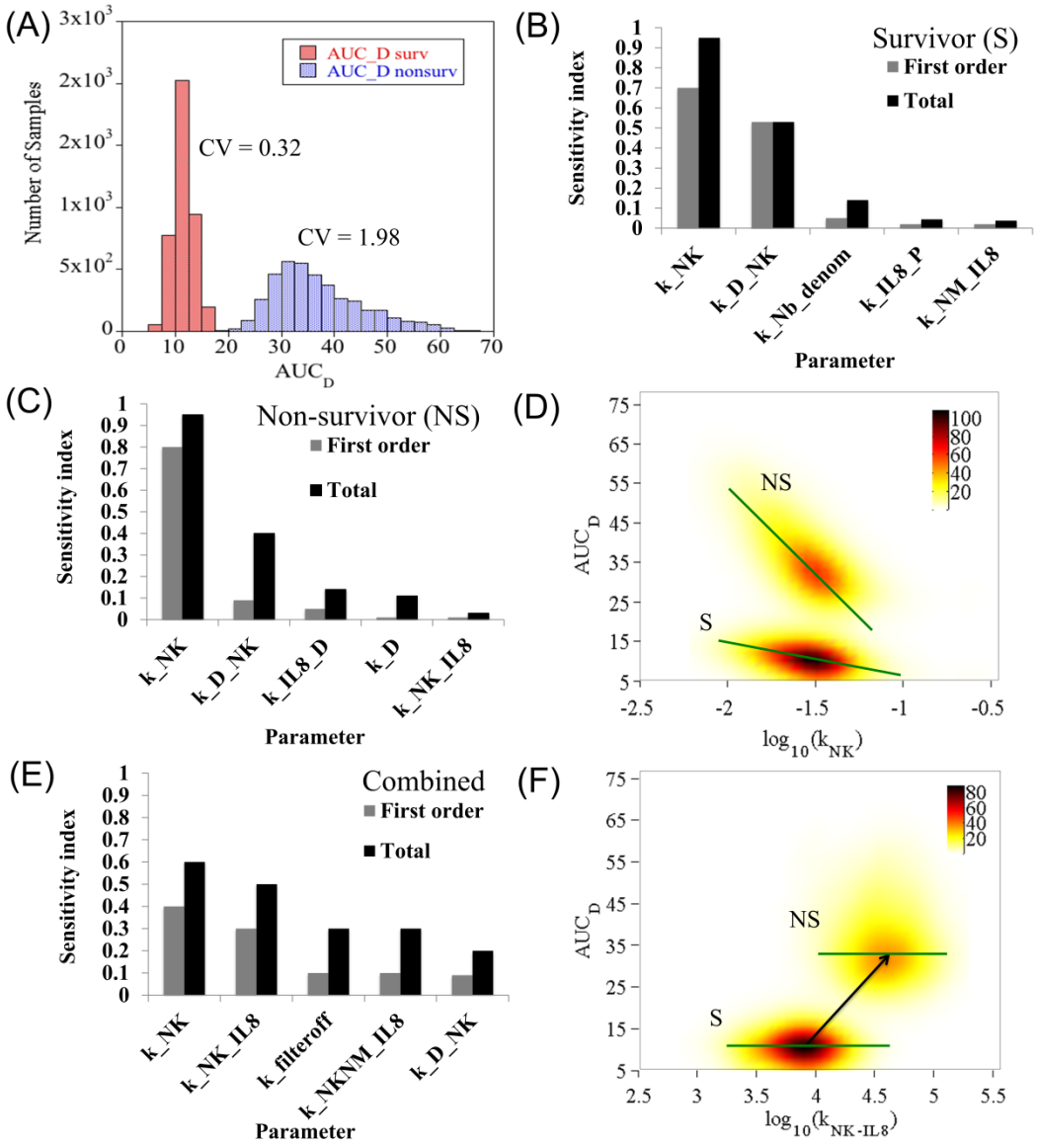

Figure 7 Factors affecting cumulative systemic damage.

(A) Cumulative damage seen in survivors and non-survivors. The histograms show the area under the damage curve until 144 hr. The rate parameters were sampled from the generated ensemble for each population. The distribution used for GSA contains 4000 samples for each population. (B-C) Prime drivers of cumulative damage. First order and total effect Sobol' indices which explained most of the variance are tabulated here for the survivor and non-survivor population respectively. (D) Functional dependence of AUCD on killer cell decay rate for the survivors (S) and non-survivors (NS). The green line has been added for visual guidance of the trend and is based on the mean trend identified by the RS-HDMR component functions. For each population, damage decreases with increase in the

decay rate of the killer neutrophil. (E) Prime drivers of cumulative damage for the combined population. (F) Functional dependence of AUCD on CXCR1 induced naïve to killer neutrophil transition rate for the survivors and non-survivors. The green line shows that within the population, damage is not particularly sensitive to the transition rate, but increased transition rate could be responsible for higher damage levels seen in non-surviving population.

For GSA conducted separately on the survivor and non-survivor ensembles, it is found that damage is mainly determined by the decay rate of the killer neutrophils, k_{N_K} (direction of influence shown in Fig 7D). The decay rate of the killer neutrophil controls the rate at which killer neutrophils are removed from the system, and the faster these neutrophils are removed, the lesser the damage. The next important term is the direct damaging effect of the killer neutrophils and this parameter has significant second order interactions with other parameters of the model as seen from the total sensitivity index. The next set of parameters has secondary importance and these parameters are different for the two populations (variance contributions of each parameter in this set is in the range, 1-10%). In survivors, damage is more influenced by the production rate of basal neutrophils and IL-8 in presence of the pathogen. In non-survivors, the effect is more pronounced for damage mediated IL-8 production (a positive feedback component), damage recovery term and killer neutrophil production rate. This indicates that overall damage in non-survivors is more sensitive to the parameters associated with killer cells, IL-8 and damage.

For GSA conducted on the combined population, the decay rate of killer neutrophils remains the most important parameter. Interestingly, the sensitivity value and ranking of three parameters increase relative to the case where the populations are analyzed separately. Among these, the transition rate of naïve neutrophils to the killer phenotype via CXCR1 (k_{N_K-IL8}) is the most important parameter. The next two parameters include the decay rate in filter equation (7) (which determines the delay between pathogen generation and resulting neutrophil entry into

circulation during sepsis) followed by the parameter controlling transition rate of killer neutrophil to the dual phenotype by CXCR2. Functional dependence of damage on these three parameters shows that they could be responsible for shift in the population from a low to a high damage region. For example, Fig 7F shows the dependence of AUC_D on parameter k_{N_K-IL8}. Within each population, no particular trend is visible, but relative increase in the transition rate in the non-survivors correlates well with increased damage. Results in Fig 2 showed that the ranges of two of the parameters, k_{N_K-IL8} and k_{filter_off} were significantly different for the survivors and non-survivors. Results from sensitivity analysis support this prediction and further show that the parameter values correlate well with the transition in observed damage.

2.3.4 Treatment implementation

Extracorporeal devices are emerging as promising therapies for treatment of sepsis[135–138]. In this instance we propose extracorporeal treatment which directly modulates CXCR-1/2 levels using a bioactive surface which interacts with unbound neutrophil surface receptors upon contact. Such a device, which is currently under development at the University of Pittsburgh, generates targeted and controlled downregulation of neutrophil surface receptors. The dynamics of this device can be analyzed within the framework of the generated computational model to determine its proof of principle *in silico* and help optimize treatment parameters. The proposed treatment implementation is shown in Fig 8. Specifically, the receptors are allowed to go to a trapped state and become unavailable for activation by IL-8 for the indicated time of treatment. To evaluate the potential of such an immunomodulatory treatment, we next performed an *in*

silico trial by varying (1) the time when the treatment is introduced and removed and (2) the strength of interaction between the trapping device and the unbound neutrophil surface receptors.

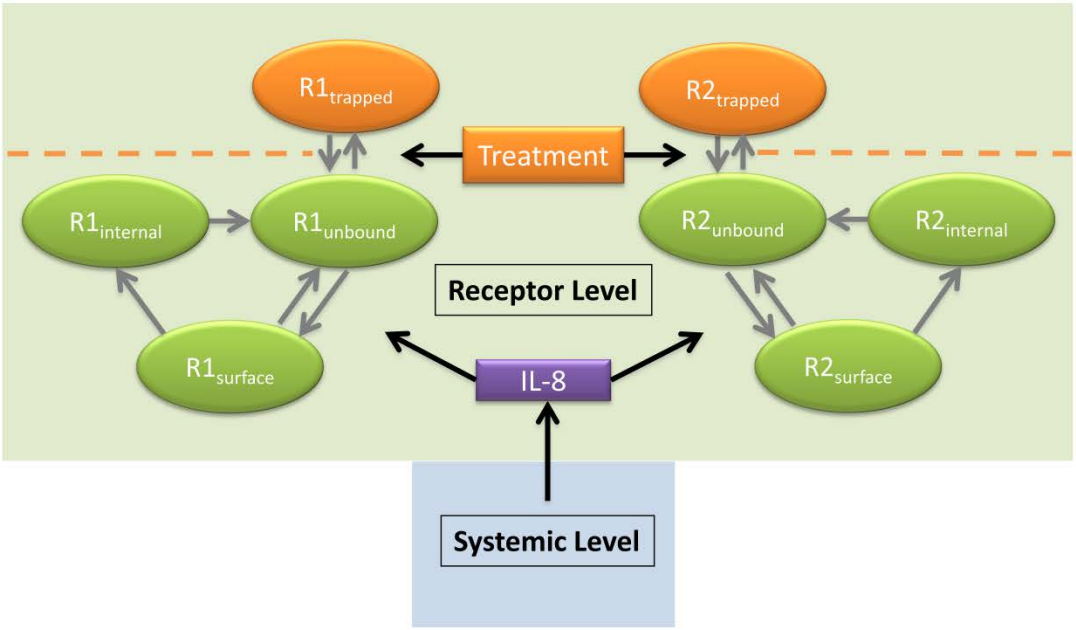

Figure 8 Model diagram showing receptor level treatment implementation.

The extracorporeal treatment introduces a trapped receptor state for CXCR-1/2. This state prevents IL-8 induced phenotype transition, which limits NK generation. The treatment is modeled entirely in the receptor level of model, leaving the systemic level (see Fig 1) unchanged.

2.3.4.1 Impact of treatment parameters For the analysis, the treatment initiation time was varied between 0 and 12 hours after the initial infection and the treatment discontinuation time was varied between 0 and 100 hours after infection. To modulate the treatment intensity, the device-receptor K_d was varied between the $1x10^{-2}$ M and $1x10^{-5}$ M, with 2.5e-3 M representing

the K_d of IL-8 and the receptors. The treatment was tested on a simulated population constructed by randomly selecting 69% of parameter sets from the non-survivor ensemble and 31% of parameter sets from the survivor ensemble, as observed in the experimental population. Survivor rate was measured for each set of proposed treatment parameters, as determined by the logistic regression classifier trained on the parameter ensembles with no treatment. A survivor rate above 31% was considered an improvement over baseline, and below 31% indicated the treatment causing overall harm.

Fig 9 shows the survival rate following different treatment strengths and start-end times. In general, the optimal time for beginning treatment was between 3 and 6 hours after the original infection, resulting 40-80% survival rates depending on treatment strength. Starting the treatment after six hours was typically too late to have a strong effect on survival. Starting treatment within 3 hours of infection would often have neutral or deleterious effects, as it would dampen the initial inflammatory response that is critical to fighting off the infection. This led to an increase in pathogen growth and an increased late inflammatory response once treatment was removed. In the worst case scenarios following early treatment of a short duration, survival rates dipped as low as 13.2%, and this trend could be seen across all treatment strengths.

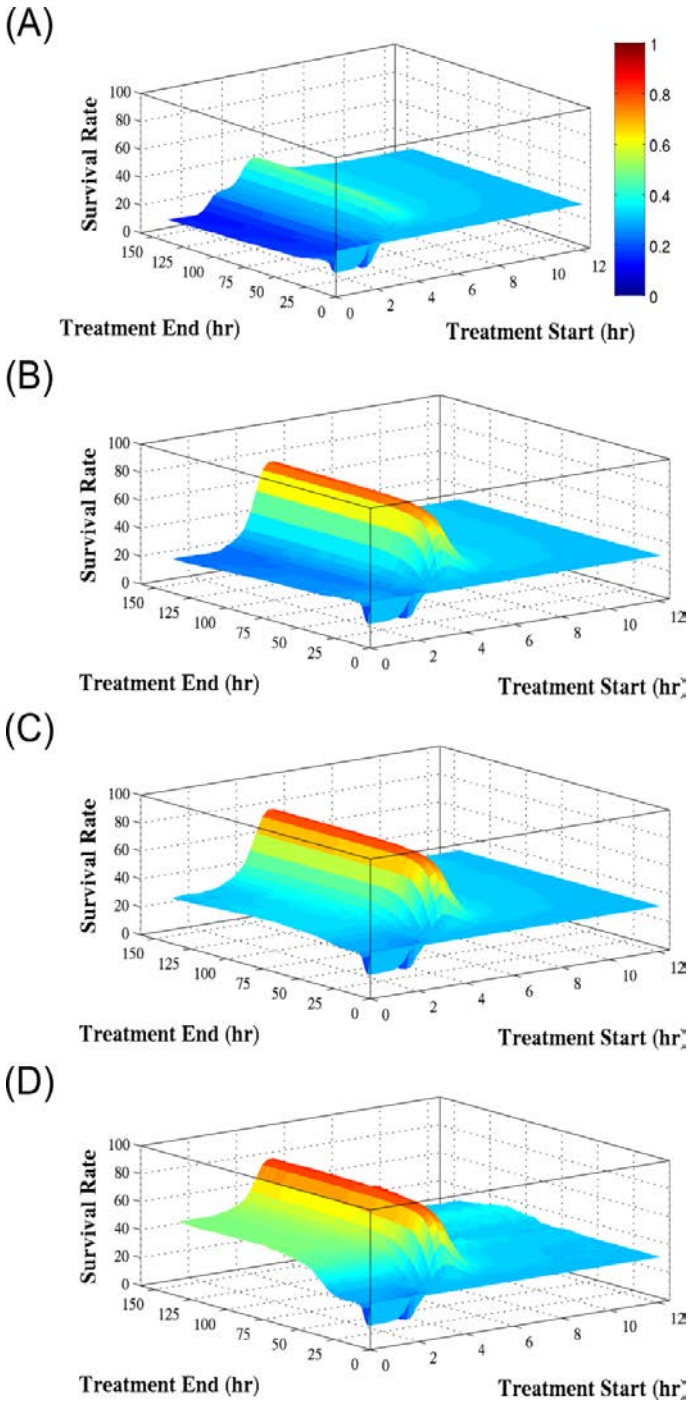

Figure 9 Effects of simulated treatment on animal survival rates.

Survival rates of a simulated population of animals following treatment with the proposed extracorporeal device considering a device-receptor affinity of (A) 1x10-2 M, (B) 1x10-3 M, (C) 1x10-4 M, (D) 1x10-5 M. In all cases the time of treatment was varied between 0 and 12 hours post infection and ended between 0 and 100 hours post infection.

When treated at the optimal time, survival rates increased from the 31% baseline to greater than 80% with sufficient device-receptor affinity. Using a K_d of 1e-2 M results in a maximum survival rate of 47%, and decreasing the K_d to 1e-3 M further increases this rate to 80.3%. Further decreases in the K_d to 1e-4 M and 1e-5 M results in increases in survival rate to 83.1% and 84.4%, showing there is a diminishing return to continuously increasing the device affinity. As the affinity increases, we see a new trend emerge in the simulation results, where treatment that begins as early as the onset of infection and is significantly long lasting leads to increased survival rates, and a less strictly defined optimal treatment time (Fig 9(D)). In this case, the treatment is so strong and long-lasting that the inflammatory response is very strongly suppressed, implying that overwhelming pathogen growth leading to death cannot be reached within the bounds of this. However, this suppression of the immune system allows for significant pathogen growth and could leave the subject vulnerable to secondary infections which are not considered in this model.

Trends in response to treatment also appear to be robust to individual parameter values. The two most sensitive parameters k_{N_K} and k_{N_K-IL8} were varied, increasing and decreasing each by 10% and 50% and recalculated the simulated population response to treatment. In general response trends remained the same, with a defined peak in survivorship when treatment is administered 2-4 hours after infection. The magnitude of responses varied predictably, as strongly increasing k_{N_K}, the death rate of damage-causing neutrophils, resulted in a higher peak of survival. Conversely, increasing k_{N_K-IL8}, which corresponds to a faster induction of damaging-causing cells, leads to a slight decrease in survivorship. Varying k_{N_K} had a larger

effect on these results, as expected following its identification as the model's most sensitive parameter affecting damage (Fig 7).

2.4 DISCUSSION

This chapter discusses the development of a mechanistic computational model of IL-8 mediated activation of CXCR-1/2 receptors in baboons which were administered intravenous *E. coli*. Neutrophil phenotypes, which dictate neutrophil functional response, were generated *in silico* based on CXCR-1/2 surface receptor levels, linking receptor level dynamics with neutrophil functional response. Parameter ensembles were generated for survivor and non-survivor populations, allowing for *in silico* observation of sepsis progression. Additionally, an extracorporeal treatment which modulates CXCR-1/2 levels on neutrophils was introduced *in silico*. This proof of concept evaluation allowed for preliminary device evaluation and optimization of treatment parameters.

To our knowledge, this is the first model describing dynamic interactions of neutrophils which specifically takes into account information sharing between the systemic variables and the receptor levels. The receptor level dynamics of the model function on a rapid time scale, adjusting to systemic IL-8 levels in a matter of minutes. These changes in receptor signaling dictate changes in neutrophil phenotype, which dictates neutrophil function and hence mortality. This link thus provides a valuable mechanistic framework that can be subjected to clinically relevant treatment scenarios. For example, the experimental treatment could be implemented purely on the receptor level. Alternatively, systemic variables such as IL-8 levels or neutrophil

phenotype could be modulated to evaluate performance of hemoadsorption or neutrophil sequestration extracorporeal devices.

Application of parallel tempering approach for parameter estimation allowed for the efficient generation of ensembles of parameters and resulted in a model that could fit experimental data well [124], allowing reasonably accurate simulations of the system without making strong claims about the values of single parameters which are notoriously difficult to measure and are likely to vary between individuals. This allows for robust, population-level predictions rather than point predictions of model parameters and model behavior. However, the computed multi-dimensional posterior distribution in parameter space reflects constraints imposed by empirical data, as well as data sparsity and uncertainty. These constraints impose a covariance structure in the posterior distribution such that there is robustness in model behavior, despite large uncertainties in individual parameter values. Learning this structure is likely crucial in building predictive model [139,140]. Yet, the method is making no claim that individual parameter sets in the ensemble represent individuals in a population. At best, an individual could be represented by a smaller ensemble, reflecting uncertainty relating to this particular individual. Yet, it is fair to say that the ensemble is meant to represent uncertainly about a population of individuals, so that simulating the ensemble will provide expected behaviors across a population of individuals, as long as such behaviors are compatible with the empirical data used to generate the ensemble.

One trend that arose in the estimated parameter ensembles was a large difference in the magnitudes of different rate constants, sometimes spanning many orders of magnitude. This is not surprising, due to the inclusion of biological events spanning many time scales, ranging from fast molecular events to cell phenotype transitions and finally to the full duration of infections

lasting for days. This suggests that future iterations of the model would benefit from a multiscale approach optimized towards handling these different time scales. Previous efforts [141–143] have worked out approaches that allow for efficient deterministic simulation of fast-scale molecular events, combined with more accurate stochastic simulation of slow-scale or rare events, and such techniques have resulted in impressive results [144,145].

Sensitivity analysis on the parametric ensembles enabled identification of the relative importance of the model parameters to state variables of the model. In general, sensitivity analysis is an important step in systems biology workflows and provides valuable information on model characteristics [146,147]. Most models in the literature resort to a local analysis which is sufficient if the parameters are well defined. For nonlinear dynamic models based on sparse experimental data and for systems which have inherently high parametric uncertainty, a global analysis needs to be done. Global techniques perform combinatorial perturbations of the parameters utilizing samples from the high-dimensional space. Application of meta-modeling approximations via RS-HDMR as was done in this work can significantly reduce the computational cost of sampling requirements for global methods. Additionally, if the sampling process takes into account parameter covariance computed from an ensemble model, biologically relevant sensitivity indices can be obtained. The systematic integration of ensemble modeling and global sensitivity analysis in this work allowed for identification of the parameters that control biological outcomes like sepsis induced tissue damage.

In addition to parameter fits, the behavior of the non-fitted state variables were inspected to check for features relevant to a clinical prognosis. Sepsis progression was analyzed by comparing differences between survivor and non-survivor populations. Neutrophil phenotypes in particular give insight into the differences between survivors and non-survivors. Of importance

is the killer neutrophil population, which is highly elevated in the non-survivor population (see Fig 5 & 6). This neutrophil phenotype is associated with neutrophil induced tissue damage in the model. With support from sensitivity analysis, killer neutrophil decay rate, which sets the levels and dynamics of N_K, was found to be the most important contributor to total damage in both the populations. Multiple studies support this finding, indicating that non-survivors or those with more severe sepsis experience increased levels of neutrophil induced tissue damage and MPO generation [102,148–151] . Furthermore, the importance of this term is supported by studies on neutrophil apoptosis and lifespan. Research by Taneja [152] and Fialkow [153] determined that neutrophil apoptosis was reduced in cases of severe sepsis, leading to increased lifespan of primed and activated neutrophils. Damage caused by these neutrophils was partially responsible for the progression of sepsis in these severe cases. Upon completion of the combined GSA, $k_{N_K-IL8}$was also found to be a significant contributor to total damage. Increase of this term leads to preferential generation of the N_K neutrophil phenotype, which directly contributes to tissue damage.

On the other hand neutrophils in the migratory phenotype were similar in survivor and non-survivor populations. These findings agree with the data from Cummings *et al* [150] which found neutrophil's harvested from septic and non-septic patients migrated to IL-8 at similar levels. Interestingly, survivors and non-survivors had similar levels of neutrophil kill/migrate phenotype, indicating that both ensembles had adequate neutrophil populations to eliminate the source pathogen. Therefore, the additional damage in non-survivors was neutrophil induced resulting from elevated neutrophil killer phenotype levels. The IL-8 mediated killing functions of neutrophils are primarily triggered through CXCR-1 rather than CXCR-2. Modulation of CXCR-

1 levels in particular may reduce the killing neutrophil phenotype and reduce neutrophil induced organ damage.

A number of experimental treatments for sepsis and other acute inflammatory diseases have targeted the CXCR-1 receptor with success in animal models [154–156]. However, translation to humans has been difficult for two main reasons [12]. First are inherent species dependent differences between human and animal immune systems that must be recognized and accounted for in pre-clinical studies. Second is the misuse of animal models and misinterpretation of pre-clinical data [157]. The recent debate on the translational fidelity of critical disease mouse models is a prime example where two separate comparisons of the human versus mouse genomic leukocyte responses using the same database resulted in two contradictory conclusions [158,159]. In the case of IL-8 signaling, which is not present in murine models, homologous cytokines and their associated surface receptors must be examined in IL-8's place [160]. In this context, in silico modeling is an attractive alternative given that it allows preliminary evaluation of experimental human treatments at minimal costs.

Multiple extracorporeal sepsis treatments are currently under investigation with promising results. Blood purification techniques such as hemoadsorption [135,136,161–163] allow for cytokines and other detrimental proteins to be removed directly from the blood during the cytokine storm, curbing the patient's immune response. Another approach called activated neutrophil sequestration [138,164], selectively removes harmful neutrophil phenotypes from circulation. In this instance we propose extracorporeal treatment which directly modulates CXCR-1/2 levels using a bioactive surface which interacts with unbound neutrophil surface receptors upon contact, resulting in CXCR-1/2 downregulation. This approach is advantageous because no components of blood are removed from circulation, allowing for a healthy immune

response after appropriate modulation of neutrophil surface receptors. In addition, all necessary cell-cell interactions are allowed to occur within well-controlled microcirculation of the device. Such a setup also allows treatment to be easily titrated or halted by adjusting blood flow through the device. The dynamics of such a device were analyzed within the framework of the generated ensemble model to determine its proof of principle *in silico* and to evaluate its benefits in rescuing individuals marked as non-survivors by the parameter ensembles.

When evaluated *in silico* the proposed extracorporeal CXCR-1/2 modulation device improved mortality from 31% to above 80% when deployed under certain ranges of conditions. This substantial improvement in survival supports the hypothesis that a CXCR-1/2 modulatory device may improve patient outcomes. However, time and length of treatment implementation are critical parameters tied to this success. The importance of quickly beginning sepsis treatment has been well established [165], particularly for antibiotic administration. Our simulations showed a well-defined optimal time for the initiation of treatment, between 3 and 6 hours after the onset of severe infection. Treatment, if started within this time frame, had a high degree of success over a large range of treatment durations and strengths. This window is specific to the animal model under study and will not directly translate to a clinical setting for two main reasons. First, the model was calibrated with experimental data obtained from baboons, and differences between the baboon and human immune systems must be considered. Second, the baboons were exposed to a well-controlled bacterial infusion at a known time point, followed by a predictably quick and strong immune response. In this instance the pathogen load is well controlled and a large portion of the ensemble can therefore be addressed by a single treatment setting. In clinical practice, patients present with varied pathogen loads and they may be in different stages of infection and immune response. So, future experiments will need to combine

clinical knowledge with additional data gathering and simulation to obtain treatment timing relevant for human patients.

Clinicians are actively searching for biomarkers to track sepsis disease progression and prescribe treatment [166–168]. Neutrophil phenotype may be a valuable indicator of disease state and individual patient response, but this information is difficult to collect in the clinic. Currently neutrophil phenotype can be evaluated either through functional testing or flow cytometry analysis of critical neutrophil surface receptors. In addition to CXCR-1/2 which are the focus of this model, CD11b, CD88, and CD62L all have roles in dictating neutrophil phenotype [169] and surface receptor expressions vary depending on severity of the inflammatory response. To more readily exploit phenotype data it may be possible to map neutrophil function to easily measurable biomarkers. Using these indirect measures of neutrophil phenotype can guide clinicians to ideal treatment regimens.

In conclusion, the ensemble model presented in this report provided key insights into the progression and mechanisms involved in progression of sepsis. We underline the role of relative abundance of killer, migratory and dual neutrophil phenotypes in deciding survivorship in an animal model. In addition, an *in silico* extracorporeal treatment which modulates CXCR-1/2 neutrophil surface receptors showed promising results. Further study and collection of experimental data will help further refine both the model and experimental device. Incorporation of data from a diverse patient population and expansion of current ensembles would increase the model's generalizability, improving the potential for translation. Additional model parameters related to the device such as flow rate, surface area, and form factor could be included, allowing the model to streamline device development.

2.5 CONTRIBUTIONS

I assisted in the construction of model equations with AM, SM, and GC. I performed the parameter estimation. SM did the sensitivity analysis. I assisted in the implementation of the model treatment scenarios with AM, SM, GC, and WF. I performed the classification of patient outcomes. HR performed the experiments. I assisted in writing the manuscript with AM and SM.

3.0 TCR SIGNALING STRENGTH CONTROLS DIFFERENTIATION DECISIONS IN CD4$^+$ T CELLS

Sections 3.2.1-5 and 3.3.1 of this chapter were originally published in *The Journal of Immunology*. Hawse, WF, Sheehan, RP, Miskov-Zivanov, N, Menk, AV, Kane, LP, Faeder, JR, Morel, PA. 2015. Cutting edge: differential regulation of PTEN by TCR, Akt, and FoxO1 controls CD4+ T cell fate decisions. J. Immunol. 194: 4615-4619.

3.1 INTRODUCTION

3.1.1 Role of T cell differentiation in the immune response

Regulatory T (Treg) cells play a critical role in maintaining self-tolerance and in controlling the immune response to pathogens [170]. Thymic (t)Tregs arise in the thymus and are generally specific for self-antigens, whereas peripheral (p)Tregs arise when naïve T cells encounter either self or foreign antigens in the periphery. Proper differentiation and expansion of Tregs is critical, as insufficient expansion of Treg cells has been shown to cause type 1 diabetes[171] and other autoimmune disorders [172]. Tregs can also play an important role in controlling the rejection of solid organ transplants and many therapeutic interventions are aimed at not only suppressing the rejection response but also to enhance the number and function of the necessary Treg

populations. Transplanted organs are highly immunogenic and they trigger strong immune responses that, if left unchecked, will reject the transplanted organ. Transplant rejection is mediated by helper T (Th) cells that respond to the foreign MHC molecules expressed by the transplanted organ. Alternatively, an overabundance of Tregs can make it difficult for the immune system to target tumors in cancer patients leading to a search for therapies that can titer Treg populations[173,174]

3.1.2 Signaling through the T Cell Receptor controls the dynamics of Akt and influences differentiation decision making

Th and pTreg cells are induced when naïve CD4 T cells recognize peptide antigens derived from external proteins that presented from antigen presenting cells (APC) by MHC molecules. The T cell receptor (TCR) is a unique receptor that recognizes peptide (p)MHC complexes presented on the surface of APC and which exhibits both exquisite sensitivity and specificity [175–177]. Activation of CD4 T cells via the TCR triggers a complex signaling cascade that results in the proliferation and differentiation of Th or pTreg cells, depending on the conditions. It has become clear that the strength of the TCR signal perceived by the naïve T cell is a critical factor that determines CD4 T cell fate. It has been shown that that low dose stimulation of naïve peripheral T cells results in Treg induction, whereas high doses are required to induce Th cells [178–180]. Analysis of the signaling pathways induced in conditions of high and low dose stimulation has revealed an important role for the Akt/mTOR pathway. High levels of Akt activation downstream of the TCR have previously been shown to correlate with the Th versus Treg decision [181,182], and high dose stimulation induces strong Akt activation. Despite this insight the precise mechanisms by which signaling pathways downstream of TCR activation determine

T cell fate remain obscure. We have found that mathematical modeling of this pathway has provided critical new insights into these mechanisms.

3.1.3 Combined experimental and modeling approaches allow for novel predictions of signaling dynamics

One way to handle the complexity of TCR signaling and its relationship with T cell activation and differentiation is through mathematical modeling. Mathematical modeling has previously been used to great effect to explore the effects of TCR signaling on T cell activation [183–185], antigen discrimination [186,187], and bistable responses to stimulation [88,57,188,189]. Previous Boolean modeling attempts explored the effects of dose on TCR signaling and subsequent T cell differentiation, as discussed in section 1.3.1.2, to study possible TCR signaling network architectures on a large, coarse-grained level [21,190]. The original model [21] produced a novel prediction that PTEN exhibited differential dynamics following stimulation by low and high doses of antigen. Following low dose stimulation, PTEN levels briefly dipped before returning to high levels, whereas following high dose stimulation PTEN levels dropped and were maintained at low levels [21]. This sparked additional model development and experimental work examining the regulation of PTEN, creating the need for a novel Boolean model with a more narrow focus on the regulation of PTEN and Akt, and allowing me to test out novel network architectures in an effort to better understand the dynamics of this protion of the pathway.

This led to a new experimental focus on the regulation of PTEN. This included additional study of post-translational modifications (PTMs) on PTEN [191,192], showing that TCR activation leads to the ubiquitination of PTEN following high dose conditions and

phosphorylation of PTEN under both high and low dose conditions. Additionally, new experiments showed that PTEN transcription is regulated by FoxO1, which in turn is regulated by phosphorylation via Akt, induced downstream of TCR activation. This outlined a novel positive feedback loop involving PTEN, Akt, and FoxO1 [190].

Further exploration of the details of this feedback loop and its role in differentiation were difficult to answer with a Boolean model, due to the coarse grained nature of all modeled elements, the lack of explicit time in the model, and the inability to directly calibrate the model to data. These details are more easily modeled using rule-based modeling. The rule-based modeling approach [82,84,193–195] is ideally suited to integrated modeling and experimental efforts being because it allows the direct translation of biochemical mechanisms into model elements. It is also robust to the combinatorial complexity that arises from multi-site phosphorylation and formation of protein complexes [82,84,195], which makes it possible to build models of increasing complexity without hitting overwhelming computational bottlenecks [93]. This approach has been previously been used to model immunological cell signaling systems [88,196,87,94] and is a convenient framework for this system due to the importance of site-specific phosphorylation events and protein trafficking, which are easily modeled.

Here we use rule-based modeling to explore the relationship between PTEN and Akt activation in the differentiation of Treg versus Th cells. The model is based on the observation that Akt activity is differentially regulated by phosphorylation at two regulatory sites Serine 473 (S473) and Threonine 308 (T308). Low dose stimulation induces phosphorylation at only the T308 site whereas high dose is required for both sites to be phosphorylated. This has consequences for T cells differentiation, as FoxO1 is itself phosphorylated by Akt following high dose stimulation, reducing transcription.

3.2 METHODS

3.2.1 Mice

C57BL/6 mice were obtained from Jackson Laboratories. All mice were housed in a specific pathogen-free facility at the University of Pittsburgh and treated under Institutional Animal Care and Use Committee-approved guidelines in accordance with approved protocols.

3.2.2 $CD4^+$ T cell isolation and activation

$CD4^+$ T cells were isolated from C57BL/6 spleens using a $CD4^+$ negative selection kit (Miltenyi Biotech). In some experiments $CD25^+$ T cells were removed using CD25 microbeads. T cell activation assays were performed with low (0.25 μg/mL) or high (1μg/mL) dose plate-bound anti-CD3 monoclonal antibody (mAb) in the presence of soluble anti-CD28 mAb (1μg/mL). For inhibition studies, T cells were treated for one hour with the following drugs prior to stimulation: caspase inhibitor (ZVAD, 80 μM), PTEN inhibitor (SF1670, 10 μM) and Akt inhibitor (Akti1/2, 10 μM).

3.2.3 Flow cytometry

Activated $CD4^+$ T cells were stained with the following mAb: anti-CD3-APC-eFluor780, anti-CD4-APC, anti-CD25-PE, anti-Foxp3-Pac blue (eBioscience), and anti-pS6 (Ser235)-FITC (Cell Signaling Technology) using buffers from eBioscience. The stained cells were analyzed on a LSR II flow cytometer and data were analyzed with the Flowjo software package.

3.2.4 Western blotting

Western blotting was performed using the following antibodies from Cell Signaling Technology: β-Actin, PTEN (138G6), Phospho-FoxO1 (Thr24), and Akt (Thr308 and Ser473).

3.2.5 Boolean modeling

The Boolean model was specified using the logical rules shown in Appendix A. These rules are used to determine the next state of each element in the system as a logical function of its inputs, which are binary variables that take the values 0, representing the inactive state, or 1, representing the active state. The logical functions used in the rules are constructed using standard operators such as AND, OR, and NOT. For example, mTORC2 activation is described by the following rule: MTORC2′ = (TCR_LOW or TCR_HIGH) and not AKT, meaning that mTORC2 is activated when either TCR_LOW or TCR_HIGH input is present and AKT is inactive. At the initial time of the simulation, all variables are set to inactive except PTEN_total, FoxO1, and either TCR_LOW or TCR_HIGH depending on the stimulation scenario. The system is then allowed to evolve in time according to the General Asynchronous update scheme [197]. For the simulations performed here, the logical rules were translated into the BioNetGen rule-based modeling language using an automated tool called Boolean2BNGL included in the BioNetGen package [82] (http://bionetgen.org). Both the Boolean model rules and the derived BioNetGen language file are available online at http://bionetgen.org/index.php/PTEN_model. The BioNetGen model was simulated using a modified version Gillespie's Direct Stochastic Simulation Algorithm [198].

3.2.6 Rule-based modeling

The model was written and simulated using the BioNetGen software [82,199]. Model code is included in Appendix B. The model contains 15 molecule types, 78 parameters, and 60 rules, which are expanded into a network of 58 species and 115 reactions. The network is simulated as a set of ordinary differential equations.

3.2.7 Parameter estimation

The model contains 78 free parameters. Parameter values were inferred using a Bayesian parallel tempering approach as described on pp. 21-24 of Chapter 2.

3.2.8 Simulation protocols

3.2.8.1 Bifurcation We systematically tested the effects of varying the antigen dose on the system. Starting from a low concentration of antigen, the concentration was increased in a stepwise manner, allowing the system to re-equilibrate at each step. The steady-state concentrations of PTEN, Akt phosphorylated at Ser473, nuclear FoxO1, and active NEDD4 were recorded at each step and normalized to a maximum value of one. The process was then reversed, decreasing the antigen and measuring the steady state concentration of each variable at each step.

3.2.8.2 Pulses The system was simulated with one, two, or three pulses of high dose antigen, separated by a rest period where antigen was entirely removed. The concentrations of PTEN and

doubly phosphorylated Akt were recorded for the entire time course and normalized to a maximum of value of one.

3.2.8.3 Phase Diagrams The antigen dose and length of stimulation were systematically varied. For every dose and time, the system was stimulated with the given dose maintained at a constant level for the given length of time. All antigen was then removed, and the system was allowed to reach steady state. Levels of PTEN and doubly phosphorylated Akt were measured at steady state and normalized to a maximum value of one.

3.2.9 Population model

A population of 50 naïve T cells was modeled as 50 iterations of our rule-based model with identical rules and kinetic parameters, but heterogeneity in initial conditions. Initial concentrations of molecules were taken from lognormal distributions, using our original parameter set as a mean and using a coefficient of variation of 0.11 for membrane bound elements and 0.41 for intracellular elements [200]. Each model is simulated independently for 30 minutes. Then, IL-2 secreted by each cell during this 30 minute block is added to a pool of free IL-2 that is available to each cell. Simulation is then resumed for the next 30 minute block for each cell. This continues for a total of 28 simulated days.

Cells are allowed to differentiate following 24 hours of exposure to antigen. A two-step threshold is set on the total activity of Akt over that time. A high level of Akt activity causes the cell to become a Th cell, a medium level of Akt activity causes the cell to become a Treg cell, and sub-threshold Akt activity allows the cell to remain naïve. The transition to the Th and Treg states is permanent and a cell cannot switch once it has committed to one state. Cells are allowed to divide following 12 hours of exposure to antigen, and sufficient IL-2 signaling. Cells can

divide symmetrically or asymmetrically. In symmetric division the two resulting daughter cells maintain the same phenotype as the original cell, and maintain identical protein concentrations. In asymmetric division, one daughter cell maintains the phenotype and protein concentrations of the parent cell, while the second daughter cell is initialized as a naïve cell with randomized initial conditions. Cells are allowed to die based on their lifetime following exposure to antigen, with an average lifetime of three days.

3.3 RESULTS

3.3.1 Boolean modeling reveals the multi-tiered regulation of PTEN as a critical control point in the signaling pathway

Using components and interactions from our previous model of T cell differentiation [21], we developed a more limited model focusing on the regulation of PTEN, Akt, and FoxO1 (Fig. 10, left), with the goal of maintaining essential behaviors from both our previous model and new experiments while utilizing a minimal network size. Simpler architectures were tested, but were unable to recreate all experimental features.

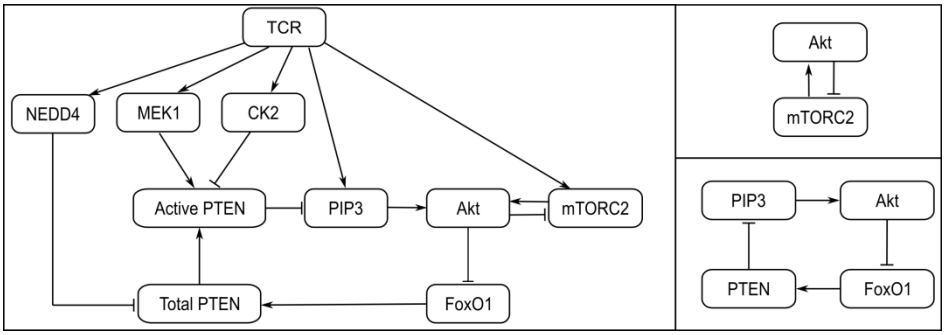

Figure 10 Boolean model structure.

A reduced logical model of PTEN and Akt dynamics was developed (left panel). Two key feedback loops can be identified: negative feedback, in which Akt inhibits mTORC2 activity, (top right panel) and positive feedback, in which Akt inactivates FoxO1 (bottom right panel).

Simulations exhibited rapid and sustained loss of PTEN (Fig. 11 far left) at high antigen dose, as well as transient and incomplete loss of PTEN at low dose, in agreement with experimental findings. Under both conditions there was a rapid initial increase in Akt activity (Fig. 11 left), sustained by positive feedback involving the loss of nuclear FoxO1 (Fig. 10 bottom right bottom, Fig. 11 right). At high dose, the activation of CK2 blocked PTEN activity and sustained Akt activation. At low dose, PTEN activity rebounded as negative feedback through mTORC2 (Fig. 10, top right) decreased Akt activity, increasing nuclear FoxO1 and, consequently, PTEN transcription. PTEN activity then further suppressed Akt, permitting full restoration of PTEN expression. Insertion of our reduced model back into our previous model of T cell differentiation resulted in sustained induction of Foxp3 in about 70% of cells at low dose and only transient induction of Foxp3 at high dose, in agreement with results from the previous model and experiments (Fig. 11, far right).

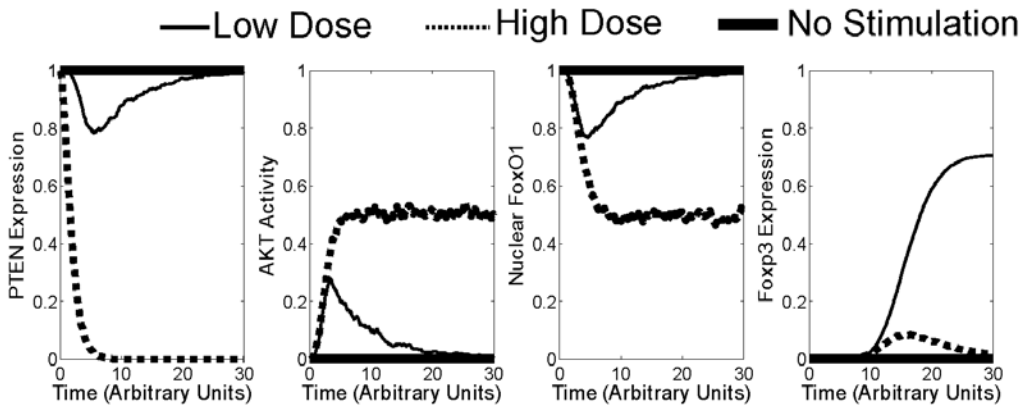

Figure 11 Boolean model results.

Average levels of total PTEN (far left panel), active Akt (left panel), and nuclear FoxO1 (right panel) from the reduced model, and average levels of Foxp3 (far right panel) from the full model with inclusion of new regulatory elements from the reduced model for no TCR stimulation (thick solid line), low TCR stimulation (thin solid line) and high stimulation (dashed line) as a function of simulated time computed from 10,000 simulated trajectories.

Transient suppression of PTEN at low dose arises from the inclusion of two regulatory mechanisms in the model: the requirement for MEK1 to activate PTEN [201], and inhibition of mTORC2 by Akt [202]. Prior to MEK1 activation by TCR [203], PTEN is inactive, allowing the transient induction of Akt, even at low dose, which may be necessary for T cell activation and proliferation regardless of differentiation outcome. Subsequent activation of PTEN by MEK1 then inhibits Akt in concert with the negative feedback provided by indirect Akt inhibition of mTORC2 [202].

3.3.2 Positive feedback leads to a bistable switch resulting in two steady states

3.3.2.1 Rule-based model of antigen-induced T cell differentiation The Boolean model allowed for easy exploration of our proposed network and the potential dynamics resulting from

the PTEN-Akt-FoxO1 positive feedback loop; however, Boolean models are limited due to the fact that they are coarse-grained in both the description of the biochemical states of the system and with respect to time, which is roughly equated with the number of update rounds. In order to explore in detail the dynamic signals downstream of the TCR, we developed a novel rule-based model of the T cell differentiation pathway that is based on our Boolean model, but also considers concentrations of signaling elements and reaction rates that cannot easily be incorporated in the Boolean framework. Thus, rule-based simulations results reflect realistic time scales of protein interactions and enzyme kinetics, in addition to changes in protein and mRNA abundance, that allow tight integration between model predictions and experimental data. In addition to protein interactions, transcription, and translation, the rule-based model of T cell differentiation explicitly defines post-translational modifications central to the receptor activated signaling pathways (Fig 12, Appendix B).

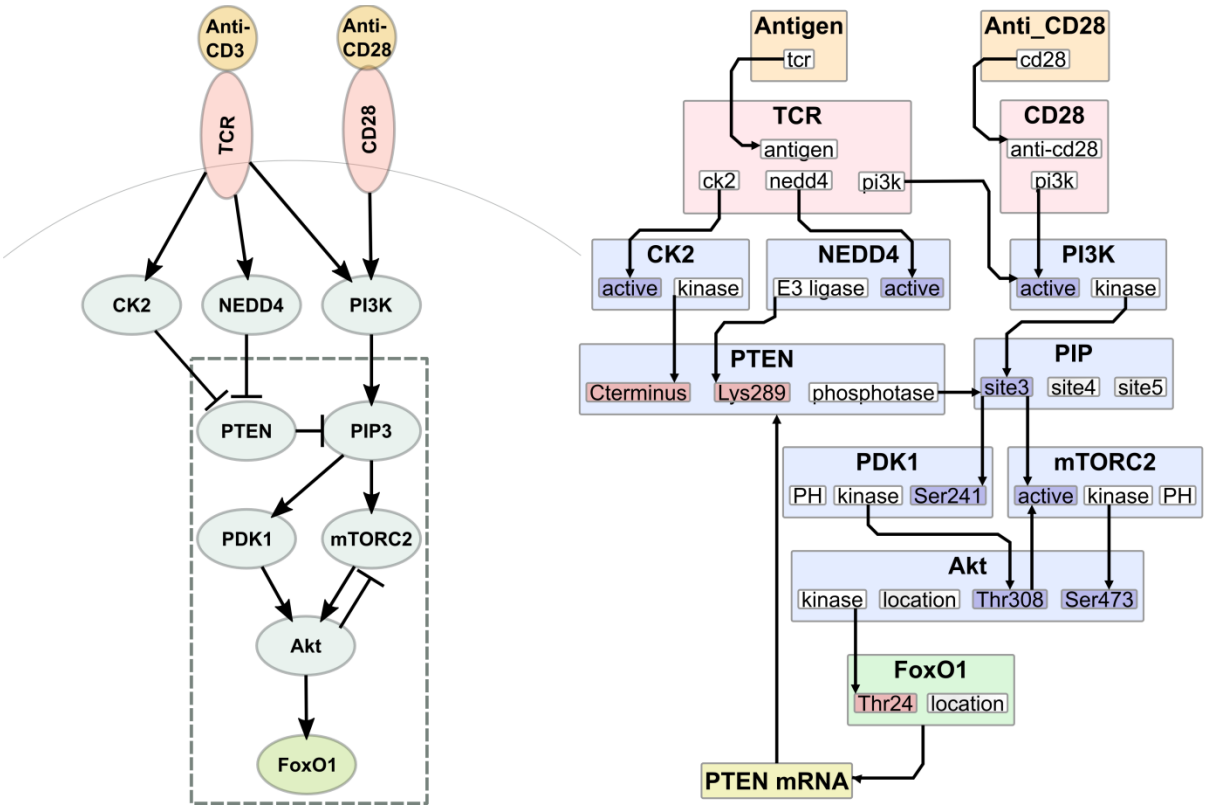

Figure 12 T cell receptor signaling model diagram.

(A) The cartoon abstraction shows all molecules considered in the model. Orange elements represent extracellular ligands. Pink elements represent membrane bound receptors. Blue elements indicate intracellular signaling intermediates. Green elements indicate transcription factors. Yellow elements indicate mRNA. (B) The contact map specifies all signaling proteins considered in the model, as well as sites for post-translation modifications, localization signals, and additional activation sites. Sites colored red indicate an inhibitory modification and sites colored blue indicate an activating modification.

Antibody ligation of TCR and CD28 induces a cascade of kinase, phosphatase, ubiquitin ligase, and transcriptional activity to coordinate the differentiation of naïve T cells. Of key importance is the regulation of PTEN through inhibitory phosphorylation by CK2 [204], K45 ubiquitination by NEDD4 [205] and transcriptional control through FoxO1 [190]. Additionally, two feedback loops are critical in defining model behavior. Negative feedback, modeled as Akt

inhibiting mTORC2 and representing the inhibitory phosphorylation on mTORC2 by S6K1 [202,206] can suppress phosphorylation of Akt on Ser473. Positive feedback controls the abundance and activation state of key players PTEN, PIP3, Akt, and FoxO1. This arises due to the opposing inputs on PIP3 through PI3K and PTEN. High levels of PTEN lead to an accumulation of PIP2, rather than PIP3 [207], limiting the activation of Akt downstream. Alternatively, strong PI3K signaling leads to an increase in PIP3 [208,209], and consequently phosphorylation and activation of Akt [202,206,210–212], phosphorylation and nuclear export of FoxO1 [213], and decreased transcription and translation of PTEN [190]. This allows for an increased accumulation of PIP3, followed by an increase in Akt and FoxO1 phosphorylation.

3.3.2.2 Model calibration reveals two steady states distinguished by levels of PTEN expression and Akt activity

To calibrate our model, we used a replica exchange Markov chain Monte Carlo approach, also known as parallel tempering, to estimate the values of unmeasured kinetic rate constants. This approach results in the selection of a posterior distribution for each parameter in the model. This allows us to use an ensemble of values to represent each parameter, which can be used to simulate the system, generating an ensemble of results, which we use to compare to measured experimental data, or make new predictions. Using this framework we obtained model fits for five key observables in the system, PTEN protein abundance, PTEN mRNA abundance, Akt phosphorylation on its Threonine 308 and Serine 473 sites, and FoxO1 phosphorylation on its Threonine 24 site under high and low dose conditions.

Our model is successfully able to recreate key features of individual experimental trajectories and capture key differences in TCR response under high and low dose stimulation conditions. The model recovers the transient dip and recovery PTEN abundance that correlates with Treg development following low dose TCR stimulation, as well as the sustained loss in

PTEN following high dose stimulation that correlates with Th development as observed in our Boolean model and experiments[190] (Fig 13A).

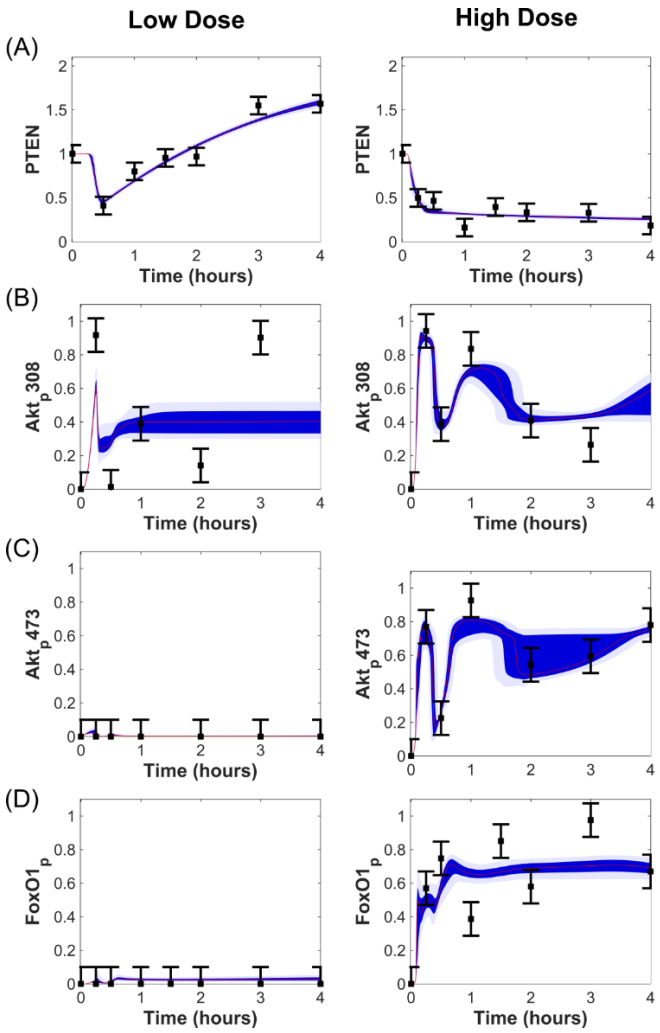

Figure 13 Time course dynamics of TCR signaling differ following low and high dose stimulation.

Mean (red), 25th-75th percentile (dark blue), and 5th-95th percentile trajectories of the simulated ensemble are shown. Experimental data points are shown in black with error bars representing one standard deviation above and below the mean averaged across the observable. The model was simulated for 4 hours under both low and high dose conditions. (A) Under low dose conditions PTEN transiently dips but then returns to high levels. Under high dose conditions PTEN dips to and remains at low levels. (B) Under both low and high dose conditions Akt Thr308 exhibits high, fluctuating levels of phosphorylation. (C) Under low dose conditions Akt Ser 473 is not phosphorylated. Under high dose conditions it is phosphorylated at high levels. (D) Under low dose conditions FoxO1 is not phosphorylated. Under high dose conditions is phosphorylated at high levels.

Using the rule based model, we further examined how exposure to low or high concentrations of antigen affects the dynamics of Akt activation (Fig. 13C). The model assumes that Akt must be phosphorylated on Thr308 and Ser473 before it can phosphorylate FoxO1. Because our rule-based model specifies each of these residues on Akt, we followed the phosphorylation state of each residue over time. The model also captures early fluctuations in Akt Threonine 308 phosphorylation under both low and high dose antigen stimulation, but shows minimal phosphorylation of the Serine 473 residue under low dose, distinctly different from high dose stimulations which again show strong fluctuations in phosphorylation (Fig 13 C-D). This low dose behavior is due in part to the negative feedback present in the model leading to limited activation of mTORC2, which correlates with the induction of a Treg phenotype [214,215]. Due to the contrasting phosphorylation of the Serine 473 residue on Akt, the model also predicts little to no phosphorylation of FoxO1 following low dose stimulation, whereas high levels are seen following a high dose (Fig 13F). The model therefore predicts that phosphorylation of Akt at Ser473 is a limiting factor for phosphorylation of FoxO1, and therefore a mechanism for T cells to discriminate between exposure to low and high concentrations of antigen and influence differentiation.

Simulations of TCR stimulation using our rule based model agree with experimental data, and illustrate important differences in signal transduction that depend on antigen concentration. These results suggest that a four-fold difference in antigen concentration can induce two distinct cellular states. The first state, for a cell exposed to a low concentration of antigen, has incomplete activation of Akt due to reduced phosphorylation of S473, in addition to a greater abundance of PTEN and active FoxO1 in the nucleus and correlates to Treg development. The second state, for a cell exposed to a high concentration of antigen, produces maximal S473-

dependent Akt activity and lower abundances of PTEN and active FoxO1 and correlates with Th development.

3.3.2.3 Bistability in Akt activation gives rise to T cell memory of encounters with antigen and a threshold for Th differentiation We identified two distinct T cell states when using the rule based model to simulate responses to low and high antigen concentrations, suggesting that the TCR-activated signaling network may be a bistable system. To test for bistability, we modeled the steady state response of simulated T cells exposed to a range of different antigen concentrations. This analysis identified a concentration threshold that separates the two cellular states (Fig 14). For cells in the first state, PTEN is predicted to remain at high abundance after exposure to increasing antigen concentrations below the threshold, after which the cell irreversibly switches to a second cell state with low PTEN abundance (Fig 14A). Conversely, phosphorylation of Akt on Ser473 switches from low to high abundance for antigen concentrations greater than the threshold (Fig 14B). The nuclear abundance of FoxO1, an Akt substrate, consequently shows a rapid decrease following phosphorylation-dependent nuclear export (Fig 14C).

Levels of PTEN abundance, Akt phosphorylation, and FoxO1 nuclear localization all exhibit hysteresis. When antigen is removed from a cell that has already switched to the second state the cell will remain in that state, suggesting that conversion is irreversible. Our model further suggests a role for a positive feedback loop between PTEN, PIP3, Akt, and FoxO1 in the bistability of these variables (Fig 12). A cell in the state with low PTEN abundance will maintain high levels of PIP3 and Akt activity that promote nuclear export of FoxO1. These kinase activities indirectly prevent transcription of PTEN and therefore quench PTEN-mediated phosphatase activity that otherwise inactivates PIP3. Although signaling molecules within this

feedback loop all exhibit bistability and hysteresis, this is not true for other molecules in the TCR-induced signaling network. NEDD4 activity, for example, is regulated outside of this feedback and does not exhibit bistability or hysteresis (Fig 14D). NEDD4 does exhibit a dose-response relationship where higher dose stimulation leads to increased production, however this effect is reversible, and decreasing antigen levels leads to decreasing activity. Overall, our simulations agree with experiments and provide mechanistic insight into how antigen dose shifts the balance of Treg and Th differentiation. Our results lead to the hypothesis that irreversibility of T cell lineages with distinct effector functions result from bistability in the TCR signaling network.

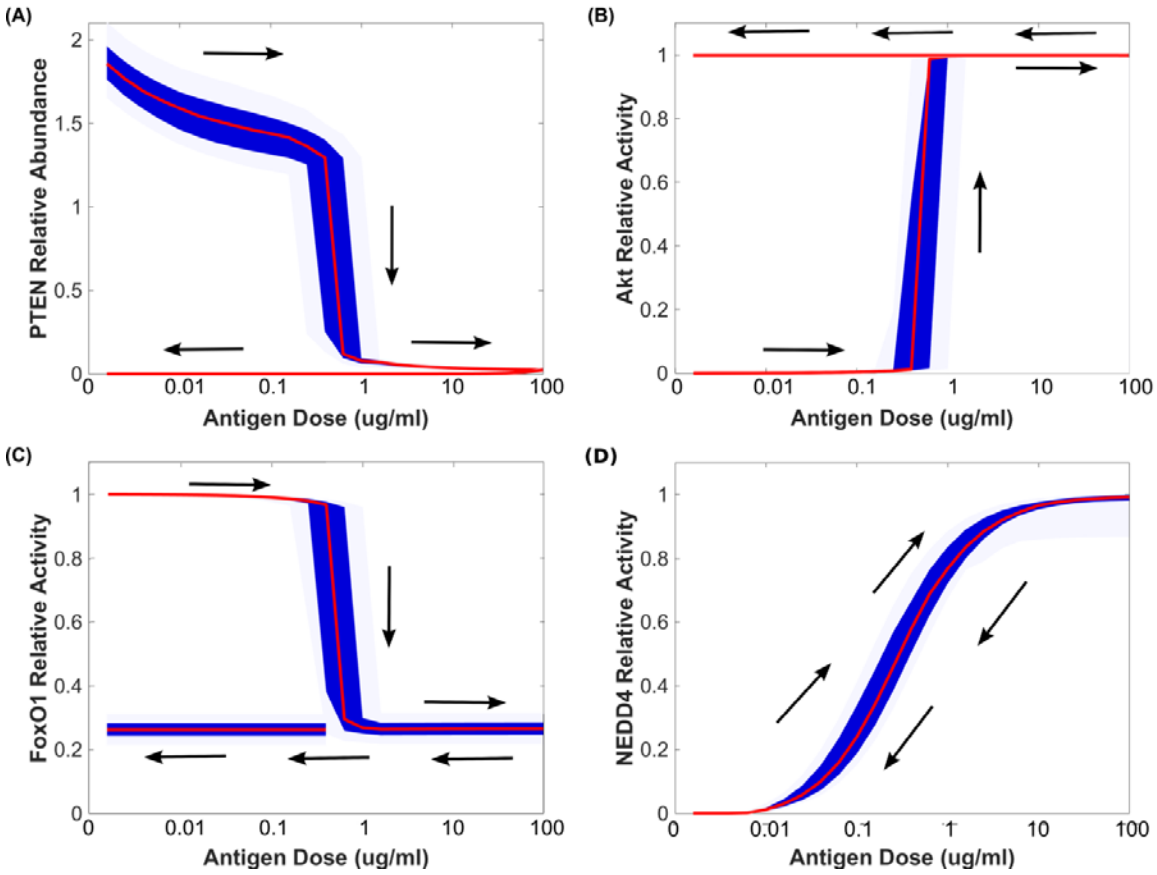

Figure 14 Bifurcations PTEN, Akt, and FoxO1 exhibit bistability.

Mean (red), 25th-75th percentile (dark blue), and 5th-95th percentile trajectories of the simulated ensemble are shown. Antigen is increased in a stepwise fashion to a maximal high dose. Under low doses PTEN (A) and nuclear FoxO1 (C) levels remain high, while Akt activity (B) and NEDD4 activity (D) remain low. Antigen is then removed in a stepwise fashion. PTEN (A) and nuclear FoxO1(C) levels remain stably low in the absence of antigen, while Akt phosphorylation (B) remains high. Alternatively, Nedd4 activity (D) drops back down to baseline levels following antigen removal.

3.3.3 Pulsatile stimulation reveals the duration of antigen exposure influences cell fate decisions

Model simulations revealed two distinct outcomes based on antigen dose; however, T cells may not be exposed to a static, sustained dose of antigen. So, we next investigated the effects of varying the length of time cells are exposed to a given dose of antigen. The system was simulated using pulses of high doses of antigen, allowing the simulated cells to experience the dose for a limited time before antigen was removed. When the full parameter ensemble is stimulated with a high dose pulse for 30 hours, all trajectories switch to their PTEN-low, Akt-high state, and are able to maintain it after antigen is removed. However, when antigen is pulsed for only 12 hours, the cells experienced a transient dip and PTEN and rise in Akt activity, and once antigen was removed levels returned to baseline (Fig 15A-B). Simulations were then run with two 12 hour pulses, with a two hour gap in between (Fig 15C-D). Once again, during the initial pulse levels of PTEN fell and Akt activity rose. During the two hour gap when antigen was removed, these trends began to reverse, but did not have time to recover all the way to baseline. The second pulse then resulted in another spike in Akt activity. Once antigen was removed, in a slight majority of simulated trajectories (51%), levels of PTEN and Akt activity were again able to return to their respective baselines in most simulations. However, the remaining 49% of trajectories received enough activation to trigger long term commitment to the active state. When simulations were run with three 12 hour pulses of antigen all PTEN was lost by the end of the third pulse, and Akt levels reached higher levels then seen in the previous simulation (Fig 15E-F). Once antigen was removed, Akt activity stayed high and PTEN levels stayed low. Sufficient stimulation had occurred to commit the system to the PTEN low, Akt high steady state we had seen previously.

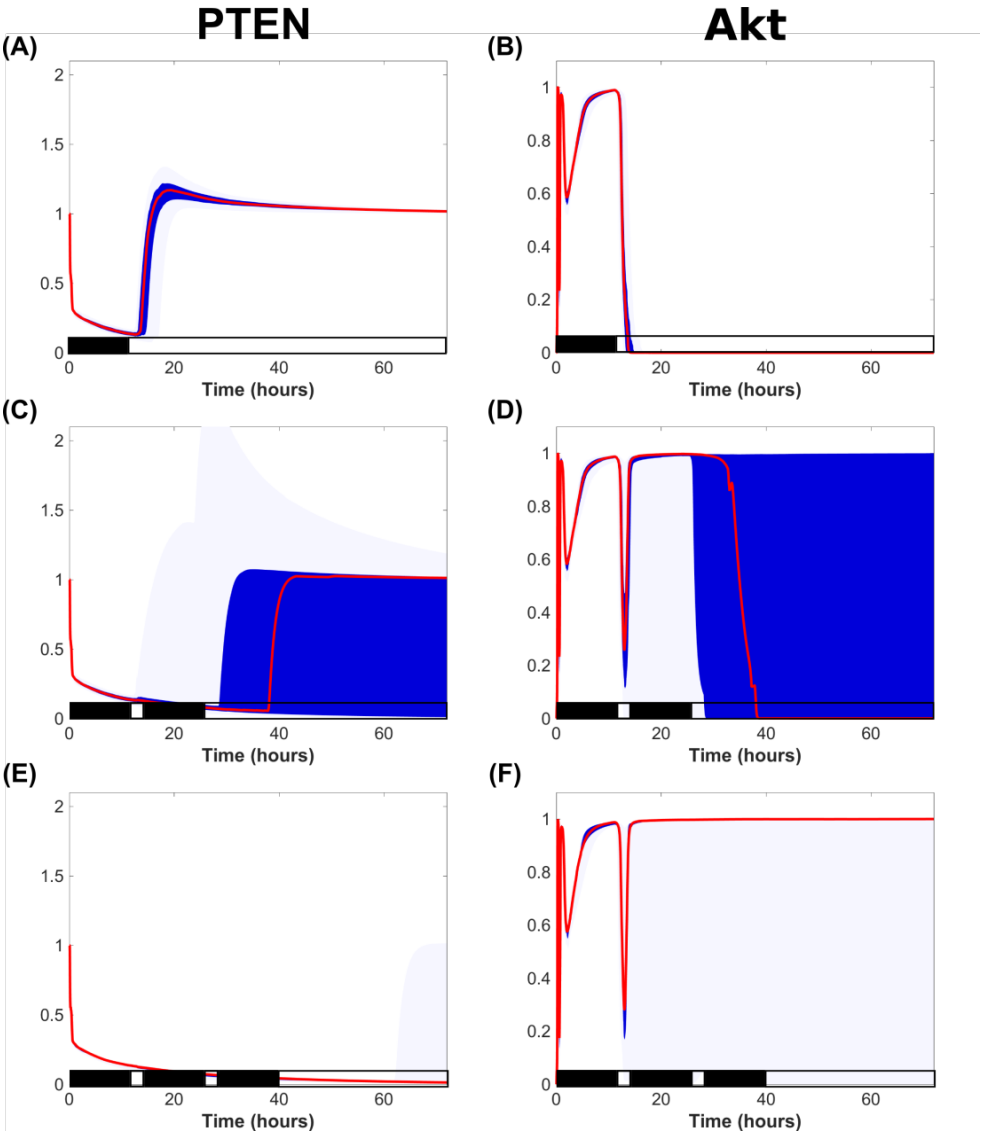

Figure 15 Consecutive pulses of antigen can stably induce the PTEN high, Akt low state.

Mean (red), 25th-75th percentile (dark blue), and 5th-95th percentile trajectories of the simulated ensemble are shown. One (A-B) and two (C-D) 12 hour pulses of high dose antigen transiently reduce PTEN levels and increase Akt activity, but the effect is lost following antigen removal. Three (E-F) pulses sufficiently activate the system to retain low levels of PTEN and high levels of Akt activity following antigen removal.

3.3.4 Model predicted thresholds are confirmed experimentally using Nur77 as a proxy for integrated dose and time

Our model predicts that the total signal through the TCR, as a combination of dose and activation time, determines Akt activation and Th commitment. To test this, we stimulated T cells from Nur77-GFP transgenic mice. Nur77 is a transcription factor that is activated downstream of the TCR and independent of PI3K activation [216]. It has been previously used as indicator of TCR signal strength [179,189]. Here, we use it as representative of the combination of our two variables of dose and time. Our model predicts a sharp threshold in signal strength as captured by total Nur77 production, resulting in distinct populations with low or high levels of Akt activity.

Further experimental efforts confirm this threshold. Following stimulation with a high dose of anti-CD3 antibody (1 ug/ml) for two hours, cells were sorted based on their amount of Nur77, based on GFP fluorescence levels. Cells exhibiting low levels of fluorescence uniformly show low levels of S6 phosphorylation, indicative of low levels of Akt activation. As fluorescence levels increase, there is a sudden and distinct shift to high levels of S6 phosphorylation (Fig 16). This pattern is consistent across experiments, resulting in two populations of cells, Nur77-lo, pS6-lo cells and Nur77-hi, pS6-high cells. Moderate levels of Nur77 can produce some heterogeneity, showing a bimodal distribution of pS6, corresponding to cells that have activated Akt and those that have not.

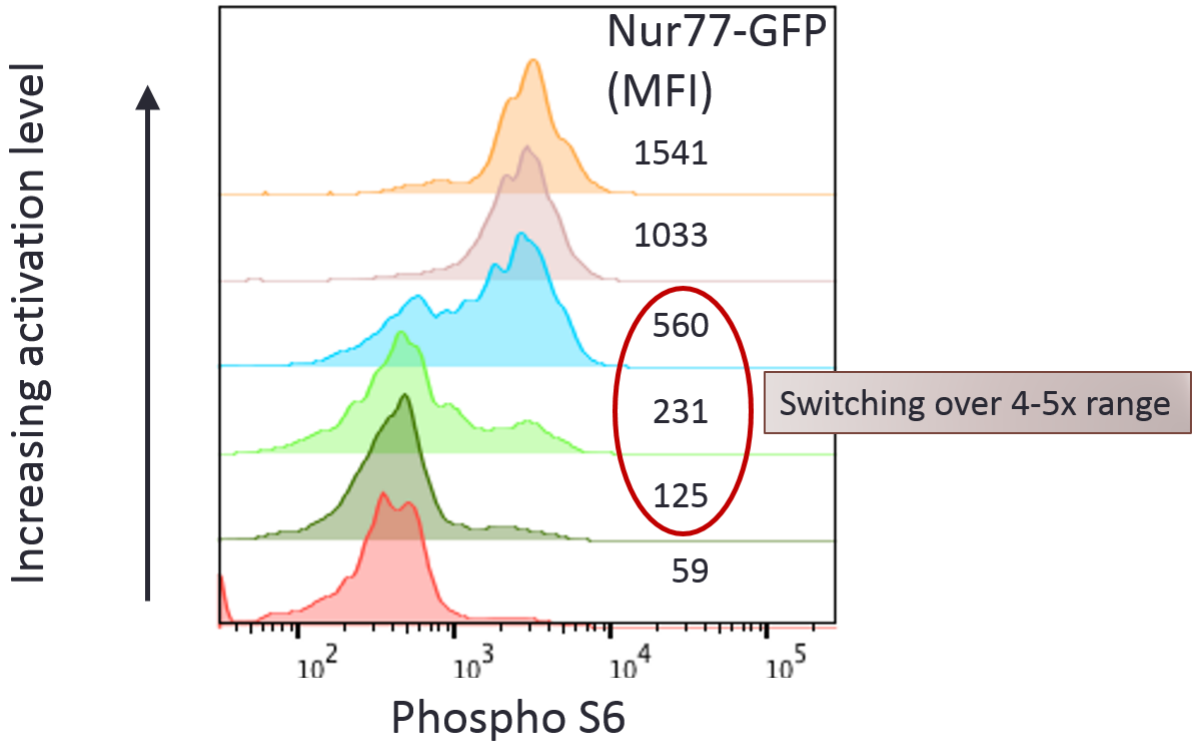

Figure 16 A threshold in total TCR activation causes the activation of Akt in T cells.

Integrated activation of the T cell receptor, indicated by the mean fluorescent intensity of cells expressing Nur77-eGFP corresponds to the levels of phosphorylated S6. A transition between the pS6-lo and pS6-hi populations occurs sharply over a small range of MFI.

3.3.5 A two-dimensional threshold dependent on antigen concentration and exposure time controls cell state transitions

Our model predicts that both the dose of antigen and the duration of antigen exposure affect T cell responses. To test if these two variables act in concert both were systematically varied, to test a wide range of combinations. The resulting phase diagram reveals a two dimensional threshold between the two steady states of the system. A minimum dose and duration of stimulation are required to switch to the PTEN-low and Akt-high (Fig 17A) state. Higher antigen

doses require a shorter stimulation, as the two variables combine to determine the total signaling input. The exact threshold varies as a function of parameters, but is qualitatively consistent.

We next wanted to test if it was possible to shift this threshold. We re-ran the simulations initializing the system with half of the baseline concentration of PTEN. Reducing PTEN levels is known to have physiological effects, as PTEN heterozygosity has been shown to induce tumor growth and hasten cancer progression, due to its role as a tumor-suppressor gene [217,218] and leads to autoimmunity and increased lymphoproliferation [219]. Additionally, PTEN inhibitors lead to an increased expansion of Th cells and reduced expansion of Treg cells [190]. Our model predicts that decreasing PTEN levels reduces the dose and duration of signal necessary to cross the threshold.

We tested this prediction by activating T cells taken from wild type and PTEN heterozygous mice with various concentrations of anti-CD3 antibody for varying lengths of time, and measuring the amount of S6 phosphorylation, a marker for Akt activity, 44 hours following the initial activation (Fig 17B). Following stimulation with the lowest dose of antigen (0.625 ug/ml), there was minimal Akt activity regardless of length of stimulation, as predicted by the model. Similar results were seen in the heterozygous cells. Successively increasing the dose wild type cells were exposed to led to increased activation, at increasingly earlier times. At the highest dose (2.5 ug/ml), most cells were activated following 28 hours of stimulation. PTEN heterozygous cells experienced activation more quickly. At 1.25 ug/ml up to 50% of cells started exhibiting activation following 24 hours of stimulation rather than 28 hours in the WT. At the highest dose most cells were active after 24 hours of stimulation and many were following 20 hours. This agrees well with the model prediction, which showed that less time was required for commitment in cells with less PTEN, with the threshold shifting by 5-10 hours.

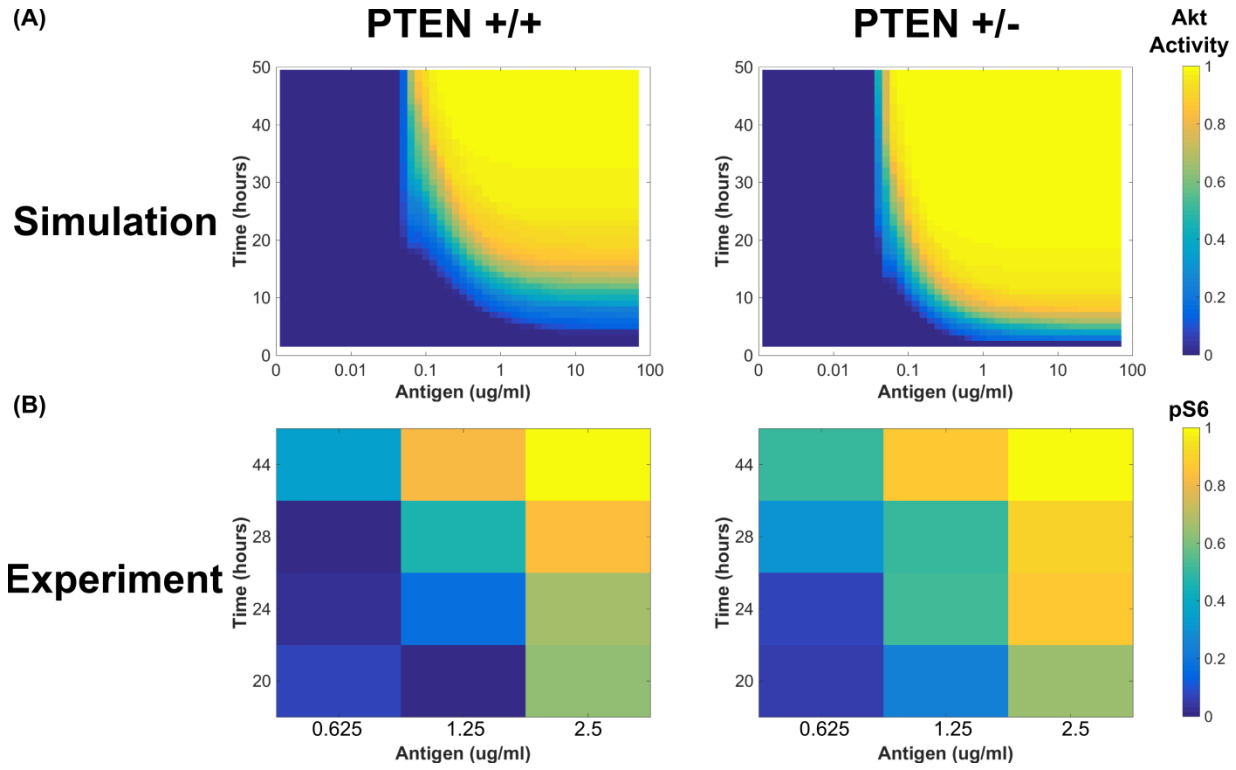

Figure 17 Signal dose and duration set a two dimensional threshold.

(A) Model simulations predict that a minimum dose of antigen and time of exposure to antigen are required to transition between steady states from low to high levels of Akt activity. Increasing the antigen dose decreases the time needed for transition. Reducing the basal concentrations of PTEN allows this transition to take place at lower doses and shorter times. (B) Stimulating WT T cells with varying doses of antigen and for varying lengths of time confirms the model prediction of a threshold. PTEN heterozygous cells exhibited a shifted threshold.

3.3.6 Population modeling

We next investigated the effects of imbedding our signaling model in a population of cells. This provided insight into the wider impact of the hypothesized network architecture and resulting bistability and how dynamic changes in antigen levels, such as in an infection, could affect the emergence of Th and Treg populations. T cells exist in a heterogeneous population, which can complicate their response to a stimulus and make it difficult to accurately capture their dynamics

with a single ODE model with a single parameter set. To address this, we expanded our model of TCR signaling, adding the production of IL-2 and CD25, which and are critical to the survival and expansion of populations of T cells (Fig 18).

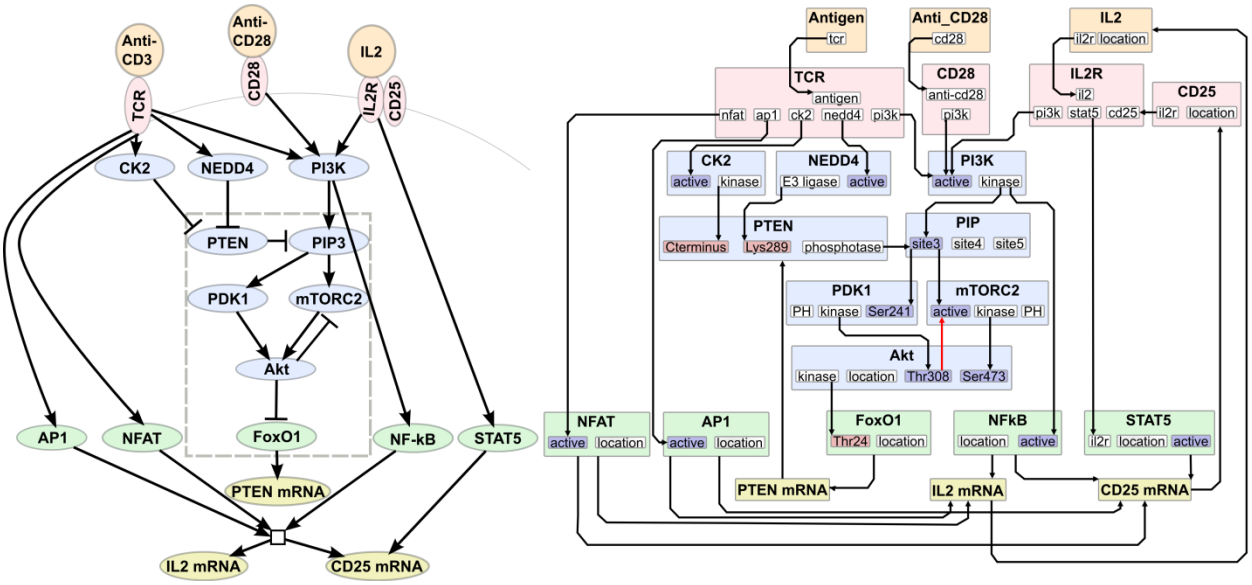

Figure 18 Multiscale T cell population model signaling diagram.

The previous rule-based model is expanded to include the transcription factors necessary to induce IL2 and CD25 expression, as well as signaling through IL2R to STAT5.

We then simulated a set of 50 cells, each containing an identical copy of our proposed signaling network (Fig 19A), but heterogeneity in their initial conditions, accomplished by selecting initial concentrations of model elements from lognormal distributions, using our original parameter set as a mean and using a coefficient of variation of 0.11 for membrane bound elements and 0.41 for intracellular elements[90]. In response to antigen, each cell can independently differentiate into Treg or Th cells as a function of total Akt activity, with high levels of Akt activity leading to Th cells and low levels of activity leading to Treg cells. Cells can also divide as a function of IL-2 signaling, or die based on the lifetime of the cell following

exposure to antigen. Cells interact through the secretion of IL2 into a shared pool that is available to all cells.

To simulate the system, we vary the concentration of antigen to mimic the time course of an infection, examining how the T cells expand and differentiate in response to dynamic antigen. Cells can thus be exposed to a wide range of antigen doses, allowing us to see how this affects the emergence of Th and Treg populations. We first simulate the system forcing all cells to divide symmetrically (Fig 19B), forcing both daughter cells to have the same protein concentrations and differentiation state as the parent cell. Under this condition, following the user-defined increase in antigen, the T cell population expands and a population of Th cells grows. As the antigen is removed, the total population of T cells returns to its baseline and the Th population is lost. No Tregs appear in this simulation. We hypothesized that this was due to the uniform symmetric division of all cells. As naïve cells were exposed to sustained high doses of antigen, they experienced high levels of Akt activation and becoming Th cells, while also producing large amounts of IL-2 and dividing. When these cells divide, the daughter cells would also become Th cells. With no other influx of cells, there were no naïve cells available to respond to decreasing levels of antigen later in the simulation as possibly become Treg cells.

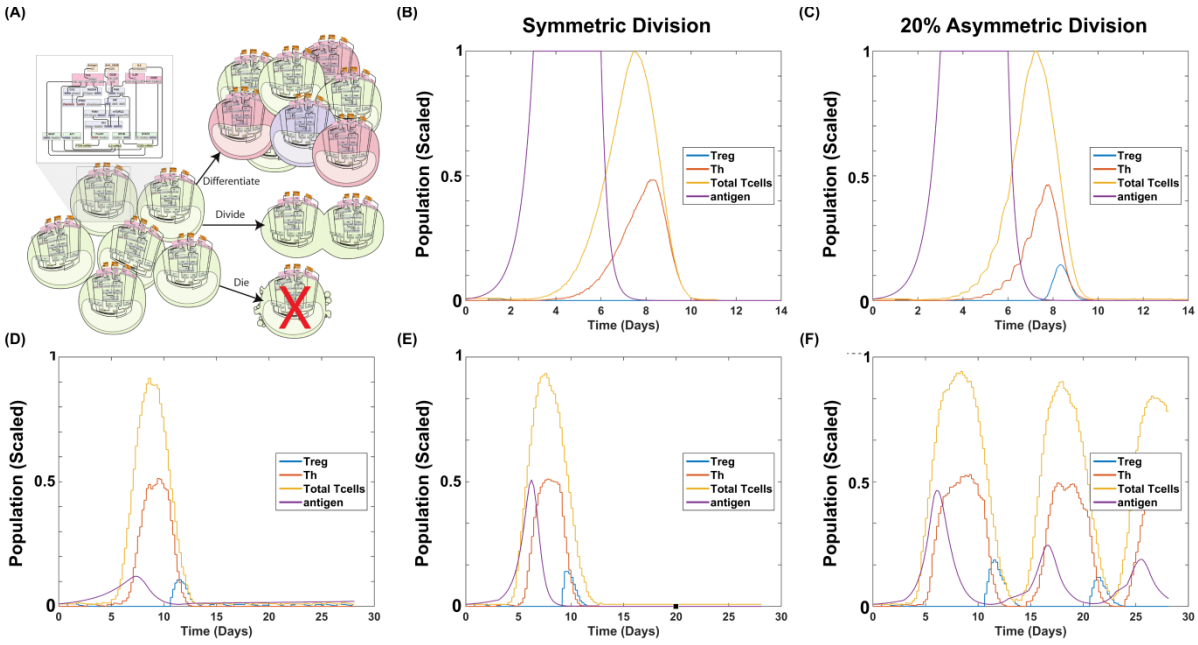

Figure 19 The induction of Tregs in a population can alter the clearance of infection.

The rule-based signaling model was simulated as a population model (A) under varying conditions. When antigen levels are manually increased and decreased, and T cells are allowed to divide only symmetrically, the overall T cell population expands, and a Th population appears (B). When asymmetric division is allowed as well, a population of Treg cells also appears (C). When the T cells control antigen removal, with Th cells clearing antigen and Treg cells slowing clearance, three scenarios can arise depending on the balance of Th and Treg populations. Antigen can be maintained at low levels indefinitely (D), antigen can be cleared entirely (E), or antigen levels can fully rebound to high levels (F).

To address this, we allowed the cells to divide asymmetrically a portion of the time. It has been shown that T cells can divide asymmetrically, producing non-identical daughter cells [220,221]. In particular, factors key to differentiation, such as Tbet, have been shown to strongly segregate to one daughter cell in certain circumstances[222]. So for the next round of stimulation, we allowed cells divide asymmetrically 20% of the time, with a differentiated parent cell producing one differentiated daughter cell and one non-differentiated daughter cell. When we repeat our simulation protocol, we again see a strong expansion of the T cell population, and

a large Th subpopulation. However, now we also see a small population of Treg cells, representing 15% of the total T cell population appear late in the simulation, as the antigen has been removed and the total population is returning to normal.

Next, we wanted to see the effects of these emergent populations of Th and Treg cells could affect the clearance of an actual infection. To test this, we allow the antigen to be responsive to T cells instead of manually changing its degradation. We now allow three sources for antigen removal, a basal term for antigen death that is unchanged, killing facilitated by Th cells, and an additional term for generic immune involvement that turns on late. Additionally, we allow Treg cells to reduce the effectiveness of killing. This allows the antigen to grow initially, while the T cell population is small. As Th cells are made, the antigen can then be killed more effectively and decreases. The late growth of Treg cells also now has the potential to slow the killing and allow for antigen survival.

Our simulations reveal three important scenarios. When the Treg population sufficiently balances out the killing of the antigen, it is possible to maintain a steady low level of antigen, and consequently retain a population of TRegs (Fig 19C). This can be important in the context of certain infections such as leishmaniasis, where long lasting Treg populations allow for concomitant immunity and prevent reinfection[223]. When there is reduced Treg function, they are not able to balance the killing of the Th cells and the antigen is completely eliminated (Fig 19D). However, if there is too much Treg activity and the immune response is too suppressed, the antigen may not be killed sufficiently. This can lead to a reoccurring infection where the antigen is able to resume growing while the immune system is suppressed.

3.4 DISCUSSION

We have demonstrated that differential regulation of PTEN determines CD4 T cell fate. In Th differentiation, stimulated by high TCR strength, multiple mechanisms suppress PTEN activity by lowering protein levels and enzymatic activity. Low TCR signal strength, resulting in Treg induction, also involves early downregulation of PTEN, but requires that PTEN activity is re-established at longer times in order to suppress Akt activity and adopt a Treg fate. Additionally, we identified a critical feedback loop driven by Akt/mTOR signaling that regulates PTEN transcription via the FoxO1 transcription factor. By combining biochemical and computational modeling approaches, our work defined how differential regulation of PTEN can produce alternate $CD4^+$ T cell fate outcomes.

By building a novel rule based-model of TCR signaling we gained significant additional insight into the detailed mechanisms and of the signaling pathway, and how they are affected by exposure to varying antigen signals. We were able to improve on the results of our previous Boolean model by adding mechanistic detail to signaling events. By considering distinct phosphorylation sites on proteins, as well as their localization patterns, we were able to add considerable detail to a small number of considered proteins and better explain the differential effects induced by low and high doses of antigen stimulations. This is most clear in the Akt phosphorylation dynamics. We saw the Thr308 residue behaves similarly under low and high dose antigen stimulation. However, the Ser473 residue, which is influenced by a negative feedback loop between Akt and mTORC2 deactivation, exhibits minimal phosphorylation under low doses, while showing significant phosphorylation following high dose stimulation. Akt activation plays a key role, leading to the phosphorylation of FoxO1 and loss of PTEN transcription under high doses.

Additionally, we now have the ability to incorporate the effects of real time scales and protein concentrations. Calibration to experimental data allowed us to replicate dynamic time course experimental data and make more quantitative predictions, not only on network architecture as past model versions have provided, but also on the timing of key events, the effects of antigen doses, and the effects of perturbations of the pathway. This provided a framework that will allow us to systematically add new experimental data to improve model behavior, and to add new elements to the model itself.

The predictions made by our model allowed us to explore how the magnitude and duration of stimulation combine to control the activation and differentiation of naïve T cells. The combination of these variables creates a threshold, below which Akt activity is low, PTEN levels are high, and the T cell is capable of committing to a Treg phenotype and above which Akt activity is high and the cell commits to a Th phenotype. The existence of this threshold was then confirmed experimentally, using Nur77 as an indicator of the combination of input variables, with stimulation leading to the growth of two distinct cell populations, Nur77-lo pS6-lo, and Nur77-hi, pS6-hi. Positive feedback downstream of the TCR maintains these two steady states, which could represent the first full step towards commitment to the Th phenotype. Our pulse simulations predicted that there needs to be a sufficient integration of the TCR signal as influenced by antigen dose and stimulation time to eliminate PTEN and commit to irreversibly high levels of Akt activity. Removing the signal for a period of time can partially or fully reset this response. This showed that the amount of exposure a cell has to antigen, as well as the contact duration of the TCR with the APC could have an impact on differentiation decisions the cell makes. Models of contact duration [187,224,225], synapse formation [226,227], and the

formation of multiple contacts, particularly in LN [228–230] have been studied and could make a substantial expansion of this signaling model.

Our new model gave us the freedom to explore a number of hypotheses involving perturbations of the signaling pathway and how they might affect a cell's response to antigen. Heterogeneity in initial conditions across the population of cell and differences in the local environment each cell experiences add an additional layer of complexity onto this problem and have significant implications on how a population of cells will respond to an infection that may be different from an average cell's response. By developing a multiscale population model we began to address these questions, while also leveraging our insights into the signaling pathway, and how perturbations in this pathway can alter differentiation. By utilizing a very basic preliminary model we have already raised new, experimentally testable questions regarding the mechanisms of asymmetric T cell division and its possible role in maintaining a pool of undifferentiated T cells that can respond to changes in antigen levels. It also predicts a late growing population of Treg cells that could play an important role in the clearance of infections and down regulation of the immune response, greatly altering the final outcome of an infection. Further expansion of this basic model will be critical to developing a better understanding of in vivo responses to infection. Extending it to consider spatial effects, the impact of other cell types, and the production of memory T cells would significantly enhance model predictions, as seen in previous multi-scale models [185,231,232]. It can also be specialized to model the time course of specific infections, taking into account their unique growth dynamics, type and amount of antigens they can present, and the potential perturbations they can induce on the immune system, including the cytokine environment and skewing the type of T cell response.

4.0 REGULATION OF NF-KB DOWNSTREAM OF IL-17 IS CONTROLLED BY THE FORMATION AND MAINTENANCE OF UBIQUITIN SCAFFOLDS

4.1 INTRODUCTION

4.1.1 IL-17 mediates the killing of fungal infections while also playing a role in inflammatory disorders

Interleukin 17 (IL-17) is the signature cytokine produced by $CD4^+$ T_H17 cells [233]. It has been shown to lead to inflammation through the activation of NF-κB[234] primarily in epithelial, endothelial, and fibroblastic target cells [235] through the activation of the IL-17 receptor. The ligand and receptor can present in a variety of hetero- and homodimers, but the homodimer IL-17A ligand, paired with the heterodimeric IL-17RA-IL-17RC receptor have come to prominence due to its strong signaling strength [236–238]. This signaling pathway is critical in immune defense against fungal pathogens, such as *Candida albicans* [239]. However it has also been linked to autoimmune disorders such as Psoriasis [22–24] and Rheumatoid Arthritis [240,241].

To better understand how these disorders arise and how they can be effectively treated, it is important to understand the cellular machinery involved in processing the IL-17 signal. The activation of NF-κB involves intermediates TRAF6, TAK1, IKK, and IκB, which accounts for significant overlap with other signaling pathways downstream of the TLR4, IL-1β, and TNFα receptors [242]. Making the IL-17 pathway unique are its receptors, which contain the SEFIR

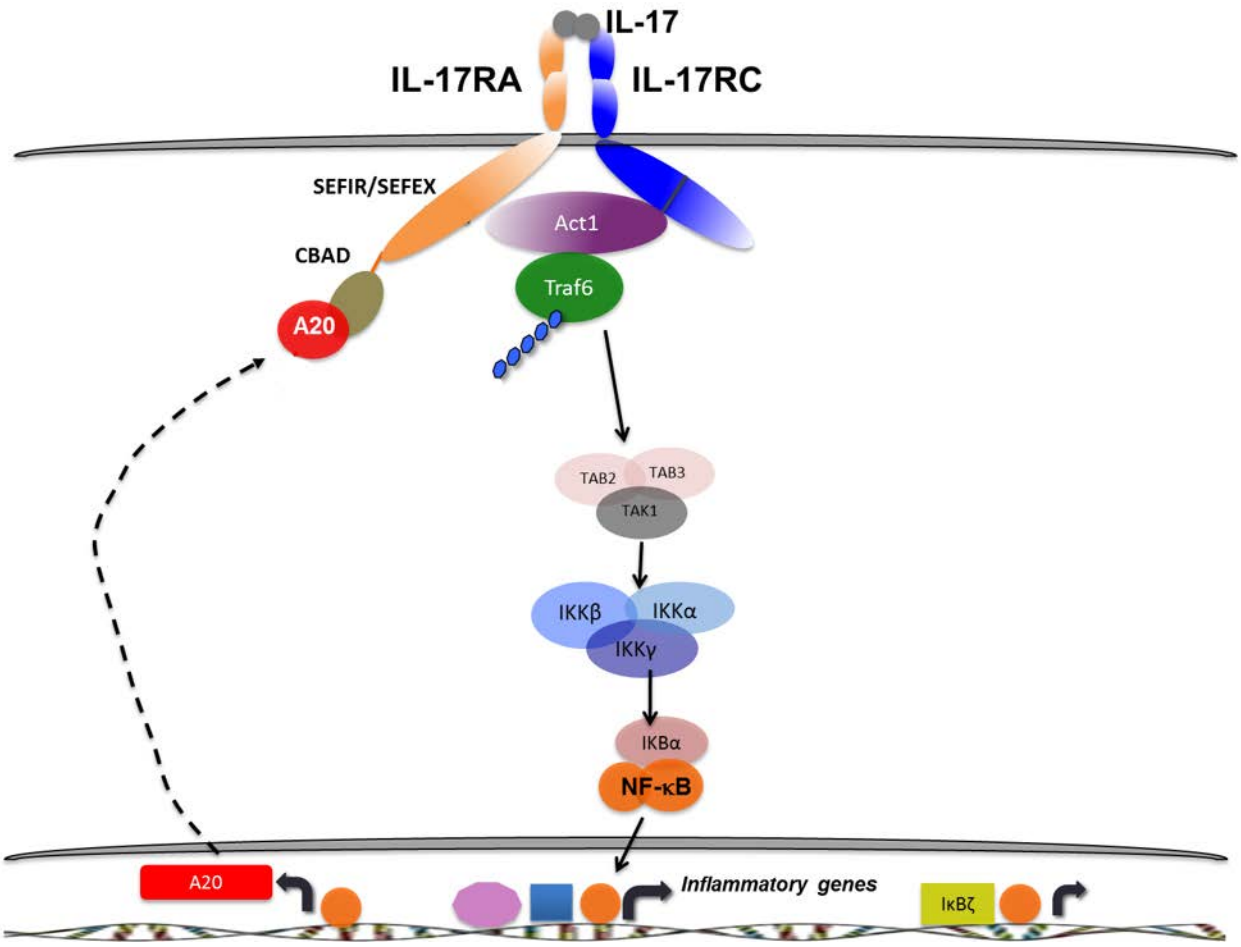

Figure 20 IL-17 signaling pathway.

Activation of the IL-17 receptor leads to the activation of NF-κB through the TAK1 and IKK kinases. Negative feedback mediator A20 is induced by NF-κB

domain allowing for binding E3 ubiquitin ligase Act1, which is also specific to the IL-17 pathway, at the top of the cascade [243]. Act1, together with TRAF6, functions to build K63-linked ubiquitin scaffolds that form a critical piece of the signaling cascade [15,16]. These scaffolds allow for the attraction and activation of key kinases TAK1 and IKK, a necessary step in the activation of NF-κB. They also serve as an fulcrum for negative feedback in the system, as NF-κB-induced ubiquitin-editing enzyme A20 can break these chains, dampening the signal [246,247]. A20 has previously been shown to be a key regulator in TLR4 and TNFR signaling

through the deubiquitination of TRAF6 [247], IKK [248], and RIP1 [249]. Additionally it has been shown that defects in A20 can lead to autoimmune disorders such as rheumatoid arthritis [27]. Recently, A20 has been shown to play an important role in down-regulating the IL-17 signal [26].

Feedback loops often play a significant role in determining the dynamics of a signaling system, adding complexity and leading to non-intuitive responses to the range of potential stimulations and perturbations of the system. These loops also serve as likely targets for failures in the system, as evidenced by A20's ties to inflammatory disorders, and could serve as targets for intervention. Thus, better understanding and predicting the dynamics of this feedback represents an important area of study, which can most easily be tackled using computational modeling.

4.1.2 Rule-based modeling allows for the modeling of ubiquitin oligomerization

In order to efficiently study this complex signaling pathway, we incorporate computational modeling. Computational modeling has been shown to be an effective way to gain new understanding in similarly large and complex systems. Numerous models of signaling systems resulting in the activation of NF-κB have been developed, with varied purposes such as better understanding feedback controls and signaling network layouts [250–254], mapping complex dynamics such as oscillations and bistable responses to stimuli [255–258,35], understanding information processing by the network [259,260], and understanding single cell versus population effects [259,261]. These models allow for a deeper and more quantitative understanding of complex biological systems and offer a framework for making novel predictions. However, traditional modeling approaches also have their limitations when dealing

with the scale and complexity involved in cell signaling pathways. Specifically, modeling the formation of large oligomers, such as the K63-linked ubiquitin scaffolds in this system, presents a difficult problem both in terms of model specification and computation time using traditional methods, such as systems of ODEs. If we tried to specify this oligomerization in such a manner, it would require writing an equation for every possible oligomer size, and every possible combination of binding partners for each oligomer. If we do not place a strict limit on the oligomer size, the number of equations necessary would be infinite, making the model impossible to specify. Because of this, we instead use a rule-based modeling approach [82] combined with network-free simulation methods [93] to accurately capture the detail of IL-17 induced activation of NF-κB.

Rule-based modeling allows us to model each signaling molecule of interest as a structured object, with rules describing their biochemical interactions. This approach has previously been used to great effect in immune signaling systems [88,87], due to the ease with which it handles model specification for systems that have a large degree of combinatorial complexity, a common problem in signaling networks. Additionally, it allows us to simulate the modeling using the NFsim software [93], which elegantly handles the case of oligomerization, a problem that would choke traditional computational methods. Recent advances in parameter estimation, including the BioNetFit software [97], which directly interfaces with NFsim, allow us to calibrate this type of model to experimental data, making it possible to make quantitative predictions about the system. This set of software makes it possible for us to include the explicit modeling of ubiquitin oligomerization into a model of NF-κB activation for the first time, an aspect of the system that has long been neglected in the field despite playing a critical role as a fulcrum for negative feedback mediated by A20. This allows us to use a systems biology

approach to learn the mechanisms of A20 and its effect on the activity of NF-κB-activating kinases by making novel, falsifiable predictions with a model calibrated to experimental data.

4.2 METHODS

4.2.1 Modeling

The model was written using the BioNetGen software [82] and simulated stochastically using NFsim [93]. Model code, including all model rules and parameters is included in Appendix C. The model contains 16 molecule types, 64 parameters, and 56 reaction rules.

4.2.2 Parameter estimation

The model was calibrated using BioNetFit [97], which utilizes a genetic algorithm compatible with rule-based models to identify best fit parameter values. Western blot data showing time course dynamics of A20 and IkBα protein levels following IL-17 stimulation and qRT-PCR data showing time course dynamics of *Tnfaip3* and *Nfkbia* expression levels were used for calibration.

4.2.3 Cell cultures and reagents

ST2 stromal cells were cultured in α-MEM (minimum essential medium, Sigma) containing 10% fetal bovine serum (FBS) supplemented with L-glutamine and antibiotics (Invitrogen). Recombinant murine IL-17 protein was purchased from PeproTech and used at a final concentration of 200 ng/ml.

4.2.4 Western blotting

Whole cell lysate was boiled in SDS sample buffer, resolved on 10% SDS-PAGE, transferred to nitrocellulose, and blotted with appropriate antibodies. Anti-A20 antibody was from Cell Signaling Technology; anti-IkBα antibody was from Santa Cruz Biotechnology; anti-tubulin antibody was obtained from Invitrogen. Bands on blots corresponding to proteins of interest were analyzed by ImageJ software. Western blots were developed with a FluorChem E imager (ProteinSimple).

4.2.5 qRT-PCR

Total RNA was isolated from cells with an RNeasy Mini Kit (Qiagen). Complementary DNA synthesis was performed with SuperScript III First-Strand (Invitrogen). The extent of expression of *Tnfaip3* and *Nfkbia* was determined by qPCR analysis with PerfeCTa SYBR Green FastMix ROX (Quanta BioSciences). The PCRs were performed on a 7300 Real-Time PCR System (Applied Bio- systems). The abundances of the mRNAs of interest were normalized to that of Gapdh. Primers were purchased from Super Array Biosciences (Qiagen).

4.3 RESULTS

4.3.1 Model description

In this model we consider the downstream signaling events mediated by IL-17 receptor

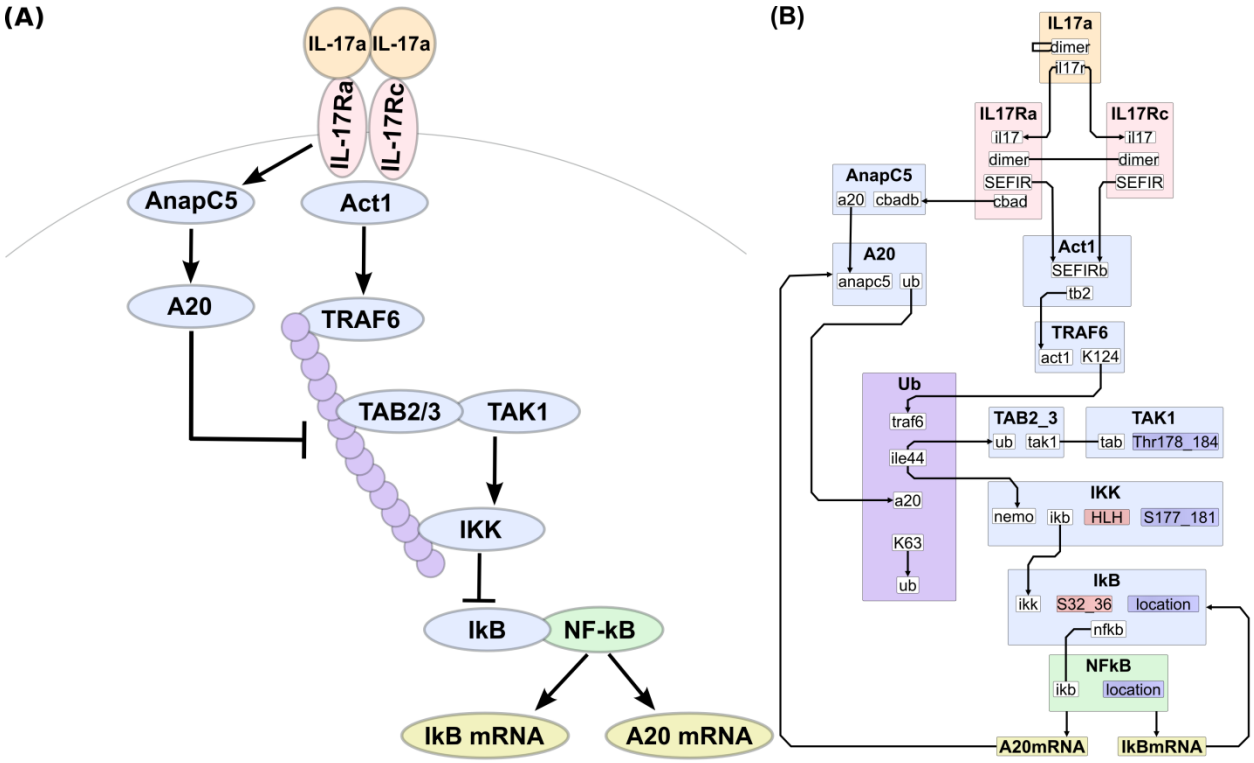

Figure 21 IL-17 signaling model diagram.

(A) The cartoon abstraction shows all molecules considered in the model. Orange elements represent extracellular ligands. Pink elements represent membrane bound receptors. Blue elements indicate intracellular signaling intermediates. Green elements indicate transcription factors. Yellow elements indicate mRNA. Purple elements represent the ubiquitin scaffold. (B) The contact map of the rule-based model specifies all signaling proteins considered in the model, as well as sites for post-translation modifications, localization signals, and additional activation sites. Sites colored pink indicate an inhibitory modification and sites colored blue indicate an activating modification.

after activation by its ligand, IL-17 (Fig 21). For simplicity, we consider only the receptor heterodimer composed of IL-17RA and IL-17RC, as well as the ligand homodimer composed of two IL-17a subunits [262]. Receptor activation is modeled by the single-step binding of the dimeric ligand to the dimeric receptor. This allows the adaptor and E3 ubiquitin ligase Act1 to bind to the active dimer through a SEFIR domain interaction [263]. TRAF6 binds to the TB2 domain of receptor-bound Act1 [244]. Act1 then induces K63-linked polyubiquitination of TRAF6 on its K124 residue [244]. In our model, Act1-TRAF6 binding allows for the initiation and extension of ubiquitin oligomers on TRAF6. Both active ligases are required for chain elongation, the presences of multiple active copies of the ligases increases the rate of elongation. The complex containing TAK1 and TAB2 or TAB3, modeled as a preformed complex, can bind ubiquitin oligomers through TAB2/3's zinc finger domain [264,265]. This binding leads to the activation of TAK1, through autophosphorylation of the threonine 178 and 184 residues in the activation loop [266,267]. The IKK complex, including IKKα, IKKβ, and IKKγ/NEMO, modeled here as a single entity, also binds to the K63-linked ubiquitin oligomers through its NEMO subunit [268,269]. Once bound, IKKβ is phosphorylated on serine 177 and 181 residues by activated TAK1 [265,270], rendering it catalytically active. Active IKK can then autophosphorylate on its helix-loop-helix (HLH) motif, inhibiting kinase activity [270], and phosphorylate IκBα on its serine 32 and 36 residues [271,272]. This phosphorylation targets IκB for K45-linked ubiquitination and proteosomal degradation [273,274]. This degradation is modeled as a deletion of the IκB molecule, releasing the bound NF-κB. Free NF-κB can then be transported to the nucleus. We do not explicitly model the nucleus as a separate compartment, but instead maintain a tag on the NF-κB molecule which indicates its location as being cytoplasmic or nuclear. Once NF-κB has reached the nucleus, it is responsible for the

transcription of IκB [275] and A20 [276] mRNA, leading to the translation of the appropriate protein. Both newly produced proteins act as negative feedback elements on the system. Nascent IκB can travel to the nucleus, again modeled as a change in its location tag, and is able to bind NF-κB, transporting it back to the cytoplasm where it is inactive [277]. A20 binds to adaptor AnapC5, which in turn binds to the IL-17 receptor [278]. A20 is then able to bind to K63-linked ubiquitin chains, breaking them to inhibit the signaling pathway [26]. The final model included 16 molecule types, 64 parameters, and 56 reaction rules.

4.3.2 Model behavior

Using a genetic algorithm encoded in the BioNetFit software[97], the model was calibrated to experimental data illustrating the time course dynamics of A20 and IκB mRNA and protein abundance following stimulation of cells with IL-17. The calibrated model recovers the experimentally seen oscillations in these variables (Fig 22).

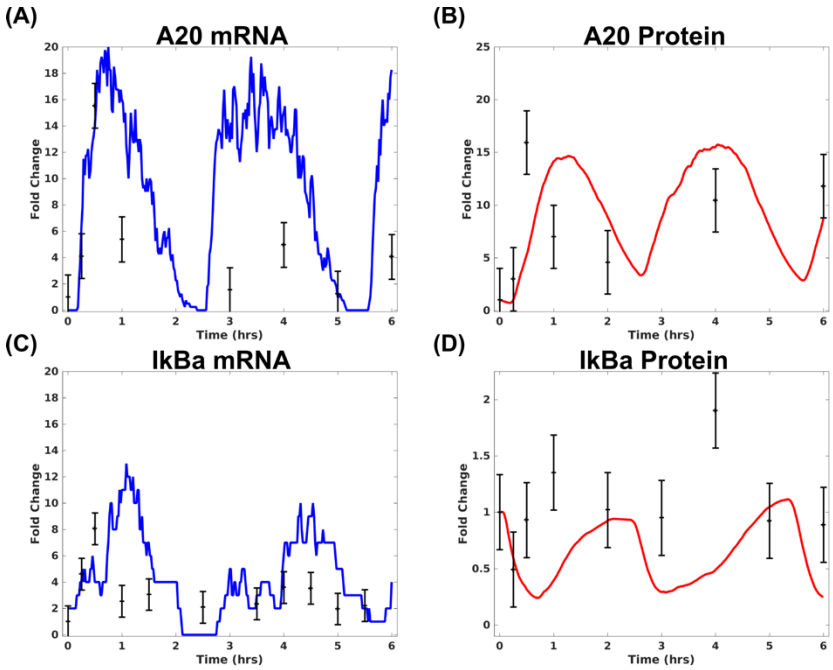

Figure 22 Model time course dynamics of A20 and IκB agree with experimental results.

The NFsim model was fit to qRT-PCR and Western blot time course data for (A-B) A20 and (C-D) IκBα mRNA and protein dynamics for six hours following IL-17 stimulation.

Additionally, NF-κB, responsible for the transcription of both genes, exhibits oscillatory behavior, as has been seen in previous literature studying stimulation by other cytokines [279,280]. Oscillations in the model arise at the level of ubiquitination of TRAF6, due to interactions with A20. Upstream of this ubiquitination, Act1 and TRAF6 are recruited to the receptor and maintained at high levels for the duration of the simulation, as the ligand is maintained in excess and these elements are unaffected by negative feedback (Fig 23A). The subsequent growth of ubiquitin oligomers following Act1-TRAF6 binding acts as a key step, allowing for the activation of TAK1, IKK, and NF-κB, resulting in A20 production, which tempers activation by breaking ubiquitin oligomers. This negative feedback, with a delay

introduced by transcription and translation, results in oscillations in all of the elements involved (Fig 23B).

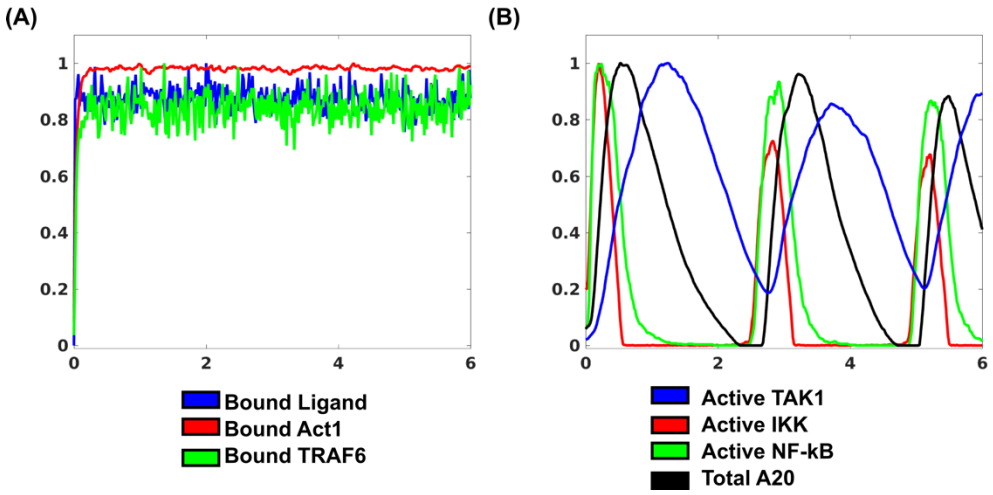

Figure 23 IL-17 signaling dynamics.

(A) Following ligand addition, ubiquitin ligases Act1 and TRAF6 form a complex with the IL-17 receptor. (B) A20-mediated negative feedback causes oscillations in the activation of TAK1, IKK, and NF-κB.

We can better understand the behavior of the system by tracking the formation of ubiquitin scaffolds. Ubiquitin quickly oligomerizes, forming scaffolds containing as many as 13 monomers within 15 minutes. These large scaffolds are also quickly lost; by 30 minutes the largest oligomer size is 4 monomers, coinciding with the nascent production of A20. The growth of large scaffolds (>5 monomers) bears qualitative resemblance to A20 kinetics, showing three distinct peaks at 15 minutes, 2.5 hours, and 5 hours with these scaffolds dissipating each time A20 levels rise (Fig 24 A). Similarly, ubiquitin binding kinases TAK1 and IKK show oscillatory patterns of aggregation. This leads to oscillating levels of kinase activity, indicated by the phosphorylation of activating sites on each (Fig 24 B-C).

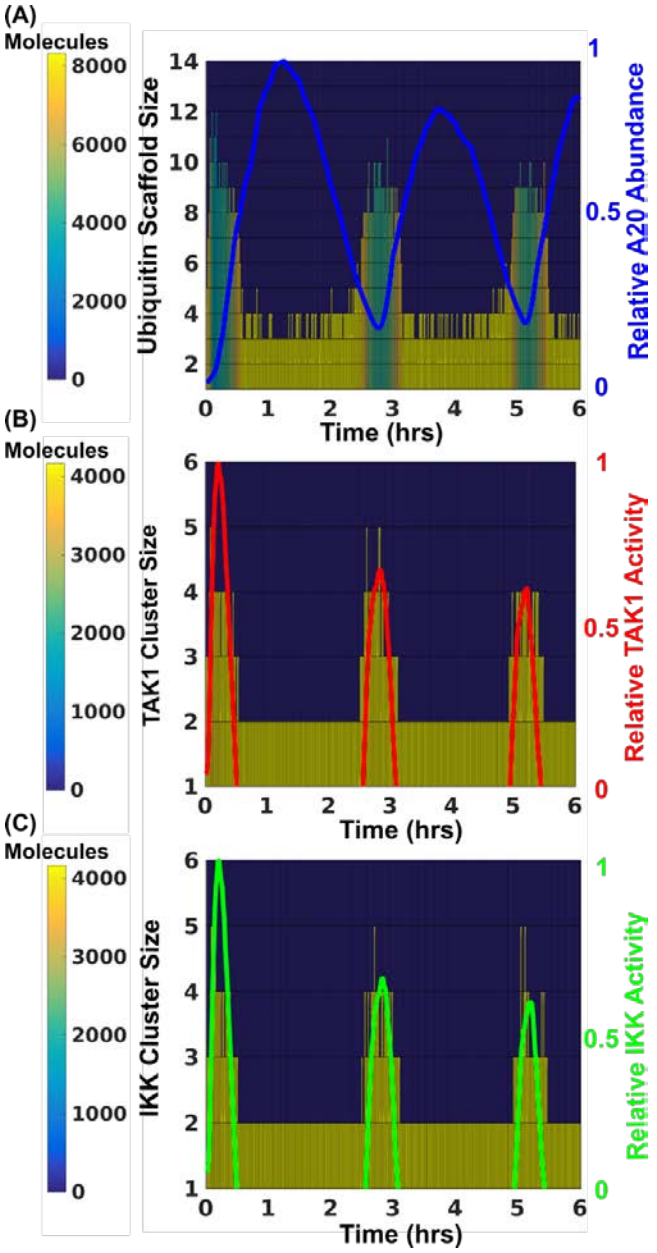

Figure 24 Dynamics of ubiquitin scaffold formation.

(A) Ubiquitin scaffolds composed of up to 13 monomers exhibit oscillatory growth and decay, corresponding to the dynamics of A20 abundance. (B-C) Ubiquitin-binding kinases TAK1 and IKK also exhibit oscillatory behavior in cluster formation and activity.

4.3.3 A20 knockouts

We can knockout A20 in our simulations by setting transcription and translation rate constants to zero. This has no effect on the upstream binding of Act1 and TRAF6 to the IL-17 receptor (Fig 25A), which are not dependent on ubiquitin oligomerization. However, there is a significant effect on the activation of ubiquitin-dependent kinases TAK1 and IKK, and consequently the activation of NF-κB (Fig 25B). All three elements exhibit high levels of activation, increased over their activity levels in WT simulations. Additionally, the higher level of activity is sustained throughout the simulation, as the oscillations they previously exhibited are lost. This corresponds to a sustained increase in ubiquitin oligomerization (Fig 25C). Instead of the oscillations in ubiquitin oligomer size seen in WT simulations, we see the consistent presence of higher order ubiquitin oligomers consisting of 7-12 monomers. This pattern is also seen in TAK1 and IKK clustering (Fig 25D), resulting in the sustained levels of IKK activity. As a result, NF-κB is active throughout the length of the simulation. These simulations compare favorably with previously published experimental reports showing the increased degradation of IκBα in A20 KO MEFs stimulated with IL-17 (Fig 25E-F) [26].

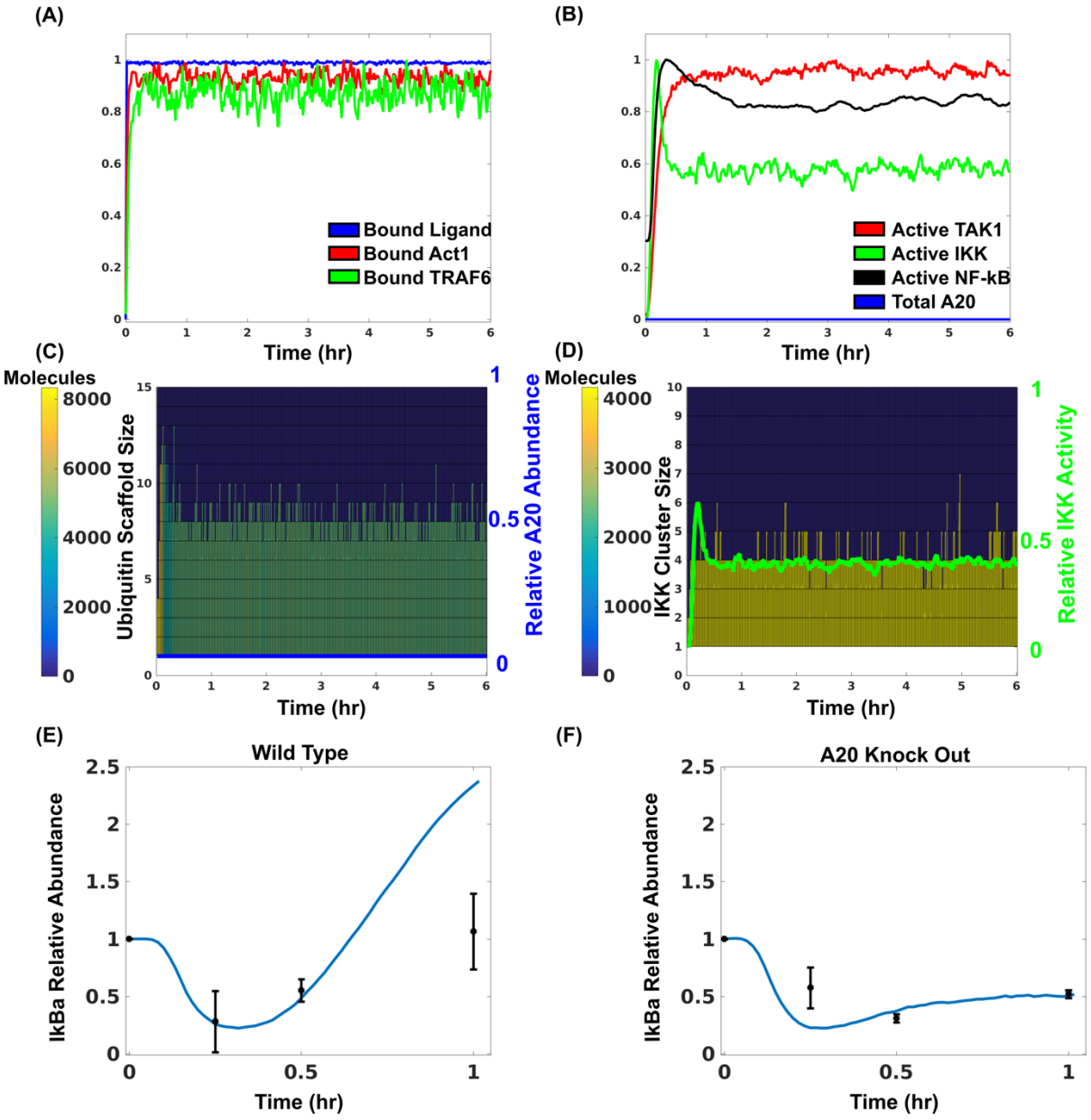

Figure 25 A20 knockout behavior.

(A-B) Despite no change in Act1- or TRAF6-receptor binding, knocking out A20 results in sustained levels of TAK1, IKK, and NF-κB activation. (C-D) Long lasting ubiquitin scaffold formation induces sustained IKK activation. (E-F) Experimental and simulation results agree that A20 knock outs exhibit reduced levels of IκBα following IL-17 stimulation.

4.3.4 Overexpression experiments

By explicitly modeling the oligomerization of ubiquitin and subsequent binding of downstream signaling elements, additional questions are raised. One key consideration is the nature of competitive binding of the ubiquitin-dependent TAK1 and IKK complexes. In our model, these complexes can bind K63-linked ubiquitin chains interchangeably, with their binding affinities and concentrations determining the resulting stoichiometry and consequently their activity levels. As a result, the model predicts that overexpression or underexpression of either of these activators of NF-κB has the potential to lead to the preferential binding of one complex, saturating available ubiquitin scaffolds and squelching the activation of the other (Fig 26A-B). Since activity from both kinases is required to activate NF-κB, interfering with their balance can lead to a loss of activation. In fact, the model predicts that there is an optimal ratio of IKK:TAK1 complexes to induce maximal NF-κB activation of 1:1 (Fig 26C). Increasing the levels of IKK leads to a decrease in TAK1 and IKK activity levels, leading to reduced NF-κB activity (Fig 26D). This indicates that traditional experimental techniques relying on the overexpression or knockdown of members of these complexes could result in non-intuitive effects that are not reflective of the base state of the system, where too much of an inducer leads to repression.

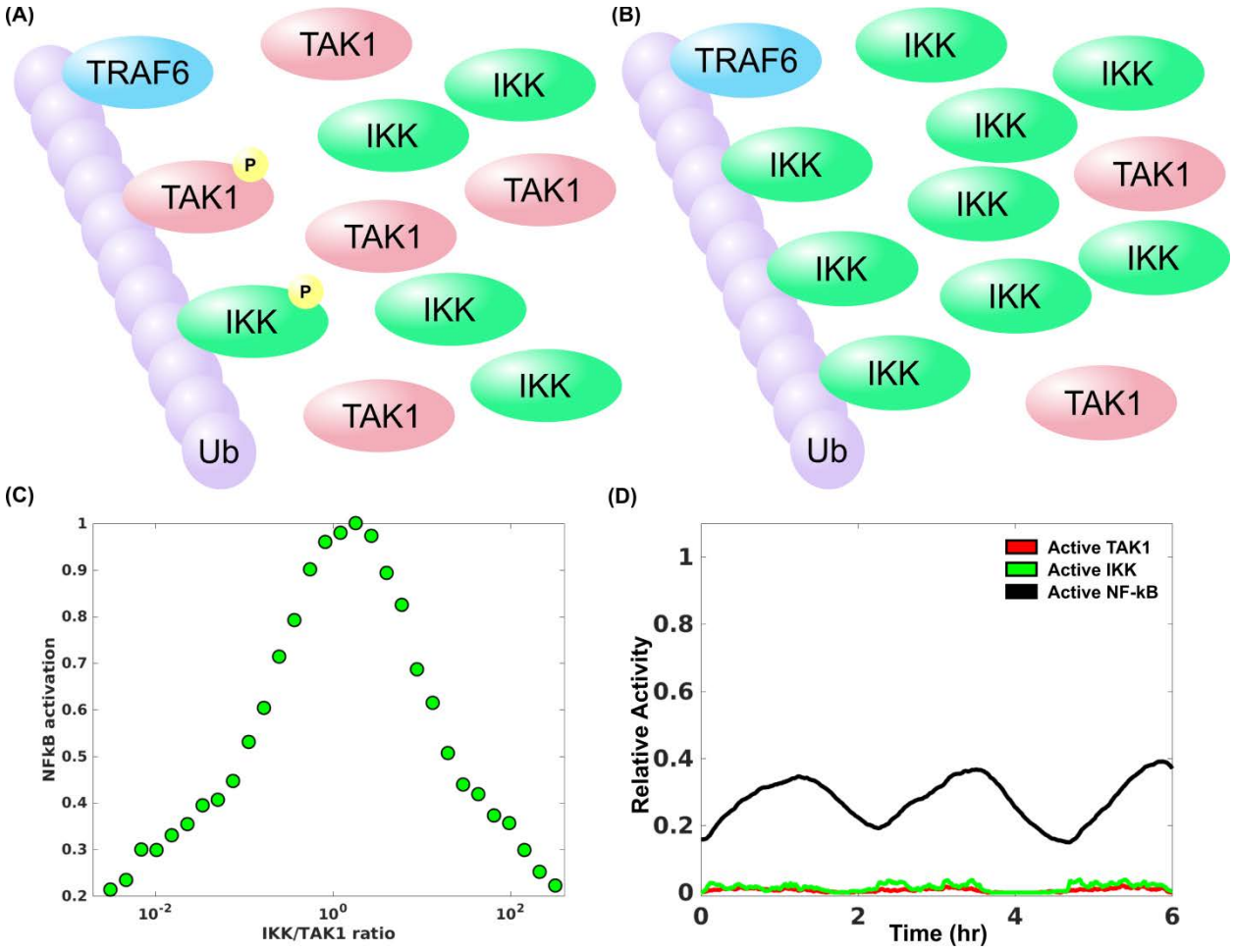

Figure 26 Overexpression of NF-κB IKK and TAK1.

(A-B) Overexpression of NF-κB activators IKK or TAK1 saturates ubiquitin scaffolds, causing reduced phosphorylation and kinase activity. (C) There exists an optimal ratio of TAK1 and IKK to induce maximal NF-κB activation. (D) Overexpression of IKK leads to minimal TAK1 and IKK activity and inhibition of NF-κB activation.

4.4 DISCUSSION

K63-linked ubiquitin scaffolds have long been known to play a key role in NF-κB activation; however, many of the details of their aggregation and dissipation remain unknown because they are difficult to study with traditional biochemical tools. These barriers can often be overcome

using computational modeling, where the costs of experiments are reduced and every species can be tracked without the need for an antibody. However this phenomenon tests even the limits of modeling, due to the theoretical and computational limits imposed by oligomerization. In this study, by using the cutting edge modeling tools now available to us, we can finally tackle this problem. This allows us to predict the size and persistence of ubiquitin scaffolds, as well as the stoichiometry of their binding partners, under various experimental scenarios. It helps us understand what happens when there are perturbations in terms of scaffold building, kinase abundance, and deubiquitinase abundance and effectiveness.

We have long known that A20 plays an important role in limiting the activation of NF-κB. By modeling ubiquitin oligomerization we gain insight into the mechanisms of A20 action, in terms of how it affects scaffold size and persistence, as well as the activation states of ubiquitin binding partners TAK1 and IKK. This allows us to explore the potential effects of mutations in A20 and how they can lead to disease states. Here we see that A20 knockouts are predicted to have long, persistent ubiquitin chains, which lead to consistently high levels of IKK, and thus NF-κB, activity, as seen in previous experimental work [281]. Additionally, by scanning the potential values for A20-ubiquitin affinity we see a range of behaviors from oscillations to persistent activations. Examining these scenarios and their effects on NF-κB activity can provide insight into disorders such as rheumatoid arthritis and psoriasis that have been linked to mutations in A20 and exhibit sustained high levels of inflammation. With this framework we can predict the effects of various potential interventions, such as breaking ubiquitin chains, blocking ubiquitin-kinase interactions with small molecule inhibitors or inhibiting the kinases themselves.

Additional insights can be gained by further extending this model. The current model considers A20's deubiqutinase activity, but A20 is also a ubiquitin ligase, inducing K48-linked ubiquitination that leads to proteosomal degradation of signaling intermediates such as RIP1 and further suppressing NF-κB activity [246]. Expanding the model to include the full range of A20 mechanisms is an important step in assessing it as a treatment target. Additionally, the modeling of ubiquitin oligomerization has been simplified in this model to only allow for K63-linkage and ignoring the effects of branching. In reality, a variety of linkages and structures are possible [282] and considering their impact will influence our understanding of the deubiquitinating and ubiquitin ligase actions of A20. Additionally, considering the spatial impact of branched ubiquitin chains, and the resulting effective proximity of TRAF6, TAK1, and IKK likely plays an important role in the expansion and maintenance of ubiquitin chains, as well as the activation of TAK1 and IKK. Recent advances in network-free spatial simulations should allow us to tackle this problem in the near future.

5.0 CONCLUSIONS

Through the use of mathematical modeling I have identified key signaling features of three immune cell signaling networks that affect immune outcomes. Modeling provided a systematic framework for defining our current understanding of these systems, and to identify important gaps in this knowledge, and new questions that can be answered. A key feature of this study was the use of experimental data to both inform and follow up on all modeling efforts. By calibrating each of the three models to experimental data, I was able to reproduce known, key behaviors of each system, allowing the models to more reliably make new predictions. By using well calibrated models, I was able use model results to directly help define the next experimental steps. In this study I used this cyclic approach combining modeling and experimental efforts to provide insights into three immune cell signaling systems: the role of neutrophil activation in sepsis, the role of T cell receptor signaling in CD4 T cell differentiation, and the role of IL-17-induced ubiquitin scaffold formation on NF-κB activation.

In Chapter 2, I explored the role of neutrophil activation in sepsis. I constructed an ODE model that incorporated the activation of the migratory and killing functions of neutrophils through two surface receptors, CXCR1 and CXCR2. Additionally, the model incorporated the ability of fully activated neutrophils to kill a dynamic infection, and for improperly activated neutrophils to cause tissue damage and inflammation, leading to further neutrophil activation. I then calibrated the model to two data sets, one from animals that survived the infection, and one

from animals that succumbed to the infection. By calibrating the model to both data sets, I was able to show how one network architecture was able to capture a range of population behaviors, through a change in parameter values. Additionally, the model made predictions on non-fitted variables, and how they varied across our two populations. Notably, the model predicted that the killer neutrophil population would be elevated in the non-surviving population. This neutrophil phenotype is associated with neutrophil induced tissue damage in the model. Multiple studies support this finding, indicating that non-survivors or those with more severe sepsis experience increased levels of neutrophil induced tissue damage and myeloperoxidase (MPO) generation, indicative of degranulation [102,148–151]. In an attempt to combat the induction of tissue damage, I modeled a treatment aimed at blocking the activation of CXCR1 and CXCR2, reducing neutrophil activation. The proposed treatment was successful in improving survival rates from 31% to above 80% under optimized treatment conditions. The most important treatment variable for optimization was the time following infection at which treatment was started. The model predicted a narrow band of time where treatment would be most effective, between 3 and 6 hours following infection. It also predicted that beginning treatment within the first two hours could be detrimental, increasing mortality. This shows that while the treatment can conceptually be quite effective, optimization of its delivery is critical, and this optimization can be most safely and efficiently done using a model calibrated to patient data.

In chapter 3 I used two modeling approaches to identify key features of T cell receptor signaling that affect CD4 T cell differentiation decision making. First, by using Boolean modeling, I identified a minimal network that could recover key experimental results regarding the dynamics of PTEN abundance and FoxO1 phosphorylation. This allowed us to narrow our focus onto a positive feedback loop containing these elements, directing further experimental

work and model construction. Additional experiments allowed us to calibrate a novel rule-based model, which allowed us to quantitatively model the dynamics of this signaling network. By calibrating the model to data gathered following two different doses of antigen, I was able to model how a small change in dose can lead to dramatically different signaling dynamics. This lead to the model prediction of a threshold in antigen dose separating two stable steady states, a $PTEN^{hi}$ Akt^{lo} state that corresponds to a Treg fate and a $PTEN^{lo}$ Akt^{hi} state that corresponds to a Th fate. The model further predicted that commitment to these two states was also affected by the duration of antigen stimulation, thus creating a two-dimensional threshold on dose and time indicative of total activation of the T cell receptor. The presence of this threshold was confirmed experimentally, as was the model prediction that threshold could be shifted by reducing the expression level of PTEN in naïve cells. This detailed model of signaling downstream of the T cell receptor was then used to build a multi-scale cell population model. This model showed that the relative size and effectiveness of Treg and Th populations has a dramatic effect on the clearance of an infection, with different scenarios leading to a recurrence or clearance of the infection. This model also has the potential for significant expansion. By adding key signaling elements to the model, such as transcription factors Foxp3 ant T-bet, both of which act as differentiation markers and play important mechanistic roles in Treg and Th stability, the model will be significantly more accurate, by including the final steps necessary to lock in differentiation. Additionally, the model could be used to tackle more specific scenarios, such as individual infections with unique dynamics and responses, and the effects of relative Treg and Th populations size on transplant rejection and vaccine development.

In chapter 4, I examined the activation of NF-κB by the cytokine IL-17, one of the less studied activators of NF-κB. The interest in this system was sparked by the experimental finding

of ubiquitin-editing enzyme A20 as a negative feedback mediator in the pathway. This led to the development of a novel rule-based model focused on the formation of K63-linked ubiquitin scaffolds and the mechanisms of A20 involved in breaking these scaffolds. The model was simulated using NFsim, allowing for the explicit modeling of ubiquitin oligomerization, and resulting in a model larger in scope than previous models of NF-κB activation that simplified this process [69,250,255,283]. Following calibration to experimental data, the model predicted the formation of ubiquitin oligomers containing up to 12 monomers. These oligomers were disrupted following the A20 transcription and translation, induced by NF-κB, which in turn led to a decrease in NF-κB activity an A20 production. A20-mediated negative feedback resulted in oscillating formation of ubiquitin scaffolds and characteristic oscillations of NF-κB. Additionally, the oscillating nature of scaffold formation led to the transient formation of clusters of IKK and TAK1, as they bound to the scaffolds, which we hope to confirm experimentally. The model also predicts that knocking out A20 breaks the oscillations, leading to sustained high levels of NF-κB activity, which was confirmed by experiments showing sustained low levels of IκB in A20 KO cells stimulated with IL-17, indicating sustained high levels of NF-κB activity. Finally, the model predicts that the relative expression levels of IKK and TAK1 play a significant role in the potential of the system to activate NF-κB. Overexpressing one protein or the other could, counterintuitively, inhibit activation of NF-κB. This model prediction leads to the conclusion that overexpressing either of these proteins in an experiment could alter results in an unintended way, and further points to the need for technologies like CRIPSR/Cas9 that allow for the expression of modified proteins at an endogenous level [284,285].

These three studies applied mathematical modeling in varied immunological systems to advance the state of the field. I showed that modeling can be effectively used to attack a wide

range of problems in a biological discipline, immunology, which requires a significant commitment on the part of the modeler to learn and understand. Additionally, by heavily incorporating data and input from experimentalists, it was possible to efficiently build and calibrate models capable of making new predictions and designing new experiments, ranging from simulations of small scale in vitro systems to testing potential clinical treatments. By applying this methodology to three different systems, I demonstrated the flexibility models provide to give insight into a wide range of problems. When combined with an initial effort to understand the biological field of interest, in this case immunology, it is possible to work on a number of problems that, while quite different, may overlap in a number of key features. In this thesis I was able to study three systems in a coherent way due to their shared relation to important immune disorders, the shared concept of positive and negative feedback fine tuning immune activation, and recurring signaling motifs and dynamics. This shared conceptual backbone allowed my approach to lead to a number of novel results in three different systems, and allows it to have great potential to be used for a wide range of studies in the future, both within the field of immunology and the wider scope of biology.

APPENDIX A T CELL BOOLEAN MODEL

```
# Translation of Boolean model in Reduced Boolean T-Cell model.txt to BNGL format within the GSP (Gillespie) update mode.
begin model
begin parameters
end parameters
begin molecule types
  tcr(state~0~1)
  tcr_low(state~0~1)
  tcr_high(state~0~1)
  mek1(state~0~1)
  pip3(state~0~1)
  pten_total(state~0~1)
  pten_active(state~0~1)
  akt(state~0~1)
  foxo1(state~0~1)
  ck2(state~0~1)
  mtorc2(state~0~1)
  nedd4(state~0~1)
end molecule types
begin seed species
  tcr(state~0) 1
  tcr_low(state~0) 1
  tcr_high(state~1) 1
  mek1(state~0) 1
  pip3(state~0) 1
  pten_total(state~1) 1
  pten_active(state~0) 1
  akt(state~0) 1
  foxo1(state~1) 1
  ck2(state~0) 1
  mtorc2(state~0) 1
  nedd4(state~0) 1
end seed species
begin observables
  Molecules TCR tcr(state~1)
```

```
  Molecules TCR_LOW tcr_low(state~1)
  Molecules TCR_HIGH tcr_high(state~1)
  Molecules MEK1 mek1(state~1)
  Molecules PIP3 pip3(state~1)
  Molecules PTEN_TOTAL pten_total(state~1)
  Molecules PTEN_ACTIVE pten_active(state~1)
  Molecules AKT akt(state~1)
  Molecules FOXO1 foxo1(state~1)
  Molecules CK2 ck2(state~1)
  Molecules MTORC2 mtorc2(state~1)
  Molecules NEDD4 nedd4(state~1)
end observables
begin functions
  tcr_func() if(TCR_LOW>0.5 || TCR_HIGH>0.5, 1, 0)
  ck2_func() if(TCR_HIGH>0.5, 1, 0)
  mek1_func() if(TCR>0.5, 1, 0)
  pip3_func() if(TCR>0.5 && PTEN_ACTIVE<0.5, 1, 0)
  mtorc2_func() if(TCR>0.5 && AKT<0.5, 1, 0)
  akt_func() if(PIP3>0.5 && MTORC2>0.5, 1, 0)
  pten_total_func() if(FOXO1>0.5 && NEDD4<0.5, 1, 0)
  pten_active_func() if(PTEN_TOTAL>0.5 && MEK1>0.5 && CK2<0.5, 1, 0)
  foxo1_func() if(AKT<0.5, 1, 0)
  nedd4_func() if(TCR_HIGH>0.5, 1, 0)
end functions
begin reaction rules
  R1: tcr(state) -> tcr(state~1) if(tcr_func()>0.5,1,0)
  R2: tcr(state) -> tcr(state~0) if(tcr_func()<0.5,1,0)
  R3: ck2(state) -> ck2(state~1) if(ck2_func()>0.5,1,0)
  R4: ck2(state) -> ck2(state~0) if(ck2_func()<0.5,1,0)
  R5: mek1(state) -> mek1(state~1) if(mek1_func()>0.5,1,0)
  R6: mek1(state) -> mek1(state~0) if(mek1_func()<0.5,1,0)
  R7: pip3(state) -> pip3(state~1) if(pip3_func()>0.5,1,0)
  R8: pip3(state) -> pip3(state~0) if(pip3_func()<0.5,1,0)
  R9: mtorc2(state) -> mtorc2(state~1) if(mtorc2_func()>0.5,1,0)
  R10: mtorc2(state) -> mtorc2(state~0) if(mtorc2_func()<0.5,1,0)
  R11: akt(state) -> akt(state~1) if(akt_func()>0.5,1,0)
  R12: akt(state) -> akt(state~0) if(akt_func()<0.5,1,0)
  R13: pten_total(state) -> pten_total(state~1) if(pten_total_func()>0.5,1,0)
  R14: pten_total(state) -> pten_total(state~0) if(pten_total_func()<0.5,1,0)
  R15: pten_active(state) -> pten_active(state~1) if(pten_active_func()>0.5,1,0)
  R16: pten_active(state) -> pten_active(state~0) if(pten_active_func()<0.5,1,0)
  R17: foxo1(state) -> foxo1(state~1) if(foxo1_func()>0.5,1,0)
  R18: foxo1(state) -> foxo1(state~0) if(foxo1_func()<0.5,1,0)
  R19: nedd4(state) -> nedd4(state~1) if(nedd4_func()>0.5,1,0)
  R20: nedd4(state) -> nedd4(state~0) if(nedd4_func()<0.5,1,0)
end reaction rules
```

```
end model

 generate_network({overwrite=>1})

# Simulate for 30 time units, outputting every time unit.
# simulate({method=>"ssa",t_end=>30,n_steps=>30,print_CDAT=>0,verbose=>1})
parameter_scan({parameter=>"x",par_min=>1,par_max=>1000,n_scan_pts=>10000,method=>"
ssa",t_end=>30,n_steps=>300,log_scale=>0})
```

APPENDIX B T CELL RULE-BASED MODEL

```
begin model

begin molecule types

Antigen(tcr)
TCR(antigen,pi3k,mek1,ck2,nedd4,active~N~Y)
Anti_CD28(cd28)
CD28(anticd28,pi3k)
PIP(site3~U~P,site4~U~P,site5~U~P)
Akt(Thr308~U~P,Ser473~U~P,location~N~C)
FoxO1(Thr24~U~P,location~N~C)
PTEN(phosphotase,Cterminus~U~P,Lys289~N~U)
mRNA_PTEN()
mTORC2(active~Y~N)
NEDD4(active~Y~N)
CK2(active~Y~N)
PDK1(Ser241~U~P)
PI3K(kinase~U~P)
DNA()

end molecule types

begin parameters
#Initial Conditions
ag_init             0#1e3
anti_cd28_init 6423600
tcr_init        222131.433804039
pip_init            268676.057686858
akt_init            13148.5790742440
foxo1_init          70437.7136425992
pten_init           0#102973.666291009
mrna_init           0#227.243338808808
mtorc2_init         369664.061790713
nedd4_init          66604.7986196980
ck2_init            252561.753786331
```

pdk1_init 89586.2452041245
pi3k_init 37411.0689919672
dna_init 2

#Rate Parameters

##############################
Receptor Activation#####
##############################

ag_bind 1.93414932224711e-10
ag_unbind 0.00421914124248945

ag_degrade 0

cd28_bind 1.01692303284445e-08
cd28_unbind 0.0630312241578351

############################
PI3K Regulation
############################

tcr_pi3k_bind 1.92290079749878e-09
tcr_pi3k_unbind 0.0394594555725759
pi3k_activate 2.30860757132927

cd28_pi3k_bind 8.35061093754634e-09
cd28_pi3k_unbind 0.0119394273501131
cd28_pi3k_activate 0.000123356909024155

pi3k_deactivate 0.0115752585350904

############################
PIP3 Regulation
############################

pi3k_pip_bind 1.12900473659142e-06
pi3k_pip_unbind 0.00604116094672570
pip_phos 5.28207208698330

pip_pten_bind 3.64067883116676e-06
pip_pten_unbind 0.00332555476889872
pip_dephos 0.0139164218145688
pip_basal_dephos 5.18125668655747e-07

##############################

mTORC2 Regulation
##############################

pip_mtorc2_bind 6.88554978507705e-07
pip_mtorc2_unbind 0.00755255942626148

mtorc2_activate 0.208188395579049
mtorc2_deactivate 0.000856554171559535
mtorc2_deactivate_akt 0.126150879675625

############################
PDK1 Regulation
############################

pdk1_pip_bind 5.43808753228395e-05
pdk1_pip_unbind 0.000323284335250397

pdk1_phos 0.0669279737743035
pdk1_dephos 0.0117743994900832

##############################
Akt Phosphorylation
##############################

pdk1_akt_bind 5.54716991168108e-06
pdk1_akt_unbind 0.0928764331259890
akt_308_phos 0.0554514172147590

akt_mtorc2_bind 4.99637687099694e-05
akt_mtorc2_unbind 0.0167431982343445
akt_473_phos 0.222582339071364

#k_akt_dephos_cyt 0.0453528916501944
k_akt_dephos_cyt_308 0.000000272678140384009
k_akt_dephos_cyt_473 0.00552041927637364
k_akt_dephos_nuc 5.790165734953087

############################
Akt Trafficking
############################

k_akt_to_nucleus 1.36668039145470
k_akt_to_cytoplasm 0.0374287215769002

##############################
FoxO1 Regulation

```
################################

akt_foxo_bind          1.37603684881592e-07
akt_foxo_unbind              0.0240779171674433

foxo_phos                    3.01201504185128
foxo_dephos                  0.0109508938521131

foxo_to_cytoplasm   0.0286091642780725
foxo_to_nucleus              2.93549890502400

####################################
##### PTEN Activity Regulation #####
####################################

tcr_ck2_bind           7.61843551839876e-06
tcr_ck2_unbind               0.00351838946742571
ck2_activate           0.00760125824376341
ck2_deactivate         0.00218552424201488

ck2_pten_bind          9.67845377018764e-06
ck2_pten_unbind              0.000166980309081892
pten_phos                    0.0299758021287826
pten_dephos                  0.000980190236401325

############################
##### mRNA Regulation #####
############################

pten_transcription     0.0418815630433629
N                                  20.1167897537963
KM_dna_foxo                  41724.8865217653

mrna_degrade           9.55128939409137e-05

####################################
##### PTEN Abundance Regulation #####
####################################

pten_translation       0.190141311816498
pten_degrade           0.00260604371372528
pten_degrade_phos      1.25062440770540e-08

tcr_nedd4_bind               1.28506698911784e-06
tcr_nedd4_unbind       0.00483638634028418
nedd4_activate               0.00383244995763267
```

```
nedd4_deactivate        0.479390168402672

nedd4_pten_bind             1.13502110339800e-07
nedd4_pten_unbind       0.00169391220994697
pten_ubiq                   0.317447278265800
pten_debuiq                 0.000151878745716983
pten_ubiq_degrade       0.0698346102188455

end parameters

begin seed species

Antigen(tcr)                                    ag_init
Anti_CD28(cd28)                                 anti_cd28_init
TCR(antigen,pi3k,mek1,ck2,nedd4,active~N)       tcr_init
CD28(anticd28,pi3k)                             tcr_init
PIP(site3~U,site4~P,site5~P)                    pip_init
Akt(Thr308~U,Ser473~U,location~C)               akt_init
FoxO1(Thr24~U,location~N)                       foxo1_init
PTEN(phosphotase,Cterminus~U,Lys289~N)          pten_init
mRNA_PTEN()                                     mrna_init
mTORC2(active~N)                                mtorc2_init
NEDD4(active~N)                                 nedd4_init
CK2(active~N)                                   ck2_init
PDK1(Ser241~U)                                  pdk1_init
PI3K(kinase~U)                                  pi3k_init
DNA()                                           dna_init

end seed species

begin observables

Molecules   pten            PTEN()
Molecules   pten_mrna       mRNA_PTEN()
Molecules   akt_p308        Akt(Thr308~P!?)
Molecules   akt_p473        Akt(Ser473~P!?)
Molecules   foxo_p          FoxO1(Thr24~P!?)
Molecules   total_foxo      FoxO1()
Molecules   active_foxo     FoxO1(Thr24~U,location~N)
Molecules   total_akt       Akt()
Molecules   active_akt      Akt(Thr308~P!?,Ser473~P!?)
Molecules   active_nedd4    NEDD4(active~Y!?)
Molecules   Bound_Ag        Antigen(tcr!+)

end observables
```

```
begin functions
        transcription() = pten_transcription*active_foxo^N/(KM_dna_foxo^N + active_foxo^N)
end functions

begin reaction rules

##############################
##### Receptor Activation#####
##############################

#Antigen-receptor binding
Antigen(tcr) + TCR(antigen) <-> Antigen(tcr!1).TCR(antigen!1)    ag_bind,ag_unbind
#TCR(antigen) <-> Antigen(tcr!1).TCR(antigen!1)  ag_init*ag_bind,ag_unbind

#Receptor activation
#Antigen(tcr!1).TCR(antigen!1,active~N)        <->        Antigen(tcr!1).TCR(antigen!1,active~Y)
        ag_rec_activate,ag_rec_deactivate
#TCR(antigen,active~N) <-> TCR(antigen,active~Y)         rec_activate,rec_deactivate

#antigen deg
Antigen(tcr) -> 0 ag_degrade

#CD28-anti_CD28 binding
CD28(anticd28)      +      Anti_CD28(cd28)      <->      CD28(anticd28!1).Anti_CD28(cd28!1)
        cd28_bind,cd28_unbind
#CD28(anticd28)                    <->                    CD28(anticd28!1).Anti_CD28(cd28!1)
        anti_cd28_init*cd28_bind,cd28_unbind
############################
##### PI3K Regulation #####
############################

#Bound receptor activates PI3K
TCR(antigen!+,pi3k,mek1,ck2,nedd4)          +          PI3K(kinase~U)          <->
TCR(antigen!+,pi3k!1,mek1,ck2,nedd4).PI3K(kinase~U!1) tcr_pi3k_bind,tcr_pi3k_unbind
TCR(pi3k!1).PI3K(kinase~U!1) -> TCR(pi3k) + PI3K(kinase~P)    pi3k_activate
TCR(antigen,pi3k!1).PI3K(kinase~U!1)      ->      TCR(antigen,pi3k)      +      PI3K(kinase~U)
        tcr_pi3k_unbind

#Bound receptor activates PI3K
CD28(anticd28!+,pi3k)  +  PI3K(kinase~U)  <->  CD28(anticd28!+,pi3k!1).PI3K(kinase~U!1)
        cd28_pi3k_bind,cd28_pi3k_unbind
CD28(pi3k!1).PI3K(kinase~U!1) -> CD28(pi3k) + PI3K(kinase~P)          cd28_pi3k_activate
CD28(anticd28,pi3k!1).PI3K(kinase~U!1)    ->    CD28(anticd28,pi3k)    +    PI3K(kinase~U)
        cd28_pi3k_unbind
```

```
#PI3K deactiavtes when unbound
PI3K(kinase~P) -> PI3K(kinase~U)  pi3k_deactivate

############################
##### PIP3 Regulation #####
############################

#PI3K converts PIP2 to PIP3
PI3K(kinase~P) + PIP(site3~U,site4~P,site5~P) <->
PI3K(kinase~P!1).PIP(site3~U!1,site4~P,site5~P)  pi3k_pip_bind,pi3k_pip_unbind
PI3K(kinase~P!1).PIP(site3~U!1,site4~P,site5~P) -> PI3K(kinase~P) +
PIP(site3~P,site4~P,site5~P)  pip_phos

#PTEN converts PIP3 back to PIP2
PIP(site3~P,site4~P,site5~P) + PTEN(phosphotase,Cterminus~U,Lys289~N) <->
PIP(site3~P!1,site4~P,site5~P).PTEN(phosphotase!1,Cterminus~U,Lys289~N)
pip_pten_bind,pip_pten_unbind
PIP(site3~P!1,site4~P,site5~P).PTEN(phosphotase!1,Cterminus~U,Lys289~N) ->
PIP(site3~U,site4~P,site5~P) + PTEN(phosphotase,Cterminus~U,Lys289~N) pip_dephos

#Basal dephos
PIP(site3~P,site4~P,site5~P) -> PIP(site3~U,site4~P,site5~P) pip_basal_dephos

#################################
##### mTORC2 Regulation ########
#################################

PIP(site3~P) + mTORC2(active~N) <-> PIP(site3~P!1).mTORC2(active~N!1)
pip_mtorc2_bind,pip_mtorc2_unbind
PIP(site3~P!1).mTORC2(active~N!1) -> PIP(site3~P) + mTORC2(active~Y)
        mtorc2_activate
mTORC2(active~Y) -> mTORC2(active~N) mtorc2_deactivate

#Akt~p308 deactivates mTORC2
mTORC2(active~Y) + Akt(Thr308~P,Ser473~?,location~C) <->
mTORC2(active~Y!1).Akt(Thr308~P!1,Ser473~?,location~C)
        akt_mtorc2_bind,akt_mtorc2_unbind
mTORC2(active~Y!1).Akt(Thr308~P!1,location~C) -> mTORC2(active~N) +
Akt(Thr308~P,location~C)  mtorc2_deactivate_akt

mTORC2(active~N!1).Akt(Thr308~?!1) -> mTORC2(active~N) + Akt(Thr308~?)
akt_mtorc2_unbind
mTORC2(active~N!1).Akt(Ser473~?!1) -> mTORC2(active~N) + Akt(Ser473~?)
akt_mtorc2_unbind

############################
```

```
##### PDK1 Regulation #####
############################

PDK1(Ser241~U) + PIP(site3~P,site4~P,site5~P) <->
PDK1(Ser241~U!1).PIP(site3~P!1,site4~P,site5~P) pdk1_pip_bind,pdk1_pip_unbind
PDK1(Ser241~U!1).PIP(site3~P!1,site4~P,site5~P) -> PDK1(Ser241~P) +
PIP(site3~P,site4~P,site5~P) pdk1_phos

PDK1(Ser241~P) -> PDK1(Ser241~U) pdk1_dephos

################################
##### Akt Phosphorylation #####
################################

#PDK1 phosphorylates Akt thr308
PDK1(Ser241~P) + Akt(Thr308~U,location~C) <->
PDK1(Ser241~P!1).Akt(Thr308~U!1,location~C) pdk1_akt_bind,pdk1_akt_unbind
PDK1(Ser241~P!1).Akt(Thr308~U!1,location~C) -> PDK1(Ser241~P) +
Akt(Thr308~P,location~C) akt_308_phos

#mTORC2 phosphorylates Akt ser473
mTORC2(active~Y) + Akt(Ser473~U,location~C) <->
mTORC2(active~Y!1).Akt(Ser473~U!1,location~C) akt_mtorc2_bind,akt_mtorc2_unbind
mTORC2(active~Y!1).Akt(Ser473~U!1,location~C) -> mTORC2(active~Y) +
Akt(Ser473~P,location~C) akt_473_phos

#Akt deactivates in cytoplasm
Akt(Thr308~P,location~C) -> Akt(Thr308~U,location~C) k_akt_dephos_cyt_308 #Implicit
phosphotase
Akt(Ser473~P,location~C) -> Akt(Ser473~U,location~C) k_akt_dephos_cyt_473 #Implicit
phosphotase

#Akt is deactivated in the nucleus
Akt(Thr308~P,Ser473~P,location~N) -> Akt(Thr308~U,Ser473~U,location~N)
        k_akt_dephos_nuc #implicit phopsphotase

############################
##### Akt Trafficking #####
############################

#Akt translocates to the nucleus when active
Akt(Thr308~P,Ser473~P,location~C) -> Akt(Thr308~P,Ser473~P,location~N)
        k_akt_to_nucleus

#Akt goes back to cytoplasm when inactive
```

```
Akt(Thr308~U,Ser473~U,location~N) -> Akt(Thr308~U,Ser473~U,location~C)
        k_akt_to_cytoplasm

################################
##### FoxO1 Regulation #########
################################

#Active Akt in the nucleus leads to phosphorylation of FoxO1
Akt(Thr308~P,Ser473~P,location~N) + FoxO1(Thr24~U,location~N) <->
Akt(Thr308~P!1,Ser473~P,location~N).FoxO1(Thr24~U!1,location~N)
        akt_foxo_bind,akt_foxo_unbind
Akt(Thr308~P!1,Ser473~P,location~N).FoxO1(Thr24~U!1,location~N) ->
Akt(Thr308~P,Ser473~P,location~N) + FoxO1(Thr24~P,location~N)  foxo_phos

#FoxO1 is dephosphorylated in the cytoplasm
FoxO1(Thr24~P,location~C) -> FoxO1(Thr24~U,location~C)  foxo_dephos

#Phosphorylated FoxO1 moves to the cytoplasm
FoxO1(Thr24~P,location~N) -> FoxO1(Thr24~P,location~C)  foxo_to_cytoplasm

#FoxO1 moves back to the nucleus once dephosphorylated
FoxO1(Thr24~U,location~C) -> FoxO1(Thr24~U,location~N)  foxo_to_nucleus

#####################################
##### PTEN Activity Regulation #####
#####################################
#TCR activates CK2
#CK2 phosphorylates PTEN
TCR(antigen!+,ck2,pi3k,mek1,nedd4) + CK2(active~N) <->
TCR(antigen!+,ck2!1,pi3k,mek1,nedd4).CK2(active~N!1)  tcr_ck2_bind,tcr_ck2_unbind
TCR(ck2!1).CK2(active~N!1) -> TCR(ck2) + CK2(active~Y)  ck2_activate
TCR(antigen,ck2!1).CK2(active~N!1) -> TCR(antigen,ck2) + CK2(active~N)
        tcr_ck2_unbind
CK2(active~Y!?) -> CK2(active~N!?) ck2_deactivate

CK2(active~Y) + PTEN(phosphotase,Cterminus~U,Lys289~N) <->
CK2(active~Y!1).PTEN(phosphotase,Cterminus~U!1,Lys289~N)
        ck2_pten_bind,ck2_pten_unbind
CK2(active~Y!1).PTEN(phosphotase,Cterminus~U!1,Lys289~N) -> CK2(active~Y) +
PTEN(phosphotase,Cterminus~P,Lys289~N)  pten_phos

CK2(active~N!1).PTEN(Cterminus~?!1) -> CK2(active~N) + PTEN(Cterminus~?)
        ck2_pten_unbind

PTEN(phosphotase,Cterminus~P,Lys289~?) -> PTEN(phosphotase,Cterminus~U,Lys289~?)
        pten_dephos
```

```
#####################################
##### mRNA Regulation #####
#####################################

#Transcription
DNA() -> DNA() + mRNA_PTEN() transcription()
#FoxO1(Thr24~U,location~N) -> FoxO1(Thr24~U,location~N) + mRNA_PTEN(stable~Y)
        pten_transcription

#mRNA degradation
mRNA_PTEN() -> 0  mrna_degrade

#####################################
##### PTEN Abundance Regulation #####
#####################################

#Translation
mRNA_PTEN() -> mRNA_PTEN() + PTEN(phosphotase,Cterminus~U,Lys289~N)
        pten_translation

#PTEN degradation
PTEN(Cterminus~U) -> 0 pten_degrade       DeleteMolecules
PTEN(Cterminus~P) -> 0 pten_degrade_phos          DeleteMolecules

#TCR activates NEDD4
#NEDD 4 ubiquitinates PTEN (K45)
TCR(antigen!+,nedd4,pi3k,mek1,ck2)              +              NEDD4(active~N)              <->
TCR(antigen!+,nedd4!1,pi3k,mek1,ck2).NEDD4(active~N!1)
        tcr_nedd4_bind,tcr_nedd4_unbind
TCR(nedd4!1).NEDD4(active~N!1) -> TCR(nedd4) + NEDD4(active~Y) nedd4_activate
TCR(antigen,nedd4!1).NEDD4(active~N!1) -> TCR(antigen,nedd4) + NEDD4(active~N)
        tcr_nedd4_unbind
NEDD4(active~Y!?) -> NEDD4(active~N!?) ck2_deactivate

NEDD4(active~Y)          +          PTEN(phosphotase,Cterminus~U,Lys289~N)          <->
NEDD4(active~Y!1).PTEN(phosphotase,Cterminus~U,Lys289~N!1)
        nedd4_pten_bind,nedd4_pten_unbind
NEDD4(active~Y!1).PTEN(phosphotase,Cterminus~U,Lys289~N!1) -> NEDD4(active~Y) +
PTEN(phosphotase,Cterminus~U,Lys289~U)          pten_ubiq
PTEN(Lys289~U!?) -> 0       pten_ubiq_degrade     DeleteMolecules
NEDD4(active~?!1).PTEN(Cterminus~?!1)          ->          NEDD4(active~?).PTEN(Cterminus~?)
        nedd4_pten_unbind
```

```
end reaction rules
end model

generate_network({overwrite=>1})
writeMexfile()
writeMfile()

#Equil
setConcentration("Antigen(tcr)",0)
setConcentration("Anti_CD28(cd28)",0)
simulate({method=>"ode",t_end=>1e7,n_steps=>250})

#Sim
setConcentration("Anti_CD28(cd28)",6423600)
##setParameter("ag_init",6423600)
setConcentration("Antigen(tcr)",1605900) #1605900, 6423600
simulate_ode({t_start=>0,t_end=>10*60*60,n_steps=>1000,atol=>1e-8,rtol=>1e-8});


########################
##### Bifurcations #####
########################

#setConcentration("Anti_CD28(cd28)","anti_cd28_init")
#setConcentration("Antigen(tcr)","ag_init")
#bifurcate({parameter=>"ag_init",par_min=>1e6,par_max=>1e7,n_scan_pts=>100,log_scale=>
0,method=>"ode",t_end=>1e7,n_steps=>1000})

##################
##### Pulses #####
##################
#setConcentration("Anti_CD28(cd28)","anti_cd28_init")
#setConcentration("Antigen(tcr)",6423600);
#simulate_ode({t_start=>0,t_end=>50000,n_steps=>100,atol=>1e-8,rtol=>1e-8});

#setConcentration("Antigen(tcr)",0);
#setParameter("ag_degrade",1e8);
#simulate_ode({continue=>1,t_start=>50000,t_end=>1000000,n_steps=>1e4,atol=>1e-
8,rtol=>1e-8});

#setParameter("ag_degrade",0);
#setConcentration("Antigen(tcr)",1e2);
#simulate_ode({continue=>1,t_start=>35000,t_end=>50000,n_steps=>100,atol=>1e-8,rtol=>1e-
8});

#setConcentration("Antigen(tcr)",0);
```

```
#setParameter("ag_degrade",1e8);
#simulate_ode({continue=>1,t_start=>50000,t_end=>150000,n_steps=>100,atol=>1e-
8,rtol=>1e-8});

#setParameter("ag_degrade",0);
#setConcentration("Antigen(tcr)",1e2);
#simulate_ode({continue=>1,t_start=>70000,t_end=>85000,n_steps=>1000,atol=>1e-
8,rtol=>1e-8});

#setConcentration("Antigen(tcr)",0);
#setParameter("ag_degrade",1e8);
#simulate_ode({continue=>1,t_start=>85000,t_end=>150000,n_steps=>100,atol=>1e-
8,rtol=>1e-8});

####################
##### Duration #####
####################
#setConcentration("Anti_CD28(cd28)","anti_cd28_init")
#setConcentration("Antigen(tcr)",1e1);
#simulate_ode({t_start=>0,t_end=>40000,n_steps=>1000,atol=>1e-8,rtol=>1e-8});
#
#setConcentration("Antigen(tcr)",0);
#setParameter("ag_degrade",1e8);
#simulate_ode({continue=>1,t_start=>40000,t_end=>200000,n_steps=>1000,atol=>1e-
8,rtol=>1e-8});
```

APPENDIX C IL-17 RULE BASED MODEL

```
begin model

begin parameters

#Initial concentrations of species
fraction = 1/10

il17_0          9.296e7*fraction
il17r_0         50000*fraction
act_0           50000*fraction
traf6_0         100000*fraction
tak1_0          50000*fraction
ikk_0           50000*fraction
#ikb_init       50000*fraction
nfkb_init       50000*fraction
anapc5_init     50000*fraction
ub_init         100000*fraction
dna_0           2

#rate constants

##########################################
#Receptor Activation
##########################################
 lig_bind                   1e-8
 lig_unbind                 1e-2

 lig_degradation        0

##########################################
#Act1 activity
##########################################

 act_bind                   1e-6
 act_unbind                 1e-2
```

```
act_bind_slow                2e-8

########################################
#TRAF6 regulation
########################################

traf_bind                    4e-7
traf_unbind          1e-2

traf6_ubiq                   0.03
ub_olig                      2.5e-8
ub_unbind_1          1e-3
ub_unbind_2          5e-3

########################################
#TAK1/TAB2_3 regulation
########################################

tab_bind                     8e-7
tak_phos                     0.05
tak_dephos                   1e-2


##############################################
#IKK Regulation
##############################################

ikk_bind                     4e-6

ikk_phos_act         5
ikk_dephos_act               5e-3
ikk_phos_inhib               1e-3
ikk_dephos_inhib     7e-2

##############################################
#IkB Regulation
##############################################

ikb_to_nuc                   5e-4
ikb_to_cyt           1e-3

ikb_bind                     5e-6
ikb_unbind                   1e-2

ikb_phos                     1
#ikb_dephos          1e-4
```

```
##############################################
#NFkB Regulation
##############################################

 nfkb_act                    1e-1
 nfkb_nuc_import             3e-1
 nfkb_nuc_export_noikb       1e-4

##########################################
#Transcription/Translation control
##########################################

 a20_transcription      0.11
 a20_translation        2.5e-2

 ikb_transcription      0.2
 ikb_translation        0.01

 KM_dna_a20             16000*fraction
 KM_dna_ikb             19000*fraction
 N_a20                  10
 N_ikb                  10


 a20_degrade            7.5e-4
 ikb_degrade            1e-5

 a20_mrna_degrade       1e-3
 ikb_mrna_degrade       1e-3

#######################################################
#A20 actions as negative regulator
#######################################################

rec_anapc5_bind         1e-5
rec_anapc5_unbind       1e-3
a20_anapc5_bind         1e-5
a20_anapc5_unbind       1e-3

a20_ub_bind             1e-2
a20_ub_unbind           1e-3

a20_ub_bind_slow        1e-7

 a20_deubiq_1           25      #Traf
```

```
 a20_deubiq_2          10      #Tak
 a20_deubiq_3          10      #IKK
 a20_deubiq_4          10      #Ub-Ub

#########################################################
#IkB actions as negative regulator
#########################################################

 ikb_nfkb_bind                  1e-3
 ikb_nfkb_unbind        0

 nfkb_nuc_export_ikb 5e-1


end parameters

begin molecule types
IL17a(dimer,il17r)
IL17Ra(il17,dimer,SEFIR,cbad)
IL17Rc(il17,dimer,SEFIR)
Act1(SEFIRb,tb2)
TRAF6(act1,K124)
TAK1(tab,Thr178_184~U~P)
TAB2_3(tak1,ub)
IKK(nemo,ikb,S177_181~U~P,HLH~U~P)
Ub(ub,traf6,ile44,K63,a20)
IkB(nfkb,ikk,S32_36~U~P,location~C~N)
NFkB(ikb,location~C~N)
A20(anapc5,ub)
AnapC5(cbadb,a20)
DNA()
IkBmRNA()
A20mRNA()

end molecule types


begin seed species

#IL17a(dimer!1,il17r).IL17a(dimer!1,il17r)                      il17_0
IL17Ra(il17,dimer!1,SEFIR,cbad).IL17Rc(il17,dimer!1,SEFIR)     il17r_0
Act1(SEFIRb,tb2)                                               act_0
TRAF6(act1,K124)                                               traf6_0
TAK1(tab!1,Thr178_184~U).TAB2_3(tak1!1,ub)                     tak1_0
IKK(nemo,ikb,S177_181~U,HLH~U)                                 ikk_0
NFkB(ikb!1,location~C).IkB(nfkb!1,ikk,S32_36~U,location~C)     nfkb_init
```

```
AnapC5(cbadb,a20)                                   anapc5_init
Ub(ub,traf6,ile44,K63,a20)                          ub_init
DNA()                                               dna_0

end  seed species

begin observables

Molecules     A20_mrna          A20mRNA()
Molecules     A20_protein       A20()
Molecules     IkB_mrna          IkBmRNA()
Molecules     IkB_total         IkB()
Molecules     TAK1_p            TAK1(Thr178_184~P)
Molecules     NFkB_nucleus      NFkB(location~N)
Molecules     NFkB_cytoplasm    NFkB(location~C)
Molecules     active_nfkb       NFkB(ikb,location~N)

end observables

begin functions
        transcription_a20() = a20_transcription*active_nfkb^N_a20/(KM_dna_a20^N_a20 +
active_nfkb^N_a20)+0.0001
        transcription_ikb() = ikb_transcription*active_nfkb^N_ikb/(KM_dna_ikb^N_ikb +
active_nfkb^N_ikb)
end functions

begin reaction rules

##########################################
#Receptor Activation
##########################################

#Homodimer ligand binds binds both monomers in one step
#Ligand_receptor_binding:\
#IL17a(dimer!1,il17r).IL17a(dimer!1,il17r) + IL17Ra(il17,dimer!2).IL17Rc(il17,dimer!2) <->\
#IL17a(dimer!1,il17r!3).IL17a(dimer!1,il17r!4).IL17Ra(il17!3,dimer!2).IL17Rc(il17!4,dimer!2)
lig_bind,lig_unbind

#More efficient ligand binding for NFsim
IL17Ra(il17,dimer!2).IL17Rc(il17,dimer!2) ->\
 IL17a(dimer!1,il17r!3).IL17a(dimer!1,il17r!4).IL17Ra(il17!3,dimer!2).IL17Rc(il17!4,dimer!2)
lig_bind*il17_0

IL17a(dimer!1,il17r!3).IL17a(dimer!1,il17r!4).IL17Ra(il17!3,dimer!2).IL17Rc(il17!4,dimer!2)  -
>\
```

```
IL17a(dimer!1,il17r).IL17a(dimer!1,il17r)  +  IL17Ra(il17,dimer!2).IL17Rc(il17,dimer!2)
        lig_unbind

IL17a(dimer!1,il17r).IL17a(dimer!1,il17r) -> 0 10 DeleteMolecules


#Ligand removal
IL17a(dimer!1,il17r!2).IL17a(dimer!1,il17r!3).IL17Ra(il17!2,dimer!4).IL17Rc(il17!3,dimer!4)  -
>\
IL17Ra(il17,dimer!2).IL17Rc(il17,dimer!2) lig_degradation DeleteMolecules

########################################
#Adatpter binding
########################################

#Act1 binds both Ra and Rc in one step
IL17Ra(il17!+,SEFIR) + Act1(SEFIRb) <->\
IL17Ra(il17!+,SEFIR!1).Act1(SEFIRb!1) act_bind,act_unbind

#Act1 unbind with no ligand
IL17Ra(il17,SEFIR!1).Act1(SEFIRb!1) -> IL17Ra(il17,SEFIR) + Act1(SEFIRb) act_unbind

#Allow some binding without ligand
IL17Ra(il17,SEFIR)  +  Act1(SEFIRb,tb2)  ->  IL17Ra(il17,SEFIR!1).Act1(SEFIRb!1,tb2)
act_bind_slow

########################################
#TRAF6 activity
########################################

#Recteptor-Act1 binds TRAF6
Act1(SEFIRb!+,tb2) + TRAF6(act1) <->\
Act1(SEFIRb!+,tb2!1).TRAF6(act1!1) traf_bind,traf_unbind

#TRAF6 unbinds free Act1
#Should rate be faster?
Act1(SEFIRb,tb2!1).TRAF6(act1!1) -> Act1(SEFIRb,tb2) + TRAF6(act1) traf_unbind

#Act1 Ubiquitnates bound TRAF6
Act1(SEFIRb!+,tb2!1).TRAF6(act1!1,K124) + Ub(ub,traf6,ile44,K63,a20) ->\
 Act1(SEFIRb!+,tb2!1).TRAF6(act1!1,K124!2).Ub(ub,traf6!2,ile44,K63,a20) traf6_ubiq

#Include this rule or not? Ub disassociating from TRAF6
#Enforce (possibly fix) very slow rate?
TRAF6(K124!1).Ub(traf6!1) -> TRAF6(K124) + Ub(traf6) ub_unbind_1
```

```
Act1().TRAF6() + Ub(traf6!+,K63) + Ub(ub,ile44,K63,a20) ->\
Act1().TRAF6() + Ub(traf6!+,K63!1).Ub(ub!1,ile44,K63,a20)        ub_olig

Act1().TRAF6() + TRAF6().Ub(ub!+,K63) + Ub(ub,ile44,K63,a20) ->\
Act1().TRAF6() + TRAF6().Ub(ub!+,K63!1).Ub(ub!1,ile44,K63,a20)        ub_olig

Ub(K63!1).Ub(ub!1) -> Ub(K63) + Ub(ub)   ub_unbind_2

#######################################
#TAK1/TAB2_3 Regulation
#######################################

#Does not enforce chain be bound to traf/act1
#Does enforce more than one ubiquitin monomer
#Will result in some free floating small chains to bind TAB2_3/TAK
Ub(ub!+,ile44,a20) + TAB2_3(tak1!1,ub).TAK1(tab!1,Thr178_184~U) ->\
Ub(ub!+,ile44!2,a20).TAB2_3(tak1!1,ub!2).TAK1(tab!1,Thr178_184~U) tab_bind

#Need unbind rule, make rate slow
Ub(ile44!2).TAB2_3(tak1!1,ub!2).TAK1(tab!1)              ->              Ub(ile44)              +
TAB2_3(tak1!1,ub).TAK1(tab!1)      ub_unbind_1

#TAK1 phosphorylates while bound to TRAF6~U, stays in complex
TAK1(tab!1,Thr178_184~U).TAB2_3(tak1!1,ub!+)                                                    ->
TAK1(tab!1,Thr178_184~P).TAB2_3(tak1!1,ub!+) tak_phos

#Tak1 can dephosphorylate regardless of binding state
TAK1(Thr178_184~P) -> TAK1(Thr178_184~U) tak_dephos

#############################################
#IKK Regulation
#############################################

#Same context as TAB2_3 binding rules
Ub(ub!+,ile44,a20) + IKK(nemo,ikb,S177_181~U) ->\
Ub(ub!+,ile44!1,a20).IKK(nemo!1,ikb,S177_181~U) ikk_bind

#Need unbind rule, make rate slow
Ub(ile44!1).IKK(nemo!1) -> Ub(ile44) + IKK(nemo)         ub_unbind_1

#Phosphorylation of IKK by TAK1
#Both need to be bound to Ubiquitin chain, and in the same complex
#IKK must be unphosphorylated on inhibitory site
TAB2_3(tak1!1,ub!+).TAK1(tab!1,Thr178_184~P).IKK(nemo!+,ikb,S177_181~U,HLH~U) ->\
TAB2_3(tak1!1,ub!+).TAK1(tab!1,Thr178_184~P)     +     IKK(nemo,ikb,S177_181~P,HLH~U)
        ikk_phos_act
```

```
#Inhibitory phosphorylation rules
#Only phosphorylated when active site is already phosphoyrlated
IKK(S177_181~P,HLH~U) -> IKK(S177_181~P,HLH~P)  ikk_phos_inhib

#Basal IKK dephosphorylation
#Dephosphorylate both regardless of context
#Allows three or four state model but doesn't enforce direction
# (U,U) <-> (P,U) <-> (P,P) -> (U,P)
IKK(S177_181~P) -> IKK(S177_181~U) ikk_dephos_act
IKK(HLH~P) -> IKK(HLH~U)        ikk_dephos_inhib


##############################################
#IkB Regulation
##############################################

#IKK~P binds cytoplasmic IkB bound to nfkb or not
IkB(ikk,S32_36~U,location~C)          +          IKK(ikb,S177_181~P,HLH~U)          <->
IkB(ikk!1,S32_36~U,location~C).IKK(ikb!1,S177_181~P,HLH~U) ikb_bind,ikb_unbind

#IKK and IkB disassociate regardles of any other context, fixes complex accumulation due to
phos changes on both
IkB(ikk!1).IKK(ikb!1) -> IkB(ikk) + IKK(ikb) ikb_unbind

#Phosphorylation of IkB bound to IKK
IkB(ikk!1,S32_36~U).IKK(ikb!1,S177_181~P,HLH~U)      ->      IkB(ikk,S32_36~P)      +
IKK(ikb,S177_181~P,HLH~U) ikb_phos

#Free IkB can traffic to the nucleus
IkB(nfkb,ikk,S32_36~U,location~C)          <->          IkB(nfkb,ikk,S32_36~U,location~N)
        ikb_to_nuc,ikb_to_cyt

##############################################
#IkB Regulation
##############################################

#Phosphorylated IkB deleted
IkB(S32_36~P) -> 0 nfkb_act DeleteMolecules

#Free NFkB transported to nucleus
NFkB(ikb,location~C) <-> NFkB(ikb,location~N) nfkb_nuc_import,nfkb_nuc_export_noikb

##############################################
#Transcription/Translation control
##############################################
```

```
DNA() -> DNA() + IkBmRNA()      transcription_ikb()
DNA() -> DNA() + A20mRNA()      transcription_a20()


#translation
A20mRNA() ->  A20mRNA() + A20(anapc5,ub)  a20_translation
IkBmRNA() -> IkBmRNA() + IkB(nfkb,ikk,S32_36~U,location~C)  ikb_translation

#protein degradation
A20(anapc5,ub) -> 0 a20_degrade DeleteMolecules
IkB(nfkb,ikk) -> 0 ikb_degrade DeleteMolecules

#mRNA degradation
A20mRNA() -> 0 a20_mrna_degrade
IkBmRNA() -> 0 ikb_mrna_degrade

########################################################
# AnacpC7 binding the receptor
########################################################

IL17Ra(SEFIR!+,cbad)  +  AnapC5(cbadb,a20)  <->
IL17Ra(SEFIR!+,cbad!1).AnapC5(cbadb!1,a20)      rec_anapc5_bind, rec_anapc5_unbind
IL17Ra(SEFIR,cbad!1).AnapC5(cbadb!1,a20)  ->  IL17Ra(SEFIR,cbad)  +  AnapC5(cbadb,a20)
        rec_anapc5_unbind

A20(anapc5,ub)  +  AnapC5(cbadb!+,a20)  <->  A20(anapc5!1,ub).AnapC5(cbadb!+,a20!1)
a20_anapc5_bind,a20_anapc5_unbind
A20(anapc5!1,ub).AnapC5(cbadb,a20!1)  ->  A20(anapc5,ub)  +  AnapC5(cbadb,a20)
        a20_anapc5_unbind

########################################################
#A20 actions as negative regulator
########################################################

#A20 binds Ub, transfered from receptor
#Only binds Ub in chains or bound to other proteins, avoids Ub monomers
AnapC5(a20!1).A20(anapc5!1,ub)  +  Ub(a20,ile44!+)  ->  AnapC5(a20)  +
A20(anapc5,ub!1).Ub(a20!1,ile44!+)  a20_ub_bind
AnapC5(a20!1).A20(anapc5!1,ub)  +  Ub(a20,traf6!+)  ->  AnapC5(a20)  +
A20(anapc5,ub!1).Ub(a20!1,traf6!+)  a20_ub_bind
AnapC5(a20!1).A20(anapc5!1,ub)  +  Ub(a20,ub!+)  ->  AnapC5(a20)  +
A20(anapc5,ub!1).Ub(a20!1,ub!+)  a20_ub_bind
A20(ub!1).Ub(a20!1) -> A20(ub) + Ub(a20) a20_ub_unbind

A20(anapc5,ub) + Ub(a20,ile44!+) -> A20(anapc5,ub!1).Ub(a20!1,ile44!+)  a20_ub_bind_slow
```

```
A20(anapc5,ub) + Ub(a20,ub!+) -> A20(anapc5,ub!1).Ub(a20!1,ub!+)  a20_ub_bind_slow

#A20 knocking enzymes off Ub
#May not be a perfect mechanistic representation, but necessary without having A20 degrade Ub (and corresponding Ub production)
TRAF6(K124!1).Ub(traf6!1,a20!2).A20(ub!2) -> TRAF6(K124) + Ub(traf6,a20) + A20(ub)
        a20_deubiq_1
TAB2_3(tak1!1,ub!2).TAK1(tab!1).Ub(ile44!2,a20!3).A20(ub!3) ->
TAB2_3(tak1!1,ub).TAK1(tab!1) + Ub(ile44,a20) + A20(ub)         a20_deubiq_2
IKK(nemo!1).Ub(ile44!1,a20!2).A20(ub!2) -> IKK(nemo) + Ub(ile44,a20) + A20(ub)
a20_deubiq_3

#A20 breaking Ub chains
Ub(K63!1,a20!2).Ub(ub!1,a20).A20(ub!2) -> Ub(K63,a20) + Ub(ub,a20) + A20(ub)
a20_deubiq_4
Ub(K63!1,a20).Ub(ub!1,a20!2).A20(ub!2) -> Ub(K63,a20) + Ub(ub,a20) + A20(ub)
a20_deubiq_4

#########################################################
#IkB actions as negative regulator
#########################################################

#IkB binds free NFkB in cytoplasm
NFkB(ikb,location~C)          +          IkB(nfkb,ikk,S32_36~U,location~C)          <->
NFkB(ikb!1,location~C).IkB(nfkb!1,ikk,S32_36~U,location~C) \
ikb_nfkb_bind,ikb_nfkb_unbind

#IkB binds free NFkB in nucleus
NFkB(ikb,location~N)          +          IkB(nfkb,ikk,S32_36~U,location~N)          <->
NFkB(ikb!1,location~N).IkB(nfkb!1,ikk,S32_36~U,location~N) \
ikb_nfkb_bind,ikb_nfkb_unbind

#IkB/NFkB complex translocates from nucleus to cytoplasm
NFkB(ikb!1,location~N).IkB(nfkb!1,ikk,S32_36~U,location~N) ->
NFkB(ikb!1,location~C).IkB(nfkb!1,ikk,S32_36~U,location~C) nfkb_nuc_export_ikb

end reaction rules
end model

#ACTIONS

visualize({type=>"contactmap"})

#equillibrate model
#setConcentration("IL17a(dimer!1,il17r).IL17a(dimer!1,il17r)",0);
setParameter("il17_0",0);
```

```
simulate_nf({suffix=>"equil",t_start=>0,t_end=>4e5,n_steps=>500,gml=>1e7});
##,param=>"-dump                                                    [0:100:1e4]-
>/home/bobby/Dropbox/MATLAB/IL17/NFanalyzeDump/equil/"

### begin simulation
##setConcentration("IL17a(dimer!1,il17r).IL17a(dimer!1,il17r)","il17_0");
setParameter("il17_0",9.296e6);
##simulate_nf({suffix=>"first",t_start=>0,t_end=>21600,n_steps=>144,gml=>5e8,param=>"-
dump [0:100:21600]->/home/bobby/Dropbox/MATLAB/IL17/NFanalyzeDump/sim/"});
simulate_nf({suffix=>"first",t_start=>0,t_end=>21600,n_steps=>144,gml=>5e8});
```

BIBLIOGRAPHY

1. Kirschner MW. The Meaning of Systems Biology Commentary. 2005;121: 503–504. doi:10.1016/j.cell.2005.05.005

2. Ryu H, Chung M, Dobrzyński M, Fey D, Blum Y, Lee SS, et al. Frequency modulation of ERK activation dynamics rewires cell fate. Mol Syst Biol. 2015;11: 838. doi:10.15252/msb.20156458

3. Zambrano S, de Toma I, Piffer A, Bianchi ME, Agresti A. NF-κB oscillations translate into functionally related patterns of gene expression. Elife. 2016;5: 1–38. doi:10.7554/eLife.09100

4. Gunawardena J. Models in biology: “accurate descriptions of our pathetic thinking”. BMC Biol. 2014;12: 29. doi:10.1186/1741-7007-12-29

5. Kitano H. Systems Biology : A Brief Overview. 2002;295: 1662–1665.

6. Liebermeister W, Wierling C, Kowald A, Lehrach H, Herwig R. Part One Introduction to Systems Biology. Basic Notion Comput Model. 2009;

7. Gunawardena J. Models in biology: “accurate descriptions of our pathetic thinking”. BMC Biol. 2014;12: 29. doi:10.1186/1741-7007-12-29

8. Shou W, Bergstrom CT, Chakraborty AK, Skinner FK. Theory, models and biology. Elife. 2015;4: e07158. doi:10.7554/eLife.07158

9. Macleod M. Strategies for Coordinating Experimentation and Modeling in Integrative Systems Biology. J Exp Zool. 2014;322: 230–239.

10. Alon U. Network motifs: theory and experimental approaches. Nat Rev Genet. 2007;8: 450–461. doi:nrg2102 [pii]\r10.1038/nrg2102

11. Kaplan D, Glass L. Understanding Nonlinear Dynamics. 1991;49: 6221.

12. Angus DC. The search for effective therapy for sepsis: back to the drawing board? JAMA. American Medical Association; 2011;306: 2614–5. Available: http://jama.jamanetwork.com/article.aspx?articleid=1104740

13. Angus DC, van der Poll T. Severe sepsis and septic shock. N Engl J Med. 2013;369: 840–51. doi:10.1056/NEJMra1208623

14. Dellinger R, Carlet J, Masur H, Gerlach H, Calandra T, Cohen J, et al. Surviving Sepsis Campaign guidelines for management of severe sepsis and septic shock. Intensive Care Med. 2004;30: 536–555. doi:10.1007/s00134-004-2210-z

15. Yealy DM, Kellum J a, Huang DT, Barnato AE, Weissfeld L a, Pike F, et al. A randomized trial of protocol-based care for early septic shock. N Engl J Med. 2014;370: 1683–93. doi:10.1056/NEJMoa1401602

16. Martin GS, Mannino DM, Eaton S, Moss M. The epidemiology of sepsis in the United States from 1979 through 2000. N Engl J Med. 2003;348: 1546–54. doi:10.1056/NEJMoa022139

17. Angus DC, Linde-Zwirble W, Lidicker J, Clermont G, Carcillo J, Pinsky MR. Epidemiology of severe sepsis in the United States: Analysis of incidence, outcome, and associated costs of care. Crit Care Med July 2001. 2001;29: 1303–1310. Available: http://ovidsp.ovid.com/ovidweb.cgi?T=JS&CSC=Y&NEWS=N&PAGE=fulltext&D=ovfte&AN=00003246-200107000-00002

18. Chiang JL, Kirkman MS, Laffel LMB, Peters AL. Type 1 Diabetes Through the Life Span: A Position Statement of the American Diabetes Association. Diabetes Care. 2014;37: 2034–2054. doi:10.2337/dc14-1140

19. Adeegbe DO, Nishikawa H. Natural and induced T regulatory cells in cancer. Front Immunol. 2013;4: 1–14. doi:10.3389/fimmu.2013.00190

20. Teng MWL, Swann JB, Von Scheidt B, Sharkey J, Zerafa N, McLaughlin N, et al. Multiple antitumor mechanisms downstream of prophylactic regulatory T-ceII depletion. Cancer Res. 2010;70: 2665–2674. doi:10.1158/0008-5472.CAN-09-1574

21. Miskov-Zivanov N, Turner MS, Kane LP, Morel PA, Faeder JR. The duration of T cell stimulation is a critical determinant of cell fate and plasticity. Sci Signal. 2013;6: ra97. doi:10.1126/scisignal.2004217

22. Nakajima K, Kanda T, Takaishi M, Shiga T, Miyoshi K, Nakajima H, et al. Distinct roles of IL-23 and IL-17 in the development of psoriasis-like lesions in a mouse model. J Immunol. American Association of Immunologists; 2011;186: 4481–9. doi:10.4049/jimmunol.1000148

23. Di Cesare A, Di Meglio P, Nestle FO. The IL-23/Th17 axis in the immunopathogenesis of psoriasis. J Invest Dermatol. The Society for Investigative Dermatology, Inc; 2009;129: 1339–50. doi:10.1038/jid.2009.59

24. Sønder SU, Paun A, Ha H-L, Johnson PF, Siebenlist U. CIKS/Act1-mediated signaling by IL-17 cytokines in context: implications for how a CIKS gene variant may predispose to psoriasis. J Immunol. 2012;188: 5906–14. doi:10.4049/jimmunol.1103233

25. Hwang S-Y, Kim J-Y, Kim K-W, Park M-K, Moon Y, Kim W-U, et al. IL-17 induces production of IL-6 and IL-8 in rheumatoid arthritis synovial fibroblasts via NF-kappaB- and PI3-kinase/Akt-dependent pathways. Arthritis Res Ther. 2004;6: R120-8. doi:10.1186/ar1038

26. Garg A V, Ahmed M, Vallejo AN, Ma A, Gaffen SL. The deubiquitinase A20 mediates feedback inhibition of interleukin-17 receptor signaling. Sci Signal. 2013;6: ra44. doi:10.1126/scisignal.2003699

27. Matmati M, Jacques P, Maelfait J, Verheugen E, Kool M, Sze M, et al. A20 (TNFAIP3) deficiency in myeloid cells triggers erosive polyarthritis resembling rheumatoid arthritis. Nat Genet. 2011;43: 908–12. doi:10.1038/ng.874

28. Bartocci E, Lió P. Computational Modeling , Formal Analysis , and Tools for Systems Biology. 2016; 1–22. doi:10.1371/journal.pcbi.1004591

29. Machado D, Costa RS, Rocha M, Ferreira EC, Tidor B, Rocha I. Modeling formalisms in Systems Biology. AMB Express. Springer Open Ltd; 2011;1: 45. doi:10.1186/2191-0855-1-45

30. Goldstein B, Faeder JR, Hlavacek WS. Mathematical and computational models of immune-receptor signalling. Nat Rev Immunol. 2004;4: 445–456. doi:10.1038/nri1374

31. Arazi A, Pendergraft WF, Ribeiro RM, Perelson AS, Hacohen N. Human systems immunology: Hypothesis-based modeling and unbiased data-driven approaches. Semin Immunol. 2013;25: 193–200. doi:10.1016/j.smim.2012.11.003

32. Blaser H, Dostert C, Mak TW, Brenner D. TNF and ROS Crosstalk in Inflammation. Trends Cell Biol. 2015;26: 249–261. doi:10.1016/j.tcb.2015.12.002

33. Kim H, Zhao Q, Zheng H, Li X, Zhang T, Ma X. A novel crosstalk between TLR4- and NOD2-mediated signaling in the regulation of intestinal inflammation. Sci Rep. Nature Publishing Group; 2015;5: 12018. doi:10.1038/srep12018

34. Schmitz ML, Weber A, Roxlau T, Gaestel M, Kracht M. Signal integration, crosstalk mechanisms and networks in the function of inflammatory cytokines. Biochim Biophys Acta - Mol Cell Res. Elsevier B.V.; 2011;1813: 2165–2175. doi:10.1016/j.bbamcr.2011.06.019

35. Pękalski J, Zuk PJ, Kochańczyk M, Junkin M, Kellogg R, Tay S, et al. Spontaneous NF-κB activation by autocrine TNFα signaling: a computational analysis. PLoS One. 2013;8: e78887. doi:10.1371/journal.pone.0078887

36. Caldwell AB, Birnbaum HA, Cheng Z, Hoffmann A, Vargas JD. Network dynamics determine the autocrine and paracrine signaling functions of TNF. Genes Dev. 2014;28: 2120–2133. doi:10.1101/gad.244749.114

37. Dinarello C a. Historical Review of Cytokines. Eur J Immunol. 2007;37: S34–S45. doi:10.1002/eji.200737772.Historical

38. O'Shea JJ, Murray PJ. Cytokine Signaling Modules in Inflammatory Responses. Immunity. 2008;28: 477–487. doi:10.1016/j.immuni.2008.03.002

39. Day J, Rubin J, Vodovotz Y, Chow CC, Reynolds A, Clermont G. A reduced mathematical model of the acute inflammatory response II. Capturing scenarios of repeated endotoxin administration. J Theor Biol. 2006;242: 237–56. doi:10.1016/j.jtbi.2006.02.015

40. Rivière B, Epshteyn Y, Swigon D, Vodovotz Y. A simple mathematical model of signaling resulting from the binding of lipopolysaccharide with Toll-like receptor 4 demonstrates inherent preconditioning behavior. Math Biosci. 2009;217: 19–26. doi:10.1016/j.mbs.2008.10.002

41. Azhar N, Ziraldo C, Barclay D, Rudnick DA, Squires RH, Vodovotz Y. Analysis of serum inflammatory mediators identifies unique dynamic networks associated with death and spontaneous survival in pediatric acute liver failure. PLoS One. 2013;8: 1–8. doi:10.1371/journal.pone.0078202

42. Song SOK, Hogg J, Peng ZY, Parker R, Kellum JA, Clermont G. Ensemble models of neutrophil trafficking in severe sepsis. PLoS Comput Biol. 2012;8.

43. Chowell G, Castillo-Chavez C, Fenimore PW, Kribs-Zaleta CM, Arriola L, Hyman JM. Model parameters and outbreak control for SARS. Emerg Infect Dis. 2004;10: 1258–1263. doi:10.3201/eid1007.030647

44. Sanchez MA, Blower S. Uncertainty and sensitivity analysis of the basic reproduction rate: tuberculosis as an example. Am J Epidemiol. 1997;145: 1127–1137.

45. Lukens S, DePasse J, Rosenfeld R, Ghedin E, Mochan E, Brown ST, et al. A large-scale immuno-epidemiological simulation of influenza A epidemics. BMC Public Health. 2014;14: 1019. doi:10.1186/1471-2458-14-1019

46. Yamada S, Shiono S, Joo A, Yoshimura A. Control mechanism of JAK/STAT signal transduction pathway. FEBS Lett. 2003;534: 190–196. doi:10.1016/S0014-5793(02)03842-5

47. Rateitschak K, Karger A, Fitzner B, Lange F, Wolkenhauer O, Jaster R. Mathematical modelling of interferon-γ signalling in pancreatic stellate cells reflects and predicts the dynamics of STAT1 pathway activity. Cell Signal. Elsevier Inc.; 2010;22: 97–105. doi:10.1016/j.cellsig.2009.09.019

48. Bachmann J, Raue A, Schilling M, Bohm ME, Kreutz C, Kaschek D, et al. Division of labor by dual feedback regulators controls JAK2/STAT5 signaling over broad ligand range. Mol Syst Biol. 2011;7: 516–516. doi:10.1038/msb.2011.50

49. Gambin A, Charzyńska A, Ellert-Miklaszewska A, Rybiński M. Computational models of the JAK1/2-STAT1 signaling. Jak-Stat. 2013;2: e24672. doi:10.4161/jkst.24672

50. Mahdavi A, Davey RE, Bhola P, Yin T, Zandstra PW. Sensitivity analysis of intracellular signaling pathway kinetics predicts targets for stem cell fate control. PLoS Comput Biol. 2007;3: 1257–1267. doi:10.1371/journal.pcbi.0030130

51. Papin JA, Palsson BO. The JAK-STAT signaling network in the human B-cell: an extreme signaling pathway analysis. Biophys J. 2004;87: 37–46. doi:10.1529/biophysj.103.029884

52. Quaiser T, Dittrich A, Schaper F, Monnigmann M. A simple work flow for biologically inspired model reduction--application to early JAK-STAT signaling. BMC Syst Biol. 2011;5: 30. doi:1752-0509-5-30 [pii]\n10.1186/1752-0509-5-30

53. Wiley HS, Shvartsman SY, Lauffenburger DA. Computational modeling of the EGF-receptor system: A paradigm for systems biology. Trends Cell Biol. 2003;13: 43–50. doi:10.1016/S0962-8924(02)00009-0

54. Kholodenko BN, Demin O V, Moehren G, Hoek JB. Quantification of short term signaling by the epidermal growth factor receptor. J Biol Chem. 1999;274: 30169–30181. doi:10514507

55. Schoeberl B, Eichler-Jonsson C, Gilles ED, Müller G. Computational modeling of the dynamics of the MAP kinase cascade activated by surface and internalized EGF receptors. Nat Biotechnol. 2002;20: 370–5. doi:10.1038/nbt0402-370

56. Orton RJ, Sturm OE, Vyshemirsky V, Calder M, Gilbert DR, Kolch W. Computational modelling of the receptor-tyrosine-kinase-activated MAPK pathway. Biochem J. 2005;392: 249–61. doi:10.1042/BJ20050908

57. Das J, Ho M, Zikherman J, Govern C, Yang M, Weiss A, et al. Digital Signaling and Hysteresis Characterize Ras Activation in Lymphoid Cells. Cell. Elsevier Inc.; 2009;136: 337–351. doi:10.1016/j.cell.2008.11.051

58. Pantazis Y, Katsoulakis M a, Vlachos DG. Parametric sensitivity analysis for biochemical reaction networks based on pathwise information theory. BMC Bioinformatics. 2013;14: 311. doi:10.1186/1471-2105-14-311

59. Villasenor R, Nonaka H, Conte-Zerial P Del, Kalaidzidis Y, Zerial M. Regulation of EGFR signal transduction by analogue-to-digital conversion in Endosomes. Elife. 2015;2015: 1–74. doi:10.7554/eLife.06156

60. Blinov ML, Faeder JR, Goldstein B, Hlavacek WS. A network model of early events in epidermal growth factor receptor signaling that accounts for combinatorial complexity. Biosystems. 2006;83: 136–51. doi:10.1016/j.biosystems.2005.06.014

61. Kiyatkin A, Aksamitiene E, Markevich NI, Borisov NM, Hoek JB, Kholodenko BN. Scaffolding protein Grb2-associated binder 1 sustains epidermal growth factor-induced mitogenic and survival signaling by multiple positive feedback loops. J Biol Chem. 2006;281: 19925–19938. doi:10.1074/jbc.M600482200

62. Huang L, Pan CQ, Li B, Tucker-Kellogg L, Tidor B, Chen Y, et al. Simulating EGFR-ERK signaling control by scaffold proteins KSR and MP1 reveals differential Ligand-Sensitivity Co-Regulated by CBL-CIN85 and Endophilin. PLoS One. 2011;6. doi:10.1371/journal.pone.0022933

63. Resat H, Petzold L, Pettigrew MF. Kinetic modeling of biological systems. Methods Mol Biol. 2009;541: 311–35. doi:10.1007/978-1-59745-243-4_14

64. Mayawala K, Vlachos DG, Edwards JS. Computational modeling reveals molecular details of epidermal growth factor binding. BMC Cell Biol. 2005;6: 41. doi:10.1186/1471-2121-6-41

65. Shankaran H, Zhang Y, Tan Y, Resat H. Model-Based Analysis of HER Activation in Cells Co-Expressing EGFR, HER2 and HER3. PLoS Comput Biol. 2013;9. doi:10.1371/journal.pcbi.1003201

66. Orton RJ, Adriaens ME, Gormand A, Sturm OE, Kolch W, Gilbert DR. Computational modelling of cancerous mutations in the EGFR/ERK signalling pathway. BMC Syst Biol. 2009;3: 100. doi:10.1186/1752-0509-3-100

67. Buch I, Ferruz N, De Fabritiis G. Computational modeling of an epidermal growth factor receptor single-mutation resistance to cetuximab in colorectal cancer treatment. J Chem Inf Model. 2013;53: 3123–3126. doi:10.1021/ci400456m

68. Bianconi F, Baldelli E, Ludovini V, Crinò L, Flacco A, Valigi P. Computational model of EGFR and IGF1R pathways in lung cancer: A Systems Biology approach for Translational Oncology. Biotechnol Adv. Elsevier Inc.; 2012;30: 142–153. doi:10.1016/j.biotechadv.2011.05.010

69. Cheong R, Hoffmann A, Levchenko A. Understanding NF-kappaB signaling via mathematical modeling. Mol Syst Biol. 2008;4: 192. doi:10.1038/msb.2008.30

70. Wang R-S, Saadatpour A, Albert R. Boolean modeling in systems biology: an overview of methodology and applications. Phys Biol. 2012;9: 55001. doi:10.1088/1478-3975/9/5/055001

71. Zhang H, Wang X, Lin X. Synchronization of boolean networks with different update schemes. IEEE/ACM Trans Comput Biol Bioinforma. 2014;11: 965–972. doi:10.1109/TCBB.2014.2338313

72. Morris MK, Saez-Rodriguez J, Sorger PK, Lauffenburger DA. Logic-based models for the analysis of cell signaling networks. Biochemistry. 2010;49: 3216–24. doi:10.1021/bi902202q

73. Chaves M, Sontag ED, Albert R. Methods of robustness analysis for Boolean models of gene control networks. Physics (College Park Md). 2006; 29. doi:arXiv:q-bio/0605004v1 [q-bio.MN] 1 May 2006

74. Liang J, Han J, Boolean S. Stochastic Boolean networks: an efficient approach to modeling gene regulatory networks. BMC Syst Biol. 2012;6: 113. doi:10.1186/1752-0509-6-113

75. Anderson CS, Dediego ML, Topham DJ, Thakar J. Boolean Modeling of Cellular and Molecular Pathways Involved in Influenza Infection. Comput Math Methods Med. Hindawi Publishing Corporation; 2016;2016. doi:10.1155/2016/7686081

76. Aldridge BB, Saez-Rodriguez J, Muhlich JL, Sorger PK, Lauffenburger DA. Fuzzy Logic Analysis of Kinase Pathway Crosstalk in TNF/EGF/Insulin-Induced Signaling. PLoS Comput Biol. 2009;5. doi:10.1371/journal.pcbi.1000340

77. Hong T, Xing J, Li L, Tyson JJ. A simple theoretical framework for understanding heterogeneous differentiation of CD4+ T cells. BMC Syst Biol. 2012;6: 66. doi:10.1186/1752-0509-6-66

78. Naldi A, Carneiro J, Chaouiya C, Thieffry D. Diversity and plasticity of Th cell types predicted from regulatory network modelling. PLoS Comput Biol. 2010;6: 9–12. doi:10.1371/journal.pcbi.1000912

79. Mendoza L. A network model for the control of the differentiation process in Th cells. BioSystems. 2006;84: 101–114. doi:10.1016/j.biosystems.2005.10.004

80. Saez-Rodriguez J, Simeoni L, Lindquist JA, Hemenway R, Bommhardt U, Arndt B, et al. A logical model provides insights into T cell receptor signaling. PLoS Comput Biol. 2007;3: 1580–1590. doi:10.1371/journal.pcbi.0030163

81. Zhang R, Shah MV, Yang J, Nyland SB, Liu X, Yun JK, et al. Network model of survival signaling in large granular lymphocyte leukemia. Proc Natl Acad Sci U S A. 2008;105: 16308–13. doi:10.1073/pnas.0806447105

82. Faeder JR, Blinov ML, Hlavacek WS. Rule-Based Modeling of Biochemical Systems with BioNetGen. Maly I V., editor. Methods Mol Biol. Totowa, NJ: Humana Press; 2009;500: 113–167. doi:10.1007/978-1-59745-525-1

83. Harris LA, Hogg JS, Tapia J-J, Sekar JAP, Gupta S, Korsunsky I, et al. BioNetGen 2.2: Advances in Rule-Based Modeling. Bioinformatics. 2016; 2006–2008. doi:10.1093/bioinformatics/btw469

84. Chylek L a, Harris L a, Tung C-S, Faeder JR, Lopez CF, Hlavacek WS. Rule-based modeling: a computational approach for studying biomolecular site dynamics in cell signaling systems. Wiley Interdiscip Rev Syst Biol Med. 2014;6: 13–36. doi:10.1002/wsbm.1245

85. Hindmarsh AC, Brown PN, Grant KE, Lee SL, Serban R, Shumaker DE, et al. Sundials. ACM Trans Math Softw. 2005;31: 363–396. doi:10.1145/1089014.1089020

86. Gillespie DT. Stochastic simulation of chemical kinetics. Ann Rev Phys Chem. 2007;58: 35–55. doi:10.1146/annurev.physchem.58.032806.104637

87. An GC, Faeder JR. Detailed qualitative dynamic knowledge representation using a BioNetGen model of TLR-4 signaling and preconditioning. Math Biosci. 2009;217: 53–63.

88. Lipniacki T, Hat B, Faeder JR, Hlavacek WS. Stochastic effects and bistability in T cell receptor signaling. J Theor Biol. 2008;254: 110–22. doi:10.1016/j.jtbi.2008.05.001

89. Barua D, Faeder JR, Haugh JM. A bipolar clamp mechanism for activation of Jak-family protein tyrosine kinases. PLoS Comput Biol. 2009;5: e1000364. doi:10.1371/journal.pcbi.1000364

90. Feinerman O, Veiga J, Dorfman JR, Germain RN, Altan-Bonnet G. Variability and robustness in T cell activation from regulated heterogeneity in protein levels. Science. 2008;321: 1081–4. doi:10.1126/science.1158013

91. Abel SM, Roose JP, Groves JT, Weiss A, Chakraborty AK. The membrane environment can promote or suppress bistability in cell signaling networks. J Phys Chem B. 2012;116: 3630–3640. doi:10.1021/jp2102385

92. Barua D, Hlavacek WS, Lipniacki T. A computational model for early events in B cell antigen receptor signaling: analysis of the roles of Lyn and Fyn. J Immunol. 2012;189: 646–58. doi:10.4049/jimmunol.1102003

93. Sneddon MW, Faeder JR, Emonet T. Efficient modeling, simulation and coarse-graining of biological complexity with NFsim. Nat Methods. 2011;8: 177–183. doi:10.1038/nmeth.1546

94. Chylek L a., Akimov V, Dengjel J, Rigbolt KTG, Hu B, Hlavacek WS, et al. Phosphorylation Site Dynamics of Early T-cell Receptor Signaling. PLoS One. 2014;9: e104240. doi:10.1371/journal.pone.0104240

95. Fricke F, Malkusch S, Wangorsch G, Greiner JF, Kaltschmidt B, Kaltschmidt C, et al. Quantitative single-molecule localization microscopy combined with rule-based modeling reveals ligand-induced TNF-R1 reorganization toward higher-order oligomers. Histochem Cell Biol. 2014;142: 91–101. doi:10.1007/s00418-014-1195-0

96. Michalski PJ, Loew LM. CaMKII activation and dynamics are independent of the holoenzyme structure: an infinite subunit holoenzyme approximation. Phys Biol. 2012;9: 36010. doi:10.1088/1478-3975/9/3/036010

97. Thomas BR, Chylek LA, Colvin J, Sirimulla S, Clayton AHA, Hlavacek WS, et al. BioNetFit: A fitting tool compatible with BioNetGen, NFsim and distributed computing environments. Bioinformatics. 2015;32: 798–800. doi:10.1093/bioinformatics/btv655

98. Lagu T, Rothberg MB, Shieh M-S, Pekow PS, Steingrub JS, Lindenauer PK. Hospitalizations, costs, and outcomes of severe sepsis in the United States 2003 to 2007. Crit Care Med. 2012;40: 754–761. doi:10.1097/CCM.0b013e318232db65

99. Iskander KN, Osuchowski MF, Stearns-Kurosawa DJ, Kurosawa S, Stepien D, Valentine C, et al. Sepsis: multiple abnormalities, heterogeneous responses, and evolving understanding. Physiol Rev. 2013;93: 1247–88. Available: http://www.pubmedcentral.nih.gov/articlerender.fcgi?artid=3962548&tool=pmcentrez&rendertype=abstract

100. Kellum JA, Kong L, Fink MP, Weissfeld LA, Yealy DM, Pinsky MR, et al. Understanding the inflammatory cytokine response in pneumonia and sepsis: results of the Genetic and Inflammatory Markers of Sepsis (GenIMS) Study. Arch Intern Med. American Medical Association; 2007;167: 1655–63. doi:10.1001/archinte.167.15.1655

101. Song SO, Hogg J, Peng Z-Y, Parker R, Kellum J a, Clermont G. Ensemble models of neutrophil trafficking in severe sepsis. PLoS Comput Biol. 2012;8: e1002422. doi:10.1371/journal.pcbi.1002422

102. Brown K, Brain S, Pearson J, Edgeworth J, Lewis S, Treacher D. Neutrophils in development of multiple organ failure in sepsis. Lancet. 2006;368: 157–169. doi:10.1016/S0140-6736(06)69005-3

103. Nylén ES, Alarifi a a. Humoral markers of severity and prognosis of critical illness. Best Pract Res Clin Endocrinol Metab. 2001;15: 553–73. doi:10.1053/beem.2001.0169

104. Simon A. Jones, Wolf M, Qin S, Mackay CR, Baggiolini M. Different Functions for the Interleukin 8 Receptors (il-8r) of Human Neutrophil Leukocytes: NADPH Oxidase and Phospholipase D are Activated through IL-8R1 but not IL-8R2. Proc Natl Acad Sci U S A. 1996;93: 6682–6686. Available: http://www.jstor.org/stable/39369

105. Nasser MW, Raghuwanshi SK, Grant DJ, Jala VR, Rajarathnam K, Richardson RM. Differential activation and regulation of CXCR1 and CXCR2 by CXCL8 monomer and dimer. J Immunol. 2009;183: 3425–32. doi:10.4049/jimmunol.0900305

106. Alves-Filho JC, Freitas A, Souto FO, Spiller F, Paula-Neto H, Silva JS, et al. Regulation of chemokine receptor by Toll-like receptor 2 is critical to neutrophil migration and resistance to polymicrobial sepsis. Proc Natl Acad Sci U S A. 2009;106: 4018–23. doi:10.1073/pnas.0900196106

107. Schlag G, Redl H, Davies J, Vuuren CJJ, Smuts P. Live Escherichia coli Sepsis Models in Baboons. Pathophysiology of Shock, Sepsis, and Organ Failure. Springer Berlin Heidelberg; 1993. pp. 1076–1107. doi:10.1007/978-3-642-76736-4_73

108. Krumsiek J, Pölsterl S, Wittmann DM, Theis FJ. Odefy--from discrete to continuous models. BMC Bioinformatics. 2010;11: 233. doi:10.1186/1471-2105-11-233

109. Wittmann DM, Krumsiek J, Saez-Rodriguez J, Lauffenburger D, Klamt S, Theis FJ. Transforming Boolean models to continuous models: methodology and application to T-cell receptor signaling. BMC Syst Biol. 2009;3: 98. doi:10.1186/1752-0509-3-98

110. Baggiolini M, Walz A, Kunkel SL, Peptide- N, Cytokine N. Neutrophil-activating peptide-1/interleukin 8, a novel cytokine that activates neutrophils. J Clin Invest. 1989;84: 1045–1049. doi:10.1172/JCI114265

111. Lenz A, Franklin G a, Cheadle WG. Systemic inflammation after trauma. Injury. 2007;38: 1336–45. doi:10.1016/j.injury.2007.10.003

112. Boyle EM, Pohlman TH, Johnson MC, Verrier ED. Endothelial cell injury in cardiovascular surgery: the systemic inflammatory response. Ann Thorac Surg. 1997;63: 277–84. Available: http://www.ncbi.nlm.nih.gov/pubmed/8993292

113. Appelberg R. Neutrophils and intracellular pathogens: beyond phagocytosis and killing. Trends Microbiol. 2007;15: 87–92. doi:10.1016/j.tim.2006.11.009

114. Badwey JA, Karnovsky ML. Active oxygen species and the functions of phagocytic leukocytes. Annu Rev Biochem. 1980;49: 695–726. Available: http://europepmc.org/abstract/MED/6250449

115. Rose JJ, Foley JF, Murphy PM, Venkatesan S. On the Mechanism and Significance of Ligand-induced Internalization of Human Neutrophil Chemokine Receptors CXCR1 and CXCR2. J Biol Chem. 2004;279: 24372–24386. doi:10.1074/jbc.M401364200

116. Gijsbers K, Van Assche G, Joossens S, Struyf S, Proost P, Rutgeerts P, et al. CXCR1-binding chemokines in inflammatory bowel diseases: down-regulated IL-8/CXCL8 production by leukocytes in Crohn's disease and selective GCP-2/CXCL6 expression in inflamed intestinal tissue. Eur J Immunol. 2004;34: 1992–2000. doi:10.1002/eji.200324807

117. Martich BGD, Danner RL, Ceska M, Suffredini AF, Martich GD. Detection of interleukin 8 and tumor necrosis factor in normal humans after intravenous endotoxin: the effect of antiinflammatory agents. J Exp Med. 1991;173: 1021–1024. doi:10.1084/jem.173.4.1021

118. Feniger-Barish R, Ran M, Zaslaver a, Ben-Baruch a. Differential modes of regulation of cxc chemokine-induced internalization and recycling of human CXCR1 and CXCR2. Cytokine. 1999;11: 996–1009. doi:10.1006/cyto.1999.0510

119. Summers C, Rankin SM, Condliffe AM, Singh N, Peters a M, Chilvers ER. Neutrophil kinetics in health and disease. Trends Immunol. 2010;31: 318–24. doi:10.1016/j.it.2010.05.006

120. Cockcroft DW, Gault MH. Prediction of creatinine clearance from serum creatinine. Nephron. 1976;16: 31–41. doi:10.1159/000180580

121. Swigon D. Ensemble Modeling of Biological Systems. In: Alexandra V. Antoniouk, Melnik RVN, editors. Mathematics and Life Sciences. Walter de Gruyter; 2012. pp. 19–42.

122. Brown K, Sethna J. Statistical mechanical approaches to models with many poorly known parameters. Phys Rev E. 2003;68: 21904. doi:10.1103/PhysRevE.68.021904

123. Swendsen R, Wang J. Replica Monte Carlo simulation of spin glasses. Phys Rev Lett. 1986;57: 2607–2609.

124. Earl DJ, Deem MW. Parallel tempering: theory, applications, and new perspectives. Phys Chem Chem Phys. 2005;7: 3910–6.

125. Mochan E, Swigon D, Ermentrout GB, Lukens S, Clermont G. A mathematical model of intrahost pneumococcal pneumonia infection dynamics in murine strains. J Theor Biol. Academic Press; 2014;353: 44–54.

126. Fernández Slezak D, Suárez C, Cecchi GA, Marshall G, Stolovitzky G. When the optimal is not the best: Parameter estimation in complex biological models. PLoS One. 2010;5: e13283.

127. Roberts G, Gelman A, Gilks W. Weak convergence and optimal scaling of random walk Metropolis algorithms. Ann Appl Probab. 1997;7: 110–120. Available: http://projecteuclid.org/euclid.aoap/1034625254

128. Gelman A, Rubin DB. lnference from Iterative Simulation Using Multiple Sequences. Stat Sci. 1992;7: 457–472.

129. Brooks S, Gelman A. General methods for monitoring convergence of iterative simulations. J Comput Graph Stat. 1998;7: 434–455. Available: http://www.tandfonline.com/doi/abs/10.1080/10618600.1998.10474787

130. Li G, Rabitz H, Yelvington PE, Oluwole OO, Bacon F, Kolb CE, et al. Global sensitivity analysis for systems with independent and/or correlated inputs. J Phys Chem A. 2010;114: 6022–32. doi:10.1021/jp9096919

131. Miller MA, Feng XJ, Li G, Rabitz HA. Identifying biological network structure, predicting network behavior, and classifying network state with high dimensional model representation (HDMR). PLoS One. 2012;7: e37664.

132. Mathew S, Bartels J, Banerjee I, Vodovotz Y. Global sensitivity analysis of a mathematical model of acute inflammation identifies nonlinear dependence of cumulative tissue damage on host interleukin-6 responses. J Theor Biol. Elsevier; 2014;358: 132–48. doi:10.1016/j.jtbi.2014.05.036

133. Mathew S, Sundararaj S, Mamiya H, Banerjee I. Regulatory interactions maintaining self-renewal of human embryonic stem cells as revealed through a systems analysis of PI3K/AKT pathway. Bioinformatics. 2014;30: 2334–42. Available: http://www.ncbi.nlm.nih.gov/pubmed/24778109

134. Hall M, Frank E, Holmes G. The WEKA data mining software: an update. ACM SIGKDD Explor. 2009;11: 10–18. Available: http://dl.acm.org/citation.cfm?id=1656278

135. Peng Z-Y, Carter MJ, Kellum JA, Manuscript A. Effects of hemoadsorption on cytokine removal and short-term survival in septic rats. Crit Care Med. 2008;36: 1573–1577. doi:10.1097/CCM.0b013e318170b9a7

136. Rimmel T, Kellum JA. Clinical review: Blood purification for sepsis. Crit Care. 2011;15: 205. doi:10.1186/cc9411

137. Humes HD, Sobota JT, Ding F, Song JH. A Selective Cytopheretic Inhibitory Device to Treat the Immunological Dysregulation of Acute and Chronic Renal Failure. Blood Purif. 2010;29: 183–190. doi:10.1159/000245645

138. Ding F, Song JH, Jung JY, Lou L, Wang M, Charles L, et al. A Biomimetic Membrane Device That Modulates the Excessive Inflammatory Response to Sepsis. PLoS One. 2011;6: e18584. doi:10.1371/journal.pone.0018584

139. Gutenkunst RN, Waterfall JJ, Casey FP, Brown KS, Myers CR, Sethna JP. Universally sloppy parameter sensitivities in systems biology models. Arkin AP, editor. PLoS Comput Biol. Public Library of Science; 2007;3: 1871–78. doi:10.1371/journal.pcbi.0030189

140. Brown K, Sethna J. Statistical mechanical approaches to models with many poorly known parameters. Phys Rev E. 2003;68: 21904. doi:10.1103/PhysRevE.68.021904

141. Haseltine EL, Rawlings JB. Approximate simulation of coupled fast and slow reactions for stochastic chemical kinetics. J Chem Phys. AIP Publishing; 2002;117: 6959. doi:10.1063/1.1505860

142. Resat H, Petzold L, Pettigrew MF. Kinetic modeling of biological systems. Methods Mol Biol. 2009;541: 311–35. doi:10.1007/978-1-59745-243-4_14

143. Swat MH, Thomas GL, Belmonte JM, Shirinifard A, Hmeljak D, Glazier JA. Multi-scale modeling of tissues using CompuCell3D. Methods Cell Biol. 2012;110: 325–66. doi:10.1016/B978-0-12-388403-9.00013-8

144. Lipniacki T, Paszek P, Brasier AR, Luxon BA, Kimmel M. Stochastic regulation in early immune response. Biophys J. 2006;90: 725–42. doi:10.1529/biophysj.104.056754

145. Prokopiou S, Barbarroux L, Bernard S, Mafille J, Leverrier Y, Arpin C, et al. Multiscale Modeling of the Early CD8 T-Cell Immune Response in Lymph Nodes: An Integrative Study. Computation. Multidisciplinary Digital Publishing Institute; 2014;2: 159–181. doi:10.3390/computation2040159

146. Kiparissides A, Kucherenko SS, Mantalaris A, Pistikopoulos EN. Global Sensitivity Analysis Challenges in Biological Systems Modeling. Ind Eng Chem Res. 2009;48: 7168–7180.

147. Kent E, Neumann S, Kummer U, Mendes P. What can we learn from global sensitivity analysis of biochemical systems? PLoS One. 2013;8: e79244.

148. Waydhas C, Nast-Kolb D, Jochum M, Trupka A, Lenk S, Fritz H, et al. Inflammatory mediators, infection, sepsis, and multiple organ failure after severe trauma. Arch Surg. 1992;127: 460–467. doi:10.1001/archsurg.1992.01420040106019

149. Ritter C, Andrades ME, Reinke A, Menna-Barreto S, Moreira JCF, Dal-Pizzol F. Treatment with N-acetylcysteine plus deferoxamine protects rats against oxidative stress and improves survival in sepsis. Crit Care Med. 2004;32: 342–9. doi:10.1097/01.CCM.0000109454.13145.CA

150. Cummings CJ, Martin TR, Frevert CW, Quan JM, Wong V a, Mongovin SM, et al. Expression and function of the chemokine receptors CXCR1 and CXCR2 in sepsis. J Immunol. 1999;162: 2341–2346.

151. Fujishima S, Aikawa N. Neutrophil-mediated tissue injury and its modulation. Intensive Care Med. 1995;21: 277–285.

152. Taneja R, Parodo J, Jia SH, Kapus A, Rotstein OD, Marshall JC. Delayed neutrophil apoptosis in sepsis is associated with maintenance of mitochondrial transmembrane potential and reduced caspase-9 activity. Crit Care Med. 2004;32: 1460–1469. doi:10.1097/01.CCM.0000129975.26905.77

153. Fialkow L, Fochesatto Filho L, Bozzetti MC, Milani AR, Rodrigues Filho EM, Ladniuk RM, et al. Neutrophil apoptosis: a marker of disease severity in sepsis and sepsis-induced acute respiratory distress syndrome. Crit Care. 2006;10: R155. doi:10.1186/cc5090

154. Moriconi A, Cesta MC, Cervellera MN, Aramini A, Coniglio S, Colagioia S, et al. Design of Noncompetitive Interleukin-8 Inhibitors Acting on CXCR1 and CXCR2. J Med Chem. 2007;50: 3984–4002. doi:10.1021/jm061469t

155. Bizzarri C, Beccari AR, Bertini R, Cavicchia MR, Giorgini S, Allegretti M. ELR+ CXC chemokines and their receptors (CXC chemokine receptor 1 and CXC chemokine receptor 2) as new therapeutic targets. Pharmacol Ther. 2006;112: 139–149. doi:10.1016/j.pharmthera.2006.04.002

156. Bertini R, Allegretti M, Bizzarri C, Moriconi A, Locati M, Zampella G, et al. Noncompetitive allosteric inhibitors of the inflammatory chemokine receptors CXCR1 and CXCR2: Prevention of reperfusion injury. Proc Natl Acad Sci U S A. 2004;101: 11791–11796. doi:10.1073/pnas.0402090101

157. Osuchowski MF, Remick DG, Lederer J a, Lang CH, Aasen AO, Aibiki M, et al. Abandon the mouse research ship? Not just yet! Shock. 2014;41: 463–75. doi:10.1097/SHK.0000000000000153

158. Seok J, Warren HS, Cuenca AG, Mindrinos MN, Baker H V, Xu W, et al. Genomic responses in mouse models poorly mimic human inflammatory diseases. Proc Natl Acad Sci U S A. 2013;110: 3507–12. doi:10.1073/pnas.1222878110

159. Takao K, Miyakawa T. Genomic responses in mouse models greatly mimic human inflammatory diseases. Proc Natl Acad Sci. 2014; 1401965111-. doi:10.1073/pnas.1401965111

160. Fu W, Zhang Y, Zhang J, Chen W-F. Cloning and characterization of mouse homolog of the CXC chemokine receptor CXCR1. Cytokine. 2005;31: 9–17. doi:10.1016/j.cyto.2005.02.005

161. Peng Z-Y, Wang H-Z, Carter MJ, Dileo M V., Bishop J V., Zhou F-H, et al. Acute removal of common sepsis mediators does not explain the effects of extracorporeal blood purification in experimental sepsis. Kidney Int. 2012;81: 363–369. doi:10.1038/ki.2011.320

162. Panagiotou A, Gaiao S, Cruz DN. Extracorporeal therapies in sepsis. J Intensive Care Med. 2013;28: 281–95. doi:10.1177/0885066611425759

163. Kang JH, Super M, Yung CW, Cooper RM, Domansky K, Graveline AR, et al. An extracorporeal blood-cleansing device for sepsis therapy. Nat Med. 2014;20: 1211–1216. doi:10.1038/nm.3640

164. Rimmelé T, Kaynar AM, McLaughlin JN, Bishop J V, Fedorchak M V, Chuasuwan A, et al. Leukocyte capture and modulation of cell-mediated immunity during human sepsis: an ex vivo study. Crit Care. BioMed Central Ltd; 2013;17: R59. doi:10.1186/cc12587

165. Gaieski DF, Mikkelsen ME, Band RA, Pines JM, Massone R, Furia FF, et al. Impact of time to antibiotics on survival in patients with severe sepsis or septic shock in whom early goal-directed therapy was initiated in the emergency department. Crit Care Med. 2010;38: 1045–1053.

166. Bozza F a, Salluh JI, Japiassu AM, Soares M, Assis EF, Gomes RN, et al. Cytokine profiles as markers of disease severity in sepsis: a multiplex analysis. Crit Care. BioMed Central; 2007;11: R49. doi:10.1186/cc5783

167. Kibe S, Adams K, Barlow G. Diagnostic and prognostic biomarkers of sepsis in critical care. J Antimicrob Chemother. 2011;66 Suppl 2: ii33-40. doi:10.1093/jac/dkq523

168. Pierrakos C, Vincent J-L. Sepsis biomarkers: a review. Crit Care. 2010;14: R15. doi:10.1186/cc8872

169. Pillay J, Hietbrink F, Koenderman L, Leenen LPH. The systemic inflammatory response induced by trauma is reflected by multiple phenotypes of blood neutrophils. Injury. 2007;38: 1365–72. doi:10.1016/j.injury.2007.09.016

170. Murphy K, Travers P, Walport M. Janeway's Immunobiology [Internet]. Schanck D, Masson S, Lawrence E, Goatly B, editors. Garland Science. Garland Science; 2008. doi:10.1086/596249

171. Turner MS, Isse K, Fischer DK, Turnquist HR, Morel PA. Low TCR signal strength induces combined expansion of Th2 and regulatory T cell populations that protect mice from the development of type 1 diabetes. Diabetologia. 2014;57: 1428–36. doi:10.1007/s00125-014-3233-9

172. Dejaco C, Grubeck- B. Imbalance of regulatory T cells in human autoimmune diseases. 2005; 289–300. doi:10.1111/j.1365-2567.2005.02317.x

173. Marabelle A, Kohrt H, Sagiv-barfi I, Ajami B, Axtell RC, Zhou G, et al. Depleting tumor-specific Tregs at a single site eradicates disseminated tumors. 2013;123. doi:10.1172/JCI64859.fits

174. Nishikawa H, Sakaguchi S, Cd F, Treg T. Regulatory T cells in cancer immunotherapy. Curr Opin Immunol. Elsevier Ltd; 2014;27: 1–7. doi:10.1016/j.coi.2013.12.005

175. Morris GP, Allen PM. How the TCR balances sensitivity and specificity for the recognition of self and pathogens. Nat Immunol. 2012;13: 121–128. doi:10.1038/ni.2190

176. Fulton RB, Hamilton SE, Xing Y, Best JA, Goldrath AW, Hogquist KA, et al. The TCR's sensitivity to self peptide-MHC dictates the ability of naive CD8(+) T cells to respond to foreign antigens. Nat Immunol. Nature Publishing Group; 2015;16: 107–17. doi:10.1038/ni.3043

177. McKeithan TW. Kinetic proofreading in T-cell receptor signal transduction. Proc Natl Acad Sci. 1995;92: 5042–5046. doi:10.1073/pnas.92.11.5042

178. Turner MS, Kane LP, Morel PA. Dominant role of antigen dose in CD4+Foxp3+ regulatory T cell induction and expansion. J Immunol. 2009;183: 4895–903. doi:10.4049/jimmunol.0901459

179. Moran AE, Holzapfel KL, Xing Y, Cunningham NR, Maltzman JS, Punt J, et al. T cell receptor signal strength in Treg and iNKT cell development demonstrated by a novel fluorescent reporter mouse. J Exp Med. 2011;208: 1279–1289. doi:10.1084/jem.20110308

180. Corse E, Gottschalk RA, Allison JP. Strength of TCR-peptide/MHC interactions and in vivo T cell responses. J Immunol. 2011;186: 5039–45. doi:10.4049/jimmunol.1003650

181. Sauer S, Bruno L, Hertweck A, Finlay D, Leleu M, Spivakov M, et al. T cell receptor signaling controls Foxp3 expression via PI3K, Akt, and mTOR. Proc Natl Acad Sci U S A. 2008;105: 7797–802. doi:10.1073/pnas.0800928105

182. Haxhinasto S, Mathis D, Benoist C. The AKT-mTOR axis regulates de novo differentiation of CD4+Foxp3+ cells. J Exp Med. 2008;205: 565–74. doi:10.1084/jem.20071477

183. Coombs D, Goldstein B. T cell activation: Kinetic proofreading, serial engagement and cell adhesion. J Comput Appl Math. 2005;184: 121–139. doi:10.1016/j.cam.2004.07.035

184. Lever M, Maini PK, van der Merwe PA, Dushek O. Phenotypic models of T cell activation. Nat Rev Immunol. Nature Publishing Group; 2014;14: 619–629. doi:10.1038/nri3728

185. Tkach KE, Barik D, Voisinne G, Malandro N, Hathorn MM, Cotari JW, et al. T cells translate individual, quantal activation into collective, analog cytokine responses via time-integrated feedbacks. Elife. eLife Sciences Publications Limited; 2014;3: e01944. doi:10.7554/eLife.01944

186. Voisinne G, Nixon BG, Melbinger A, Gasteiger G, Vergassola M, Altan-Bonnet G. T Cells Integrate Local and Global Cues to Discriminate between Structurally Similar Antigens. Cell Rep. Elsevier; 2015;11: 1208–1219. doi:10.1016/j.celrep.2015.04.051

187. Dushek O, van der Merwe PA. An induced rebinding model of antigen discrimination. Trends Immunol. Elsevier Ltd; 2014;35: 153–158. doi:10.1016/j.it.2014.02.002

188. Chakraborty AK, Das J, Zikherman J, Yang M, Govern CC, Ho M, et al. Molecular origin and functional consequences of digital signaling and hysteresis during Ras activation in lymphocytes. Sci Signal. 2009;2: pt2. doi:10.1126/scisignal.266pt2

189. Au-Yeung BB, Zikherman J, Mueller JL, Ashouri JF, Matloubian M, Cheng DA, et al. A sharp T-cell antigen receptor signaling threshold for T-cell proliferation. Proc Natl Acad Sci U S A. 2014;111: E3679-88. doi:10.1073/pnas.1413726111

190. Hawse WF, Sheehan RP, Miskov-Zivanov N, Menk a. V., Kane LP, Faeder JR, et al. Cutting Edge: Differential Regulation of PTEN by TCR, Akt, and FoxO1 Controls CD4+ T Cell Fate Decisions. J Immunol. 2015; 1–6. doi:10.4049/jimmunol.1402554

191. Wang X, Jiang X. Post-translational regulation of PTEN. Oncogene. Macmillan Publishers Limited; 2008;27: 5454–63. doi:10.1038/onc.2008.242

192. Song MS, Salmena L, Pandolfi PP. The functions and regulation of the PTEN tumour suppressor. Nat Rev Mol Cell Biol. Nature Publishing Group; 2012;13: 283–296. doi:10.1038/nrm3330

193. Blinov ML, Faeder JR, Goldstein B, Hlavacek WS. BioNetGen: Software for rule-based modeling of signal transduction based on the interactions of molecular domains. Bioinformatics. 2004;20: 3289–3291. doi:10.1093/bioinformatics/bth378

194. Sekar, John A. P. and Faeder JR. Rule-Based Modeling of Signal Tansduction: A Primer. Computationsl MOdeling of Signaling Networks Methods and Protocols. 2012. pp. 139–218. doi:10.1007/978-1-61779-833-7

195. Hlavacek WS, Faeder JR. The complexity of cell signaling and the need for a new mechanics. Sci Signal. 2009;2: pe46. doi:10.1126/scisignal.281pe46

196. Faeder JR, Hlavacek WS, Reischl I, Blinov ML, Metzger H, Redondo A, et al. Investigation of early events in Fc epsilon RI-mediated signaling using a detailed mathematical model. J Immunol. 2003;170: 3769–3781. doi:10.4049/jimmunol.170.7.3769

197. Saadatpour A, Albert I, Albert R. Attractor analysis of asynchronous Boolean models of signal transduction networks. J Theor Biol. 2010;266: 641–656. doi:10.1016/j.jtbi.2010.07.022

198. Gillespie DT. A general method for numerically simulating the stochastic time evolution of coupled chemical reactions. J Comput Phys. 1976;22: 403–434. doi:10.1016/0021-9991(76)90041-3

199. Harris LA, Hogg JS, Tapia J-J, Sekar JAP, Gupta S, Korsunsky I, et al. BioNetGen 2.2: Advances in Rule-Based Modeling. Bioinformatics. 2016; 2006–2008. doi:10.1093/bioinformatics/btw469

200. Feinerman O, Veiga J, Dorfman JR, Germain RN, Altan-Bonnet G. Variability and robustness in T cell activation from regulated heterogeneity in protein levels. Science. 2008;321: 1081–4. doi:10.1126/science.1158013

201. Zmajkovicova K, Jesenberger V, Catalanotti F, Baumgartner C, Reyes G, Baccarini M. MEK1 is required for PTEN membrane recruitment, AKT regulation, and the maintenance of peripheral tolerance. Mol Cell. 2013;50: 43–55. doi:10.1016/j.molcel.2013.01.037

202. Julien L-A, Carriere A, Moreau J, Roux PP. mTORC1-activated S6K1 phosphorylates Rictor on threonine 1135 and regulates mTORC2 signaling. Mol Cell Biol. 2010;30: 908–21. doi:10.1128/MCB.00601-09

203. Appleman LJ, van Puijenbroek AAFL, Shu KM, Nadler LM, Boussiotis VA. CD28 costimulation mediates down-regulation of p27kip1 and cell cycle progression by activation of the PI3K/PKB signaling pathway in primary human T cells. J Immunol. 2002;168: 2729–36.

204. Torres J, Pulido R. The tumor suppressor PTEN is phosphorylated by the protein kinase CK2 at its C terminus. Implications for PTEN stability to proteasome-mediated degradation. J Biol Chem. 2001;276: 993–8. doi:10.1074/jbc.M009134200

205. Wang X, Trotman LC, Koppie T, Alimonti A, Chen Z, Gao Z, et al. NEDD4-1 is a proto-oncogenic ubiquitin ligase for PTEN. Cell. 2007;128: 129–39. doi:10.1016/j.cell.2006.11.039

206. Burnett PE, Barrow RK, Cohen N a, Snyder SH, Sabatini DM. RAFT1 phosphorylation of the translational regulators p70 S6 kinase and 4E-BP1. Proc Natl Acad Sci U S A. 1998;95: 1432–1437. doi:10.1073/pnas.95.4.1432

207. Maehama T. PTEN: a tumour suppressor that functions as a phospholipid phosphatase. Trends Cell Biol. 1999;9: 125–128. doi:10.1016/S0962-8924(99)01519-6

208. Vanhaesebroeck B, Leevers SJ, Panayotou G, Waterfield MD. Phosphoinositide 3-kinases: A conserved family of signal transducers. Trends Biochem Sci. 1997;22: 267–272. doi:10.1016/S0968-0004(97)01061-X

209. Okkenhaug K, Bilancio A, Farjot G, Priddle H, Sancho S, Peskett E, et al. Impaired B and T cell antigen receptor signaling in p110delta PI 3-kinase mutant mice. Science. 2002;297: 1031–4. doi:10.1126/science.1073560

210. Alessi DR, James SR, Downes CP, Holmes AB, Gaffney PRJ, Reese CB, et al. Characterization of a 3-phosphoinositide-dependent protein kinase which phosphorylates and activates protein kinase Bα. Curr Biol. 1997;7: 261–269. doi:10.1016/S0960-9822(06)00122-9

211. Gan X, Wang J, Su B, Wu D. Evidence for direct activation of mTORC2 kinase activity by phosphatidylinositol 3,4,5-trisphosphate. J Biol Chem. 2011;286: 10998–1002. doi:10.1074/jbc.M110.195016

212. Sarbassov DD, Guertin DA, Ali SM, Sabatini DM. Phosphorylation and regulation of Akt/PKB by the rictor-mTOR complex. Science. 2005;307: 1098–101. doi:10.1126/science.1106148

213. Biggs WH, Meisenhelder J, Hunter T, Cavenee WK, Arden KC. Protein kinase B/Akt-mediated phosphorylation promotes nuclear exclusion of the winged helix transcription factor FKHR1. Proc Natl Acad Sci U S A. 1999;96: 7421–6.

214. Crellin NK, Garcia R V, Levings MK. Altered activation of AKT is required for the suppressive function of human CD4 ♀ CD25 ♀ T regulatory cells. 2014;109: 2014–2022. doi:10.1182/blood-2006-07-035279.

215. Delgoffe GM, Kole TP, Zheng Y, Zarek PE, Matthews KL, Xiao B, et al. The mTOR Kinase Differentially Regulates Effector and Regulatory T Cell Lineage Commitment. Immunity. Elsevier Ltd; 2009;30: 832–844. doi:10.1016/j.immuni.2009.04.014

216. Zikherman J, Parameswaran R, Weiss A. Endogenous antigen tunes the responsiveness of naive B cells but not T cells. Nature. Nature Publishing Group; 2012;489: 160–4. doi:10.1038/nature11311

217. Di Cristofano A, Pesce B, Cordon-Cardo C, Pandolfi PP. Pten is essential for embryonic development and tumour suppression. Nat Genet. 1998;19: 348–355. doi:10.1038/1235

218. Kwabi-Addo B, Giri D, Schmidt K, Podsypanina K, Parsons R, Greenberg N, et al. Haploinsufficiency of the Pten tumor suppressor gene promotes prostate cancer progression. Proc Natl Acad Sci U S A. 2001;98: 11563–8. doi:10.1073/pnas.201167798

219. Di Cristofano A, Kotsi P, Peng YF, Cordon-Cardo C, Elkon KB, Pandolfi PP. Impaired Fas response and autoimmunity in Pten+/- mice. Science (80-). 1999;285: 2122–2125. doi:10.1126/science.285.5436.2122

220. Chang JT, Palanivel VR, Kinjyo I, Schambach F, Intlekofer AM, Banerjee A, et al. Asymmetric T lymphocyte division in the initiation of adaptive immune responses. Science. 2007;315: 1687–1691. doi:10.1126/science.1139393

221. Arsenio J, Metz PJ, Chang JT. Asymmetric Cell Division in T Lymphocyte Fate Diversi fi cation. Trends Immunol. Elsevier Ltd; 2015;xx: 1–14. doi:10.1016/j.it.2015.09.004

222. Chang JT, Ciocca ML, Kinjyo I, Palanivel VR, McClurkin CE, DeJong CS, et al. Asymmetric Proteasome Segregation as a Mechanism for Unequal Partitioning of the Transcription Factor T-bet during T Lymphocyte Division. Immunity. Elsevier Inc.; 2011;34: 492–504. doi:10.1016/j.immuni.2011.03.017

223. Belkaid Y, Piccirillo C a, Mendez S. CD4 1 CD25 1 regulatory T cells control Leishmania major persistence and immunity. Nature. 2002;420: 633–637. doi:10.1038/nature01199.1.

224. Wu LC, Tuot DS, Lyons DS, Garcia KC, Davis MM. Two-step binding mechanism for T-cell receptor recognition of peptide – MHC. 2002;418: 1–5.

225. Germain RN. Computational Analysis of T Cell Receptor Signaling and Ligand Discrimination - Past, Present, and Future. FEBS Lett. 2010;584: 4814–4822. doi:10.1016/j.febslet.2010.10.027.Computational

226. Coward J, Germain RN, Altan-Bonnet G. Perspectives for Computer Modeling in the Study of T Cell Activation. Cold Spring Harb Perspect Biol. 2010;2.

227. Huppa JB, Davis MM. T-cell-antigen recognition and the immunological synapse. Nat Rev Immunol. 2003;3: 973–983. doi:10.1038/nri1245

228. Boer RJ De, Beltman JB. Random Migration and Signal Integration Promote Rapid and Robust T Cell Recruitment. 2014;10. doi:10.1371/journal.pcbi.1003752

229. Lee M, Mandl JN, Germain RN, Yates AJ. The race for the prize : T-cell trafficking strategies for optimal surveillance. 2016;120: 1432–1439. doi:10.1182/blood-2012-04-424655.

230. Zheng H, Jin B, Henrickson SE, Perelson AS, Andrian UH Von, Chakraborty AK. How Antigen Quantity and Quality Determine T-Cell Decisions in Lymphoid Tissue. 2008;28: 4040–4051. doi:10.1128/MCB.00136-08

231. Prokopiou S, Barbarroux L, Bernard S, Mafille J, Leverrier Y, Arpin C, et al. Multiscale Modeling of the Early CD8 T-Cell Immune Response in Lymph Nodes: An Integrative Study. Computation. Multidisciplinary Digital Publishing Institute; 2014;2: 159–181. doi:10.3390/computation2040159

232. Pienaar E, Matern WM, Linderman JJ, Bader JS, Kirschner DE. Multiscale Model of Mycobacterium tuberculosis Infection Maps Metabolite and Gene Perturbations to Granuloma Sterilization. 2016;84: 1650–1669. doi:10.1128/IAI.01438-15.

233. Steinman L. A brief history of T(H)17, the first major revision in the T(H)1/T(H)2 hypothesis of T cell-mediated tissue damage. Nat Med. Nature Publishing Group; 2007;13: 139–45. doi:10.1038/nm1551

234. Yao Z, Fanslow WC, Seldin MF, Rousseau AM, Painter SL, Comeau MR, et al. Herpesvirus Saimiri encodes a new cytokine, IL-17, which binds to a novel cytokine receptor. Immunity. 1995;3: 811–21.

235. Fossiez F, Djossou O, Chomarat P, Flores-Romo L, Ait-Yahia S, Maat C, et al. T cell interleukin-17 induces stromal cells to produce proinflammatory and hematopoietic cytokines. J Exp Med. 1996;183: 2593–603.

236. Wright J, Bennett F, Li B. The human IL-17F/IL-17A heterodimeric cytokine signals through the IL-17RA/IL-17RC receptor complex. J Immunol 2008; Available: http://www.jimmunol.org/content/181/4/2799.short

237. Ishigame H, Kakuta S, Nagai T, Kadoki M, Nambu A, Komiyama Y, et al. Differential roles of interleukin-17A and -17F in host defense against mucoepithelial bacterial infection and allergic responses. Immunity. 2009;30: 108–19. doi:10.1016/j.immuni.2008.11.009

238. Gaffen SL. Structure and signalling in the IL-17 receptor family. Nat Rev Immunol. 2009;9: 556–67. doi:10.1038/nri2586

239. Conti HR, Shen F, Nayyar N, Stocum E, Sun JN, Lindemann MJ, et al. Th17 cells and IL-17 receptor signaling are essential for mucosal host defense against oral candidiasis. J Exp Med. 2009;206: 299–311. doi:10.1084/jem.20081463

240. Kirkham BW, Lassere MN, Edmonds JP, Juhasz KM, Bird PA, Lee CS, et al. Synovial membrane cytokine expression is predictive of joint damage progression in rheumatoid arthritis: a two-year prospective study (the DAMAGE study cohort). Arthritis Rheum. 2006;54: 1122–31. doi:10.1002/art.21749

241. Lubberts E, Koenders MI, Oppers-Walgreen B, van den Bersselaar L, Coenen-de Roo CJJ, Joosten LAB, et al. Treatment with a neutralizing anti-murine interleukin-17 antibody after the onset of collagen-induced arthritis reduces joint inflammation, cartilage destruction, and bone erosion. Arthritis Rheum. 2004;50: 650–9. doi:10.1002/art.20001

242. Gaffen SL. Structure and signalling in the IL-17 receptor family. Nat Rev Immunol. Nature Publishing Group; 2009;9: 556–67. doi:10.1038/nri2586

243. Zhang B, Liu C, Qian W, Han Y, Li X, Deng J. Structure of the unique SEFIR domain from human interleukin 17 receptor A reveals a composite ligand-binding site containing a conserved-helix for Act1 binding and IL-17 signaling. Acta Crystallogr Sect D Biol Crystallogr. 2014;70: 1476–1483. doi:10.1107/S1399004714005227

244. Liu, Caini; Qian, Wen; Qian, Youcun; Giltiay, Natalia; Lu, Yi; Misra, Saurav, Deng, Li; Chen, Zhijian and Li X. Act1, a novel U-box E3 ubiquitin ligase for IL-17R-mediated signalling. Sci Signal. 2011;92: ra63. doi:10.1016/j.str.2010.08.012.Structure

245. Wertz IE, Dixit VM. Signaling to NF-kappaB: regulation by ubiquitination. Cold Spring Harb Perspect Biol. 2010;2: a003350. doi:10.1101/cshperspect.a003350

246. Wertz IE, O'Rourke KM, Zhou H, Eby M, Aravind L, Seshagiri S, et al. De-ubiquitination and ubiquitin ligase domains of A20 downregulate NF-kappaB signalling. Nature. 2004;430: 694–9. doi:10.1038/nature02794

247. Boone DL, Turer EE, Lee EG, Ahmad R-C, Wheeler MT, Tsui C, et al. The ubiquitin-modifying enzyme A20 is required for termination of Toll-like receptor responses. Nat Immunol. 2004;5: 1052–60. doi:10.1038/ni1110

248. Mauro C, Pacifico F, Lavorgna A, Mellone S, Iannetti A, Acquaviva R, et al. ABIN-1 binds to NEMO/IKKgamma and co-operates with A20 in inhibiting NF-kappaB. J Biol Chem. 2006;281: 18482–8. doi:10.1074/jbc.M601502200

249. Wertz IE, O'Rourke KM, Zhou H, Eby M, Aravind L, Seshagiri S, et al. De-ubiquitination and ubiquitin ligase domains of A20 downregulate NF-kappaB signalling. Nature. 2004;430: 694–9. doi:10.1038/nature02794

250. Werner SL, Kearns JD, Zadorozhnaya V, Lynch C, O'Dea E, Boldin MP, et al. Encoding NF-kappaB temporal control in response to TNF: distinct roles for the negative regulators IkappaBalpha and A20. Genes Dev. 2008;22: 2093–101. doi:10.1101/gad.1680708

251. Yang Q, Calvano SE, Lowry SF, Androulakis IP. A dual negative regulation model of Toll-like receptor 4 signaling for endotoxin preconditioning in human endotoxemia. Math Biosci. Elsevier Inc.; 2011;232: 151–63. doi:10.1016/j.mbs.2011.05.005

252. Lipniacki T, Paszek P, Brasier a RAR, Luxon B, Kimmel M. Mathematical model of NF-kappaB regulatory module. J Theor Biol. 2004;228: 195–215. doi:10.1016/j.jtbi.2004.01.001

253. Fu Y, Glaros T, Zhu M, Wang P, Wu Z, Tyson JJ, et al. Network topologies and dynamics leading to endotoxin tolerance and priming in innate immune cells. PLoS Comput Biol. 2012;8: e1002526. doi:10.1371/journal.pcbi.1002526

254. Lee REC, Walker SR, Savery K, Frank DA, Gaudet S. Fold change of nuclear NF-??B determines TNF-induced transcription in single cells. Mol Cell. Elsevier Inc.; 2014;53: 867–879. doi:10.1016/j.molcel.2014.01.026

255. Ashall L, Horton CA, Nelson DE, Paszek P, Harper C V, Sillitoe K, et al. Pulsatile stimulation determines timing and specificity of NF-kappaB-dependent transcription. Science. 2009;324: 242–246. doi:10.1126/science.1164860

256. Foteinou P, Calvano S, Lowry S, Androulakis I. Modeling endotoxin-induced systemic inflammation using an indirect response approach. Math …. 2009;217: 27–42. doi:10.1016/j.mbs.2008.09.003.Modeling

257. Wang Y, Paszek P, Horton C a, Yue H, White MRH, Kell DB, et al. A systematic survey of the response of a model NF-κB signalling pathway to TNFα stimulation. J Theor Biol. Elsevier; 2012;297: 137–47. doi:10.1016/j.jtbi.2011.12.014

258. Covert MW, Leung TH, Gaston JE, Baltimore D. Achieving stability of lipopolysaccharide-induced NF-kappaB activation. Science. 2005;309: 1854–7. doi:10.1126/science.1112304

259. Tay S, Hughey JJ, Lee TK, Lipniacki T, Quake SR, Covert MW. Single-cell NF-kappaB dynamics reveal digital activation and analogue information processing. Nature. 2010;466: 267–71. doi:10.1038/nature09145

260. Cheong R, Rhee a., Wang CJ, Nemenman I, Levchenko a. Information Transduction Capacity of Noisy Biochemical Signaling Networks. Science (80-). 2011;334: 354–358. doi:10.1126/science.1204553

261. Lee TK, Denny EM, Sanghvi JC, Gaston JE, Maynard ND, Hughey JJ, et al. A noisy paracrine signal determines the cellular NF-kappaB response to lipopolysaccharide. Sci Signal. 2009;2: ra65. doi:10.1126/scisignal.2000599

262. Gaffen SL, Jain R, Garg A V, Cua DJ. The IL-23-IL-17 immune axis: from mechanisms to therapeutic testing. Nat Rev Immunol. Nature Publishing Group; 2014;14: 585–600. doi:10.1038/nri3707

263. Qian Y, Liu C, Hartupee J, Altuntas CZ, Gulen MF, Jane-Wit D, et al. The adaptor Act1 is required for interleukin 17-dependent signaling associated with autoimmune and inflammatory disease. Nat Immunol. 2007;8: 247–56. doi:10.1038/ni1439

264. Kanayama A, Seth RB, Sun L, Ea CK, Hong M, Shaito A, et al. TAB2 and TAB3 activate the NF-??B pathway through binding to polyubiquitin chains. Mol Cell. 2004;15: 535–548. doi:10.1016/j.molcel.2004.08.008

265. Wang C, Deng L, Hong M, Akkaraju GR, Inoue J, Chen ZJ. TAK1 is a ubiquitin-dependent kinase of MKK and IKK. Nature. 2001;412: 346–51. doi:10.1038/35085597

266. Yu Y, Ge N, Xie M, Sun W, Burlingame S, Pass AK, et al. Phosphorylation of Thr-178 and Thr-184 in the TAK1 T-loop is required for interleukin (IL)-1-mediated optimal NF??B and AP-1 activation as well as IL-6 gene expression. J Biol Chem. 2008;283: 24497–24505. doi:10.1074/jbc.M802825200

267. Kishimoto K, Matsumoto K, Ninomiya-Tsuji J. TAK1 mitogen-activated protein kinase kinase kinase is activated by autophosphorylation within its activation loop. J Biol Chem. 2000;275: 7359–64. Available: http://www.ncbi.nlm.nih.gov/pubmed/10702308

268. Tang ED, Wang C-Y, Xiong Y, Guan K-L. A Role for NF- B Essential Modifier/I B Kinase- (NEMO/IKK) Ubiquitination in the Activation of the I B Kinase Complex by Tumor Necrosis Factor-. J Biol Chem. 2003;278: 37297–37305. doi:10.1074/jbc.M303389200

269. Wu C-J, Conze DB, Li T, Srinivasula SM, Ashwell JD. Sensing of Lys 63-linked polyubiquitination by NEMO is a key event in NF-kappaB activation [corrected]. Nat Cell Biol. 2006;8: 398–406. doi:10.1038/ncb1384

270. Delhase M, Hayakawa M, Chen Y, Karin M. Positive and Negative Regulation of ⟩ Kinase Activity Through IKK Subunit Phosphorylation. : 7–12.

271. DiDonato J a, Hayakawa M, Rothwarf DM, Zandi E, Karin M. A cytokine-responsive IkappaB kinase that activates the transcription factor NF-kappaB. Nature. 1997;388: 548–54. doi:10.1038/41493

272. Mercurio F, Sci JC, Zhu H, Murray BW, Shevchenko A, Bennett BL, et al. Activation IKK-1 And IKK-2 : Cytokine-Activated IkB Kinases Essential for NF-kB Activation. 1997;278: 860–866. doi:10.1126/science.278.5339.860

273. Chen Z, Hagler J, Palombella VJ, Melandri F, Seherer D, Ballard D, et al. Signal-induced site-specific phosphorylation targets IKBa to the ubiquitin-proteasome pathway. Genes Dev. 1995;9: 1586–1598. doi:10.1101/gad.9.13.1586

274. DiDonato J, Mercurio F, Rosette C, Wu-Li J, Suyang H, Ghosh S, et al. Mapping of the inducible IkappaB phosphorylation sites that signal its ubiquitination and degradation. Mol Cell Biol. 1996;16: 1295–304. doi:10.1128/MCB.16.4.1295

275. Sun SC, Ganchi PA, Ballard DW, Greene WC. NF-kappa B controls expression of inhibitor I kappa B alpha: evidence for an inducible autoregulatory pathway. Science. American Association for the Advancement of Science; 1993;259: 1912–5. doi:10.1126/science.8096091

276. Krikos a, Laherty CD, Dixit VM. Transcriptional activation of the tumor necrosis factor alpha-inducible zinc finger protein, A20, is mediated by kappa B elements. J Biol Chem. 1992;267: 17971–6. Available: http://www.ncbi.nlm.nih.gov/pubmed/1381359

277. Jacobs MD, Harrison SC. Structure of an IkBa/NF-kB Complex. Cell. 1998;95: 749–758. doi:10.1016/S0092-8674(00)81698-0

278. Ho AW, Garg A V., Monin L, Simpson-Abelson MR, Kinner L, Gaffen SL. The Anaphase-Promoting Complex Protein 5 (AnapC5) Associates with A20 and Inhibits IL-17-Mediated Signal Transduction. PLoS One. 2013;8: 1–10. doi:10.1371/journal.pone.0070168

279. Hoffmann A, Levchenko A, Scott ML, Baltimore D. The IkappaB-NF-kappaB signaling module: temporal control and selective gene activation. Science. 2002;298: 1241–5. doi:10.1126/science.1071914

280. Sung MH, Salvatore L, De Lorenzi R, Indrawan A, Pasparakis M, Hager GL, et al. Sustained oscillations of NF-??B produce distinct genome scanning and gene expression profiles. PLoS One. 2009;4. doi:10.1371/journal.pone.0007163

281. Lee EG, Boone DL, Chai S, Libby SL, Chien M, Lodolce JP, et al. Failure to regulate TNF-induced NF-kappaB and cell death responses in A20-deficient mice. Science. 2000;289: 2350–4. doi:10.1126/science.289.5488.2350

282. Komander D, Rape M. The Ubiquitin Code. Annu Rev Biochem. 2012;81: 203–229. doi:10.1146/annurev-biochem-060310-170328

283. Adamson A, Boddington C, Downton P, Rowe W, Bagnall J, Lam C, et al. Signal transduction controls heterogeneous NF-κB dynamics and target gene expression through cytokine-specific refractory states. Nat Commun. Nature Publishing Group; 2016;7: 12057. doi:10.1038/ncomms12057

284. Cong L, Ran FA, Cox D, Lin S, Barretto R, Hsu PD, et al. Multiplex Genome Engineering Using CRISPR/VCas Systems. Science (80-). 2013;339: 819–823. doi:10.1126/science.1231143.Multiplex

285. Mali P, Yang L, Esvelt KM, Aach J, Guell M, DiCarlo JE, et al. RNA-Guided Human Genome Engineering via Cas9 Prashant. Science (80-). 2013;339: 823–826. doi:10.1126/science.1232033.RNA-Guided